A Final Technical Report to the
National Aeronautics and Space Administration
from

President and Fellows of Harvard College
Office of Sponsored Research
Holyoke Center 458
Harvard University
1350 Massachusetts Avenue
Cambridge, MA 02138

NAG 5-2487

Grant Expiration: 2/14/96

Principal Investigator: Robert P. Kirshner
Harvard College Observatory MS-19
60 Garden Street
Cambridge, MA 02138
(617) 495-7519

Date: 22 May 1996

SUMMARY OF RESULTS

This program supported the analysis of IUE observations of supernovae. One aspect was a Target-of-Opportunity program to observe bright supernovae which was applied to SN 1993J in M81, and another was continuing analysis of the IUE data from SN 1987A. Because of its quick response time, the IUE satellite has continued to provide useful data on the ultraviolet spectra of supernovae. Even after the launch of the Hubble Space Telescope, which has much more powerful ultraviolet spectrometers, the IUE has enabled us to obtain early and frequent measurements of ultraviolet radiation: this information has been folded in with our HST data to create unique observations of supernova which can be interpreted to give powerful constraints on the physical properties of the exploding stars. Our chief result in the present grant period was the completion of a detailed re-analysis of the data on the circumstellar shell of SN 1987A.

The presence of narrow high-temperature mission lines from nitrogen-rich gas close to SN 1987A has been the principal observational constraint on the evolution of the supernova's progenitor. Our new analysis shows that the onset of these lines, their rise to maximum, and their subsequent fading can be understood in the context of a model for the photoionization of circumstellar matter.

IUE SUPERNOVA PUBLICATIONS

Kirshner, R.P., Sonneborn, G., Crenshaw, D.M, and Nassiopoulos, G.E. 1987, "Ultraviolet Observations of SN 1987A," Ap.J. 320, 602.

Dupree, A.K., Kirshner, R.P., Nassiopoulos, G.E., Raymond, J.C., and Sonneborn, G. 1987, "The Interstellar Medium Towards SN 1987A," Ap.J. 320, 597.

Sonneborn, G., Altner, B.A., and Kirshner, R.P. 1987, "Spatially-Resolved Ultraviolet Spectroscopy of SN1987A: Identification of the Progenitor," Ap.J. (Lett.) 232, L35.

Kirshner, R.P. 1987, "Ultraviolet Views and Spectroscopic Clues," in ESO Workshop on SN 1987A (I.J. Danziger, ed.) p. 121.

Kirshner, R.P. 1988, "SN 1987A: Ultraviolet Observations and Mass Loss," in IAU Colloquium 108 (K. Nomoto, ed.) (Springer-Verlag: New York) p.252.

Kirshner, R.P. 1988, "Ultraviolet Observations of SN 1987A: Clues to Mass Loss," in George Mason Symposium on SN1987A (M. Kafatos, ed.)

Kirshner, R.P 1988, "Supernova 1987A", McGraw-Hill Science Year 1988.

Kirshner, R.P. 1988, "Death of a Star," National Geographic Magazine, 173, 618.

Kirshner, R.P. 1988, "Supernovae in the South: SN 1987A y CIA," in "Progress and Opportunities in Southern Hemisphere Optical Astronomy," (ed, V. Blanco and M. Phillips), Astronomical Society of the Pacific.

Kirshner, R.P. 1988, "Observing SN 1987A with IUE" in " A Decade of UV Astronomy with the IUE Satellite," ESA SP-281.

Sanz Fernandez de Cordoba, L., Cassatella, A., Gilmozzi, R., Kirshner, R., Panagia, N., Sonneborn, G., and Wamsteker, W. 1988, "Spectral Evolution of SN 1987A in the IUE Long Wavelength Range" in " A Decade of UV Astronomy with the IUE Satellite," ESA SP-281.

Fransson, C., Cassatella, A., Gilmozzi, R., Kirshner, R.P., Panagia, N., Sonneborn, G., and Wamsteker, W. 1989, "Narrow UV Emission Lines from SN 1987A: Evidence for CNO-Processing in the Progenitor" Ap.J. 336, 429.

Arnett, W.D., Bahcall, J.N., Kirshner, R.P., and Woosley, S.E. 1989, "Supernova 1987A," Ann. Rev. Astron. Astrophys. 27, 629.

Eastman, R.G. and Kirshner, R.P. 1989, "Model Atmospheres of SN 1987A and the Distance to the LMC," Ap.J. 15 Dec 89

Kirshner, R.P. 1990, "Supernova Light Curves" in Supernovae, Petschek (ed.) Springer-Verlag, p.59.

Kirshner, R.P. and Gilmozzi, R. 1989, "SN 1987A" in Exploring the Universe with the IUE Satellite, Y. Kondo (ed.) Kluwer Academic (Dordrecht) p. 771.

Leibundgut, B., Kirshner, R.P., Filippenko, A.V., Shields, J.C., Phillips, M.M., and Sonneborn, G. 1991, "Pre-Maximum Observations of SN 1990N" Ap.J. Letters 371:L23-26.

Jeffery, D.J., Leibundgut, B., Kirshner, R.P., Benetti, S., Branch, D., Sonneborn, G. 1992, "Analysis of the Photospheric Epoch Spectra of Supernovae Ia 1990N and 1991T" Ap.J. 397, 304.

Kirshner, R.P. 1991, "Exploding Stars and the Expanding Universe," Quarterly Journal of the Royal

Astronomical Society 32, 233-244.

Kirshner, R.P 1991, "Observing SN 1987A with the International Ultraviolet Explorer," in *High-Energy Astrophysics --American and Soviet Perspectives* (Lewin, W.H.G., Clark, G.W. and Sunyaev, R.A. eds.), National Academy Press, Washington D.C., pp. 237-250.

Panagia, N., Gilmozzi, R., Macchetto, F., Adorf, H.-M., and Kirshner, R.P. 1991, "Properties of the SN 1987A Circumstellar Ring and the Distance to the Large Magellanic Cloud," Ap. J. Letters, **380**, L23.

Phillips, M.M., Wells, L.A., Suntzeff, N.B., Hamuy, M., Leibundgut, B., Kirshner, R.P, and Foltz, C.B. 1992, "SN 1991T: Further Evidence of the Heterogeneous Nature of Type Ia Supernovae" A.J. **103**, 1632.

Schmidt, B.P., Kirshner, R.P., and Eastman, R.G. 1992, "Expanding Atmospheres of Type II Supernovae and the Extragalactic Distance Scale," Astrophys. J. **395**, 366.

Jeffery, D.J., Leibundgut, B., Kirshner, R.P., Benetti, S., Branch, D., and Sonneborn, G. 1992, "Analysis of the Photospheric Epoch Spectra of Supernovae Ia 1990N and 1991T," Astrophys. J. **397**, 304-328.

Leibundgut, B., Kirshner, R.P, and 29 others... 1993, "SN 1991bg: A Type Ia Supernova with a Difference," A.J. **105**, 301.

Schmidt, B.P., Kirshner, R.P., and 34 others 1993, "Photometric and Spectroscopic Observations of SN 1990E in NGC 1035: Observational Constraints for Models of Type II Supernovae," A.J. **105**, 2236.

Kirshner, R.P., Jeffery, D.J., and 19 others 1993, "SN 1992A: Ultraviolet and Optical Studies Based on HST, IUE, and CTIO Observations," Ap.J. **415**, 589.

Schmidt, B.P., Kirshner, R.P., Eastman, R.G., Grashuis, R., Dell'Antonio, I., Caldwell, N., Foltz, C., Huchra, J.P. and Milone, A.A.E. 1993, "The Unusual Supernova SN1993J in the Galaxy M81" Nature, **364**, 600.

Wamsteker, W. Rodriguez, P.M., Gonzales, R., Sonneborn, G., and Kirshner, R.P. 1993, IAU Circular 5738.

Sonneborn, G. Rodriguez, P.M., Wamsteker, W., Fransson, C. and Kirshner, R.P. 1993, IAU Circular 5754.

Sonneborn, G. Fransson, C. Kirshner, R.P., Rodriguez, P.M., and Wamsteker, W. 1993,"UV Spectroscopy of SN 1993J and Detection of Stellar Wind Material from the Progenitor" B.A.A.S. **25**, 893.

de Boer, K.S., rodrigues Pascual, P., Wamsteker, W., Fransson, C., Bomans, D.J., and Kirshner, R.P. 1993, "Intergalactic and galactic clouds on the line of sight to SN 1993J in M81 seen in IUE spectra" Astronomy and Astrophysics, 280, L15.

Jeffery, D.J., Kirshner, R.P., Challis, P.M., Pun, C.S.J., Filippenko, A.V., Matheson, T., Branch, D., Chevalier, R.A., Fransson, C., Panagia, N., Wagoner, R.V., Wheeler, J.C., Clocchiatti, 1994, "A Hubble Space Telescope Ultraviolet Spectrum of SN 1993J," Astrophysical Journal 421, L27.

Pun, C.S.J, Kirshner, R.P., Sonneborn, G., Challis, P., Nassiopoulos, G., Arquilla, R., Crenshaw, M., Shrader, C., Teays, T., Cassatella, A., Gilmozzi, R., Talavera, A., Wamsteker, W., Fransson, C., and Panagia, N. 1995, "Ultraviolet Observations of SN 1987A with the IUE Satellite" Astrophysical Journal Supplement Series 99, 223-261.

Sonneborn, G., Fransson, C., Lundqvist, P., Cassatella, A., Gilmozzi, R., Kirshner, R.P., Panagia, N., and Wamsteker, W. 1996, "The Evolution of Ultraviolet Emission Lines from Circumstellar Material Surrounding SN 1987A" Astrophyical Journal, submitted.

THE ASTROPHYSICAL JOURNAL SUPPLEMENT SERIES, 99:223–261, 1995 July

ULTRAVIOLET OBSERVATIONS OF SN 1987A WITH THE *IUE* SATELLITE

CHUN S. J. PUN AND ROBERT P. KIRSHNER[1]
Harvard-Smithsonian Center for Astrophysics, 60 Garden Street, Cambridge, MA 02138

GEORGE SONNEBORN[1]
Laboratory for Astronomy and Solar Physics, Code 681, NASA/Goddard Space Flight Center, Greenbelt, MD 20771

PETER CHALLIS AND GEORGE NASSIOPOULOS
Harvard-Smithsonian Center for Astrophysics, 60 Garden Street, Cambridge, MA 02138

RICHARD ARQUILLA, D. MICHAEL CRENSHAW, CHRIS SHRADER,[2,3] AND TERRY TEAYS
Computer Sciences Corporation, NASA/GSFC Code 681, Greenbelt, MD 20771

ANGELO CASSATELLA,[4] ROBERTO GILMOZZI,[5] ANTONIO TALAVERA, AND WILLEM WAMSTEKER
ESA IUE Observatory, VILSPA, Villafranca, Apartado 50727, E-28080 Madrid, Spain[6]

CLAES FRANSSON
Stockholm Observatory, S-133 36 Saltsjöbaden, Sweden

AND

NINO PANAGIA[6,7]
Space Telescope Science Institute, 3700 San Martin Drive, Baltimore, MD 21218
Received 1994 September 2; accepted 1994 December 14

ABSTRACT

Ultraviolet (λ: 1150–3300 Å) observations of SN 1987A with the *IUE* satellite provide a unique data set. Observations started the day after discovery, 1987 February 24 (day 1.6), and a total of 751 spectra were obtained through 1992 June 9 (day 1567). The data have been processed to generate a complete catalog of SN 1987A ultraviolet spectra. The data reduction procedure includes careful line-by-line extraction, removing hits and hot pixels, and, most importantly, a scrupulous subtraction of the contribution from stars near SN 1987A within the *IUE* aperture. In addition to processing the data, we have also extracted light curves, and combined them with the ground-based optical data and *HST* observations (day 1278 to 2431) to extend the study in both wavelength and time. The data-processing procedures of our *IUE* study produce results that are consistent with the *HST* data where they overlap, but not with the *IUE* study by Sanz Fernández de Córdoba (1993) because of its incorrect background subtraction. The *IUE* data are consistent with the ground-based Walraven *VBLUW* photometry, while we found that flux scale of the Soviet *ASTRON* satellite spectroscopic data is low by ~15%. The UV flux plummeted during the earliest days of observations because of the drop in the photospheric temperature and the increase in opacity. However, after reaching a minimum of 0.04% on day 44, the UV flux increased by 175 times in its contribution to 7% of the total UVOIR bolometric luminosity at day 800. A revised set of bolometric data has been constructed which includes the contribution of UV from day 1 to day 1352. Studies of the UV colors show that the supernova started to get bluer in UV around the time when dust started to form in the ejecta. Our results are consistent with the possibility that the dust condensed may be metal-rich.

Subject headings: ultraviolet: stars—stars: individual (SN 1987A)

1. INTRODUCTION

SN 1987A in the Large Magellanic Cloud (LMC) provided a unique opportunity for the study of supernovae which has resulted in unprecedented coverage in both wavelength and time. No other supernova has ever been as well observed as SN 1987A—it was truly a once-in-a-lifetime opportunity which we hope to repeat! SN 1987A is the first supernova bright enough for long-term ultraviolet observations. Previous bright supernovae observed in the ultraviolet by the *International Ultraviolet Explorer* (*IUE*), Type IIs SN 1979C and SN 1980K, and Type Ib SN 1983N, only stayed bright enough for good signal-to-noise observations for less than a month (Benvenuti et al. 1982). A large volume of literature has been generated by this spectacular event. Excellent reviews by Arnett et al. (1989), Imshennik & Nadëzhin (1989), Hillebrandt & Höflich (1989), McCray (1991), Nomoto et al. (1994), Chevalier (1992), Podsiadlowski (1992), and McCray (1993) cover various issues of the supernova, such as the neutrino burst, progenitor evolution, explosive nucleosynthesis, bolometric light curve, and interactions with circumstellar mate-

[1] Guest Observer, *IUE* Observatory.
[2] Present address: Laboratory for High-Energy Astrophysics, NASA/GSFC Code 668.1, Greenbelt, MD 20771.
[3] Also at Universities Space Research Association.
[4] Present address: Instituto Astrofisica Spaziale, CNR, Via E. Fermi 21, I-00044 Frascati, Italy.
[5] Present address: European Southern Observatory, Karl-Schwarzschild Strasse 2, D-85748 Garching-bei-München, Germany.
[6] Affiliated with the Astrophysics Division, Space Science Department of ESA, ESTEC, The Netherlands.
[7] Also at University of Catania, Catania, Italy.

rial. In this paper we present the ultraviolet spectra of SN 1987A taken by the *IUE* satellite from day 1 to day 1248, covering the wavelength range 1150–3300 Å. The procedures used to process this unique data set are described. Beyond data processing, this set of data forms the basis for extensive analysis of the UV evolution of the supernova.

Early results on the *IUE* spectroscopy were reported by Kirshner et al. (1987b) and Wamstaker et al. (1987b). These results stimulated a series of papers focussing on studying and interpreting the very early UV spectra of the supernova (Cassatella et al. 1987; Fransson et al. 1987; Panagia et al. 1987b; Lucy 1987). The *IUE* spectra were also essential in identifying the supernova progenitor (Sonneborn, Altner, & Kirshner 1987; Gilmozzi et al. 1987). High-resolution *IUE* spectra ($\lambda/\Delta\lambda \approx 10^4$) with good signal-to-noise were obtained in the first few days of observations (Dupree et al. 1987; de Boer et al. 1987; Blades et al. 1988a,b; Savage et al. 1989). Interstellar absorption lines of various species with a wide range of ionization covering the heliocentric velocity range from -30 to 330 km s^{-1} were detected. Absorptions originated from the galaxy and its halo ($v < 120$ km s^{-1}), LMC ($v > 190$ km s^{-1}), and other sources other than the galaxy or LMC have been identified (Savage et al. 1989). Other studies of SN 1987A with the *IUE* satellite include the observations of the UV light echo in the vicinity of SN 1987A (Gilmozzi 1988; Panagia & Gilmozzi 1991). The UV echo spectrum could provide information about the expansion velocity and the temperature of the supernova at the time of the shock breakout.

Narrow emission lines of highly ionized species in the circumstellar matter were first detected in the UV spectra taken by the short-wavelength camera of *IUE* in 1987 May ($\sim$ day 80) (Wamsteker et al. 1987a; Kirshner et al. 1987a; Sonneborn et al. 1995). High-resolution observation by *IUE* at day 275 showed that the line widths of the C III] 1909, and the N III] 1750 multiplets were $\lesssim$30 km s^{-1} (Panagia et al. 1987a). Studies of the relative strengths of the lines showed that the circumstellar matter was highly CNO enriched (Fransson et al. 1989). This is consistent with models where the progenitor was a red supergiant before exploding as a blue supergiant, thus losing much of its hydrogen envelope before the explosion. The emission-line flux reached a maximum around day 410, and slowly decayed afterwards (Sonneborn 1991; Sonneborn et al. 1995; Sanz Fernández de Córdoba 1993, hereafter SFdC93). Panagia & Gilmozzi (1991) constructed a simple model for the emission-line light curves to determine the absolute diameter of the circular circumstellar ring. Combined with the measurement of the angular diameter by the *Hubble Space Telescope* (*HST*) (Jakobsen et al. 1991), the distance to SN 1987A, $d_{\rm SN87A}$, can be determined (Panagia et al. 1991). The result, 51.2 ± 3.1 kpc, is consistent with the other measurements of the distance to the LMC. Gould (1994a,b) adopted the emission light curve model of Dwek & Felten (1992) and obtained $d_{\rm SN87A} = 46.77 \pm 0.76$ kpc for a circular circumstellar ring and found that the results will be similar for an elliptical ring. Detailed models of the circumstellar matter also exist (Lundqvist 1991; Dwek & Felten 1992; Plait et al. 1995) and they provide good agreement with the observed light curves of the *IUE* emission lines. The effects of these models on the determination of $d_{\rm SN87A}$ still remain to be seen.

Summaries of early results from the *IUE* study of SN 1987A can be found in Kirshner & Gilmozzi (1989), Gilmozzi (1990), and Panagia & Gilmozzi (1991). A study similar to this one on the *IUE* data of SN 1987A can be found in the SFdC93 paper. In SFdC93, the *IUE* light curves of SN 1987A are computed from the time of the first *IUE* observation until 1990 March (day 1100). The results and conclusions of the SFdC93 study are generally similar to this work. However, the UV flux attributed to SN 1987A at late times in SFdC93 is about 7–15 times higher than what we find. The discrepancies are most probably caused by the improper subtraction of background stars in SFdC93. The detailed differences between our data processing procedures and the ones employed in SFdC93 are discussed in § 2.

For this paper, we processed all the low-dispersion UV spectra of SN 1987A from the *IUE* archive. The data processing procedures we applied to all the 751 *IUE* spectra of SN 1987A are described in § 2. The resulting data set is significantly different from that in the *IUE* archive. The data have been carefully selected and combined to generate spectra with the best signal-to-noise. Moreover, as the supernova dims, removing the flux from nearby field stars in the aperture becomes increasingly important. The extra flux comes mostly from Star 2 ($V = 15.03$) and Star 3 ($V \sim 15.7$) in the Walker & Suntzeff (1990) catalog of stars near SN 1987A, which are always in the *IUE* aperture. Flux from Star 4, which is periodically present in the aperture as the spacecraft rotates annually around the sun, is also removed. It is only recently that we have obtained the definitive background spectra which permit this important correction to the data. The procedures used for removing these field stars are addressed in § 2.

A total of 290 spectra spanning the epoch from day 1 to 1248 are assembled and are presented in § 3. This processed set of data forms the basis for our analysis of the UV evolution of the supernova. The UV spectra are combined with optical data to extend the wavelength coverage. We compare our data set to other UV observations of SN 1987A from the Soviet *ASTRON* satellite (Lyubimkov 1990) and the Walraven *VBLUW* photometry (Pel et al. 1987) in § 4. We show that the *IUE* results are consistent with the Walraven data within 5% and are higher than the ASTRON results by $\sim$15%. The UV light curves are shown in § 5 and are compared with the optical photometry. The ratio of ultraviolet flux to optical flux, $F_{\rm UV}/F_{\rm optical}$, is found to increase with time after about day 100. The previously published UVOIR bolometric luminosity (Suntzeff & Bouchet 1990; Suntzeff et al. 1991; Bouchet, Danziger, & Lucy 1991) includes the UV contribution for only the first week of *IUE* observations. We present the revised set of UVOIR bolometric luminosity, which includes the UV flux contributions from the *IUE* data from day 1 to 1352, in § 5. The UV color evolution is discussed in § 6. We found that the UV color became bluer just at the time that the dust started to condense in the SN 1987A ejecta. We conclude that the condensed dust does not resemble galactic or LMC interstellar dust in its extinction properties and that it probably is metal-rich. Finally, in § 7, *IUE* results are compared with the *HST* Faint Object Camera observations (day 1278–2431) obtained by the Supernova INtensive Study (SINS) collaboration. We demonstrate that the *IUE* data archive can be connected to future UV observations with imaging detectors for SN 1987A and other supernovae. With the *HST* data, we establish a long-term rec-

ord of ultraviolet flux that will continue long after the supernova became too faint for *IUE* detections. Comparing the *HST* results with the *IUE* data requires special attentions to the "red leaks" of the *HST* filters, which demand significant corrections to obtain valid results. We present a concluding discussion in § 8.

2. UV OBSERVATIONS AND DATA REDUCTION

2.1. *IUE Observations*

Taking advantage of a Target-of-Opportunity Program to observe bright supernovae, *IUE* observations of SN 1987A started at both NASA's Goddard Space Flight Center (GSFC) and ESA's Villafranca del Castillo (VILSPA) promptly after its discovery. Subsequent systematic programs to obtain UV spectroscopy of SN 1987A with *IUE* have led to a thorough coverage of the ultraviolet evolution of the supernova.

Detailed characteristics of the *IUE* satellite, its scientific instruments and performance can be found in Boggess et al. (1978). One of the many attractive features of the geosynchronous *IUE* satellite is that quick changes in observing schedules can be arranged by the ground observing stations which make the target-of-opportunity program very effective. The spectra are recorded on two image-converter SEC vidicon cameras: short wave prime (SWP) for the wavelength band 1150–1975 Å, and long wave prime (LWP) for the wavelength band 1975–3300 Å. We have processed all the spectra of SN 1987A taken in the low dispersion mode (resolution ~6–7 Å) with the large entrance aperture of size 10″ × 20″. In this mode, the spatial distribution of light projected on the long axis of the aperture is retained in the two-dimensional data. All *IUE* spectra obtained at GSFC and VILSPA were processed by the *IUE* Spectral Image Processing System (IUESIPS) (Turnrose & Thompson 1984), as updated by Mũnoz Piero (1985) for extended line-by-line (ELBL) enhancements to improve the spatial resolution of the low dispersion spectra. Each resulting ELBL file is a two-dimensional flux array with about 800 wavelength points (for SWP; 900 for LWP) and 110 lines in the spatial dimension, approximately parallel with the longer (20″) axis of the aperture. The separation between spectra of two point sources in the ELBL file corresponds to the true angular separation in the sky projected on the long axis. The angular separation between two neighboring lines corresponds to 1.″07 ± 0.″04. In a typical large aperture observation of a point source, the spectral information is contained in about 18 lines in the ELBL file. Various spurious features in the low-dispersion *IUE* spectra such as cosmic ray hits, hot pixels, and the reseaux etched on the faceplates of the cameras were flagged by the IUESIPS, enabling us to remove them from each individual line of the ELBL file where the supernova was present. This treatment is essential, especially in our late-time observations because of the diminishing flux of the supernova and the long exposure time.

Subsequent corrections are applied to adjust for the decreasing sensitivity with time of each *IUE* camera. Teays & Garhart (1990) showed that the LWP camera degradation in low dispersion observing mode between the dates of 1984.5 and 1989.5 can be represented by a linear decline. This is also true for the SWP camera degradation in low dispersion mode between the dates of 1979.5 and 1992.0 (Garhart 1992a). Both studies indicated that the sensitivity changes varied significantly with wavelength due to the granular nature of the camera faceplate. Best-fit straight line coefficients were tabulated for the performance corrections at various wavelengths, and we have applied these corrections for all the *IUE* spectra on SN 1987A, which spanned the period from 1987.2 to 1991.4. The latest broadband sensitivity monitoring confirmed the linear relation until year 1992.3 (Garhart 1992b) with a mean rate of degradation of ~0.7%/year for the SWP camera and ~1.5%/year for the LWP camera since the time of absolute calibration (1984.5–1985.0).

2.2. *Background Stars Subtraction*

SN 1987A is located in a densely populated region of the LMC and has close neighbors. Sonneborn et al. (1987) deconvolved the spatially resolved *IUE* ELBL spectral files to separate the contributions from star 2 and star 3 present in the large aperture SWP data between day 30 and day 70. The absence of any hot stars left in the aperture confirmed the identification of star 1 of the Sanduleak −69°202 system as the progenitor that exploded as SN 1987A. Gilmozzi et al. (1987) conducted a similar analysis using the 1300–1500 Å data from day 7 to day 14 and deduced the same progenitor. Moreover, Gilmozzi et al. (1987) observed stars 2 and 3 directly using the small *IUE* aperture (diameter 3″). With star 2 located 2.″9 ± 0.″1 (PA 315°) and star 3 located 1.″6 ± 0.″2 (PA 115°) from the supernova, these two stars are always present in the large *IUE* aperture (10″ × 20″). Scuderi et al. (1995) compared the small aperture *IUE* spectrum of star 2 with stellar atmosphere models with solar abundances and the *IUE* spectra of standard stars, and they classified star 2 as a B1 III star. Walborn et al. (1993) obtained the optical photometry and spectroscopy of stars 2 and 3. Star 2 is classified as a B2 III star, while star 3 shows variations in *UBVRI* photometry as large as ~0.3 mag, and in infrared photometry by about ~1 mag (Walborn et al. 1993). Combining these results with the discovery of broad Hα emission in star 3 (Wang et al. 1992), it can be concluded that star 3 is a Be object. Be stars are known to vary in the UV as well (Barylak & Doazan 1986), and thus star 3 complicates our study of the UV photometry of SN 1987A, as discussed in § 5.1.

Removing flux of the field stars in the spectra, which comes mostly from stars 2 and 3, grows more difficult and more important as SN 1987A fades. Contamination was especially severe in the SWP data where more than half of the integrated flux was from background stars as early as ~20 days after the explosion. The *IUE* spectra we obtained after day 1300 (for both the SWP and LWP cameras) remain constant in time except for the circumstellar emission lines, which suggests that they are completely dominated by flux from the background field stars instead of the supernova. These spectra (six in SWP and 11 in LWP between day 1301 and 1567) have been averaged, and carefully subtracted from all the data obtained. The combined background spectrum is shown in Figure 1. A definitive reduction of the *IUE* data for SN 1987A has not been possible without this measure of the background flux.

Even after subtracting the background spectrum of Figure 1 from earlier epochs, we still detected extra flux, with a six-month periodicity, in the remaining SWP spectra. When

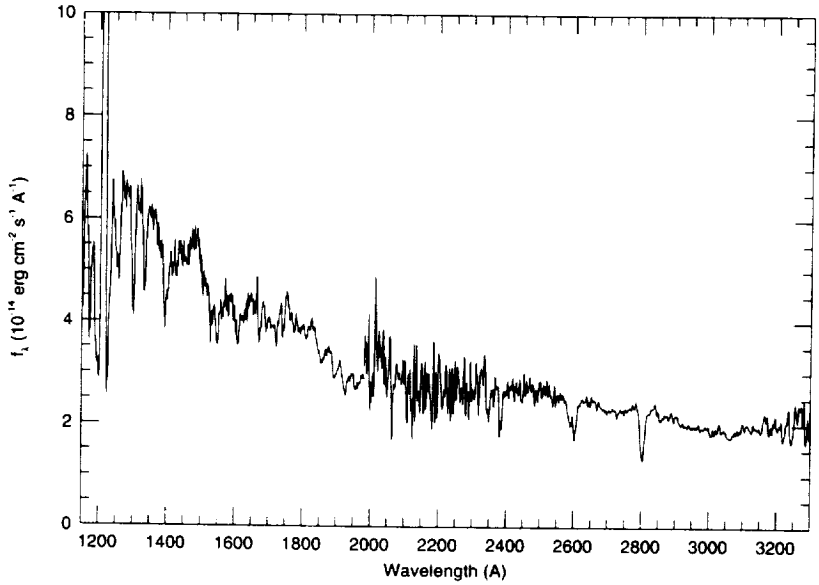

FIG. 1.—The average background spectrum (day 1301–1567) subtracted from all the *IUE* data. The spectrum is not corrected for interstellar extinction.

pointed at SN 1987A, the position angle of the *IUE* aperture rotates once a year as the satellite is oriented for maximum power output from its solar cells. This is a natural way to produce a 6 month periodic signal from additional field star(s) at a distance 5″ to 10″ from SN 1987A. We determined the maximum field star separation by studying the ELBL file and the position angle of the aperture at the epoch of maximum flux to locate the additional star(s) present. We conclude that the additional flux is from star 4 (5.″5 from the supernova; V = 18.24) in the Walker & Suntzeff (1990) catalog of stars near SN 1987A. The extra flux from star 4 is removed by removing the lines in the ELBL spectral file which contribute additional flux and are spatially resolved from SN 1987A, star 2, and star 3. All ELBL files of the SWP spectra taken after ~ day 400 are processed this way (and some before, at epochs of maximum star 4 contribution), when the flux from SN 1987A contributes only ~30% of the flux observed through the aperture and scrupulous sky subtraction is required.

Additional field stars located less than 5″ from the supernova are always present in the *IUE* aperture. Walker & Suntzeff (1991) identified stars "4" and "5" located 2.″0 and 2.″9 away from the supernova. Notice that stars "4" and "5" in Walker & Suntzeff (1991) are different from stars 4 and 5 of the Walker & Suntzeff (1990) catalog of stars near SN 1987A. Plait et al. (1995) resolved star "5" into two stars with a separation of ~0.″1 in FOC images from *HST*. Also with the *HST* images, Plait, Chevalier, & Kirshner (1992) identified a star along our line of sight to the supernova superposed on the circumstellar ring located 0.″74 ± 0.″03 away. The colors and magnitudes are consistent with an A-type dwarf in the LMC (Plait et al. 1995). Examining the *HST* images of SN 1987A (described in § 7) shows that each of these stars is more than 5 mag dimmer than either star 2 or star 3 in the UV. Therefore, they are not significant sources of contamination to our data.

The data processing procedures used in the SFdC93 paper are different from our present work in three major aspects. First, in SFdC93, not all the data from both the GSFC and VILSPA stations between day 1 and 1100 are included. Second, about 15% of the spectra included in the SFdC93 study to compute the UV light curves contained saturated pixels, which we have avoided in our data set. Third, and most important, we employed a different stellar background subtraction procedure from that of SFdC93. In SFdC93, by assuming the spectral types of stars 2 and 3 as B0 V and B1.5 V, respectively, the combined background spectrum is generated with standard *IUE* stars weighted according to the flux ratio deduced by Gilmozzi et al. (1987). This combined spectrum is scaled to the UV flux in the late-time SN 1987A spectra in the range 1300–1500 Å and is subtracted from all the *IUE* data as the background. Because they assume a hotter atmosphere for star 2 than others who have classified this star (B2 III in Walborn et al. 1993; B1 III in Scuderi et al. 1995), the SFdC93 subtraction routine underestimates the long wavelength flux from the background stars. The star 2 and 3 background flux determined by SFdC93 is about 11% lower than we find in the range 1600–1950 Å and about 25% lower in the range 1952–3200 Å. The measurement of the background flux is essential to the correct determination of the flux level from the supernova, especially during late epochs when the background is larger than the supernova flux ($t > 6$ days for SWP; $t > 800$ days for LWP). At day 1000, the UV flux attributed to SN 1987A by SFdC93 is larger than ours by a factor of ~15 in the SWP range (1250–1950 Å), and a factor of ~7 in LWP (2400–3200 Å).

2.3. *Reddening Correction*

Because SN 1987A is only ~20′ from the 30 Doradus nebula in the LMC, the supernova spectra have been corrected for interstellar extinction as derived for that region. Walker & Suntzeff (1990) have measured the reddening in the field of SN 1987A by studying the $U - B$ and $B - V$ colors of 23 early-type stars in the 30 Doradus region. The reddening for SN 1987A

was determined to be $E(B-V)_{\rm total} = 0.17 \pm 0.02$. Walborn et al. (1989) studied the existing spectroscopic data of the progenitor of the supernova, Sk −69°202, and deduced a total reddening toward SN 1987A of $E(B-V)_{\rm total} = 0.16$, with a galactic foreground reddening of $E(B-V)_{\rm galactic} \simeq 0.06$ and a LMC contribution of $E(B-V)_{\rm LMC} \simeq 0.10$. Gochermann, Goudfrooij, & Schmidt-Kaler (1989) have observed 41 galactic foreground stars in the direction of SN 1987A and deduced a galactic foreground reddening of $E(B-V)_{\rm galactic} = 0.08 \pm 0.01$, which is higher than the usually assumed values. We have adopted the reddening values of $E(B-V)_{\rm galactic} = 0.06$ and $E(B-V)_{\rm LMC} = 0.09$ for direct comparisons with the results obtained by the CTIO group (Hamuy et al. 1988). However, by modeling the UV stellar atmosphere of star 2, Scuderi et al. (1995) deduced a total reddening of $E(B-V)_{\rm total} = 0.19 \pm 0.01$, with ~10% galactic contribution, i.e., $E(B-V)_{\rm galactic} = 0.02$.

The choice of dereddening function is important in UV studies because the correction is large and is known to vary in shape from place to place. Fitzpatrick (1985) documented significant differences between the ultraviolet extinction curves of the Galaxy, the LMC generally, and the 30 Doradus region. The 30 Doradus extinction curve has a weaker 2175 Å "bump" and a steeper far-ultraviolet rise than either the galactic or average LMC extinction function. We used the 30 Doradus extinction function evaluated by Fitzpatrick (1986) and assumed the ratio of visual extinction over the color excess, $R_V = A_V/E(B-V)$, to be 3.1, the standard value for the diffuse interstellar medium. Fitzpatrick & Walborn (1990) verified that the average 30 Doradus extinction correction function was justified for Sk −69°203, a B0.7 Ia supergiant, located 2.2 north of SN 1987A, by studying its UV and optical colors and spectra. This improves our confidence that the average 30 Doradus extinction law is appropriate for the UV data of SN 1987A. For the galactic reddening component, the extinction function and the value of R_V, 3.2, formulated by Seaton (1979) are used.

3. UV SPECTROSCOPY OF SN 1987A

3.1. *UV Spectra*

We have processed the GSFC observations taken before 1991 June 9 (day 1568), and VILSPA data up to 1991 March 3 (day 1470). Some statistics of the low dispersion observations we obtained from both GSFC and VILSPA are presented in Table 1. Because of the large wavelength-dependent variations of sensitivities of both the SWP and LWP cameras (Harris & Sonneborn 1987), and the steep variations of flux with wavelength in the spectra, multiple exposures with different exposure times were often needed. We have combined them to ensure optimum coverage of a wavelength band with satisfactory signal-to-noise ratio. However, in order to preserve information on the time evolution of the supernova, only observations made within 5 hr were considered for combination. Thus many of the processed *IUE* spectra are combined from two or, less often, three observations. There were only two occasions when we combined more than three spectra.

TABLE 1

THE COMBINED STATISTICS OF THE *IUE* LOW-DISPERSION SN 1987A OBSERVATIONS OBTAINED AT GSFC AND VILSPA THROUGH 1992 JUNE

	Number of SWP Spectra	Number of LWP Spectra	Total *IUE* Spectra
Observation total	221	530	751
Background (> day 1300)	6	11	17
Raw data (< day 1300)	215	519	734
Combined data (day 1–1248)	124	166	290

The catalog of the SWP spectra taken between day 1301 and day 1568 which we used to create the background spectrum is given in Table 2A. The corresponding catalog for the LWP spectra is presented in Table 2B. The third column is the time of observation in days after core collapse of the supernova, 1987 February 23.316 (UT) (JD = 2,446,849.816), as determined at the IMB and Kamiokande II neutrino detectors (Bionta et al. 1987; Hirata et al. 1987). Complete lists of *IUE* observations of the SWP and LWP cameras on SN 1987A are given in Table 3A and 3B, respectively. The exposure time in the fourth column is corrected for the *IUE* exposure time quantization and the camera response time (Crenshaw 1988). These corrections are important for the early data where the time of exposure is short ($t_{\rm exp} < 15$ s). A total of 290 combined spectra are obtained from day 1 to day 1248. The *IUE* spectra at different epochs are presented in Figure 2, where the number to the right of a spectrum represents the number of days after outburst and the displayed spectrum is the average over the indicated time period. The vertical axis is the logarithm of observed flux and successive spectra are shifted vertically for clarity of display, except for the spectra taken in the first four days. The magnitude of shift, in dex, is shown in the parenthesis under the epoch of observation.

There had been five Type II supernovae (SNe II) observed by *IUE* before SN 1987A. However, only two, SN 1979C and SN 1980K, were bright enough for high-quality UV data to

TABLE 2

SPECTRA AVERAGED FOR BACKGROUND SUBTRACTION

IUE Image	Date (UT)	Day	$t_{\rm exp}$ (minutes)
Short-wavelength spectra (1150–1975 Å)			
SWP 39757	1990 Oct 4.02	1318.71	265
SWP 40002	1990 Oct 31.03	1345.72	270
SWP 40275	1990 Dec 5.85	1381.54	280
SWP 40858	1991 Feb 12.63	1450.32	280
SWP 41179	1991 Mar 25.68	1491.37	310
SWP 41802	1991 Jun 9.34	1567.03	290
Long-wavelength spectra (1975–3300 Å)			
LWP 18792	1990 Sep 15.57	1300.26	110
LWP 18933	1990 Oct 4.16	1318.85	120
LWP 19090	1990 Oct 31.17	1345.86	105
LWP 19356	1990 Dec 5.99	1381.68	120
LWP 19518	1991 Jan 7.42	1414.11	130
LWP 19743	1991 Feb 12.77	1450.46	120
LWP 19865	1991 Mar 3.21	1468.90	130
LWP 19985	1991 Mar 25.52	1491.21	140
LWP 20100	1991 Apr 7.95	1504.64	90
LWP 20102	1991 Apr 8.49	1505.18	140
LWP 20553	1991 Jun 9.48	1567.17	125

TABLE 3

IUE CAMERA OBSERVATIONS OF SN 1987A

IUE Image	Date (UT)	Day	t_{exp}
SWP camera (1150–1975 Å)			
SWP 30376	1987 Feb 24.87	1.55	10 s
SWP 30378	1987 Feb 24.98	1.67	8
SWP 30380	1987 Feb 25.16	1.84	10
SWP 30385	1987 Feb 25.44	2.12	10
SWP 30388	1987 Feb 25.86	2.54	10
SWP 30390	1987 Feb 25.95	2.63	18
SWP 30395	1987 Feb 26.23	2.92	20
SWP 30397	1987 Feb 26.43	3.11	30
SWP 30398	1987 Feb 26.51	3.19	30
SWP 30401, 30402	1987 Feb 26.84	3.53	1, 25 minutes
SWP 30407, 30408	1987 Feb 27.53	4.22	4.5, 90
SWP 30410, 30411	1987 Feb 27.95	4.63	10, 90
SWP 30414, 30415	1987 Mar 1.01	5.69	90, 40
SWP 30416, 30417	1987 Mar 1.28	5.97	40, 170
SWP 30421	1987 Mar 2.02	6.70	90
SWP 30422	1987 Mar 2.25	6.93	106
SWP 30427	1987 Mar 3.31	8.00	161
SWP 30428	1987 Mar 3.88	8.56	180
SWP 30429	1987 Mar 4.00	8.68	198
SWP 30433	1987 Mar 5.38	10.06	195
SWP 30472	1987 Mar 9.31	13.99	180
SWP 30512	1987 Mar 13.59	18.27	240
SWP 30522	1987 Mar 14.37	19.05	182
SWP 30547	1987 Mar 16.61	21.29	240
SWP 30551	1987 Mar 17.24	21.93	87
SWP 30592	1987 Mar 22.53	27.22	300
SWP 30637	1987 Mar 28.37	33.05	185
SWP 30743	1987 Apr 8.55	44.23	225
SWP 30841	1987 Apr 22.76	58.44	45
SWP 30871	1987 Apr 26.62	62.30	40
SWP 30882	1987 Apr 29.79	65.48	110
SWP 30907	1987 May 4.56	70.25	230
SWP 30929	1987 May 7.70	73.39	60
SWP 30932	1987 May 8.10	73.78	60
SWP 30974	1987 May 14.91	80.59	120
SWP 31000	1987 May 19.54	85.23	180
SWP 31040	1987 May 25.17	90.86	195
SWP 31064	1987 May 30.57	96.26	180
SWP 31125	1987 Jun 9.08	105.77	200
SWP 31132	1987 Jun 11.13	107.81	195
SWP 31154	1987 Jun 14.14	110.82	180
SWP 31166	1987 Jun 16.30	112.99	180
SWP 31177	1987 Jun 17.07	113.76	128
SWP 31273, 31274	1987 Jul 1.38	128.06	240, 140
SWP 31319, 31320	1987 Jul 11.99	138.68	240, 120
SWP 31334	1987 Jul 12.74	139.42	80
SWP 31371, 31372	1987 Jul 20.35	147.03	240, 105
SWP 31420, 31421	1987 Jul 29.06	154.75	240, 120
SWP 31462, 31463	1987 Aug 3.27	160.95	240, 85
SWP 31818, 31819	1987 Sep 10.12	198.81	90, 240
SWP 32030, 32031	1987 Oct 9.07	227.75	240, 90
SWP 32219, 32220	1987 Nov 3.02	252.70	240, 80
SWP 32395	1987 Nov 26.08	275.76	90
SWP 32619, 32620	1987 Dec 25.92	305.61	240, 80
SWP 32797, 32798	1988 Jan 27.83	338.51	210, 70
SWP 32879	1988 Feb 7.81	349.49	75
SWP 32910, 32911	1988 Feb 13.32	355.00	70, 212
SWP 32984	1988 Feb 25.66	367.34	60
SWP 33035, 33036	1988 Mar 4.68	375.37	240, 40
SWP 33104, 33105	1988 Mar 17.27	387.96	70, 240
SWP 33175, 33176	1988 Mar 29.66	400.34	210, 90
SWP 33279, 33280	1988 Apr 14.24	415.92	60, 200
SWP 33331, 33332	1988 Apr 21.59	423.28	240, 75
SWP 33423	1988 May 1.91	433.59	80
SWP 33492	1988 May 8.92	440.60	80
SWP 33496, 33497	1988 May 10.11	441.79	70, 240
SWP 33519, 33520	1988 May 13.49	445.18	240, 80

TABLE 3—*Continued*

IUE Image	Date (UT)	Day	t_{exp}
SWP 33644	1988 May 26.61	458.29	80
SWP 33725	1988 Jun 8.74	471.42	80
SWP 33741, 33742	1988 Jun 11.02	473.71	80, 235
SWP 33799, 33800	1988 Jun 22.40	485.09	240, 80
SWP 33832	1988 Jun 29.65	492.33	65
SWP 33868, 33869	1988 Jul 5.95	498.64	90, 195
SWP 33899	1988 Jul 12.55	505.24	80
SWP 33937, 33938	1988 Jul 18.32	511.00	240, 80
SWP 33966, 33967	1988 Jul 25.95	518.63	90, 251
SWP 34057, 34058	1988 Aug 9.24	532.93	240, 80
SWP 34087, 34088	1988 Aug 14.73	538.42	60, 200
SWP 34095	1988 Aug 17.34	541.02	110
SWP 34193	1988 Sep 7.26	561.95	120
SWP 34231, 34232	1988 Sep 12.77	567.46	80, 200
SWP 34316, 34317*	1988 Sep 26.19	580.87	120, 110
SWP 34441	1988 Oct 8.81	593.50	150
SWP 34477	1988 Oct 15.47	600.16	110
SWP 34670	1988 Nov 3.58	619.26	133
SWP 34701	1988 Nov 7.40	623.09	120
SWP 34751, 34752	1988 Nov 17.05	632.73	240, 42
SWP 34807	1988 Nov 24.40	640.09	135
SWP 34871	1988 Dec 4.98	650.66	163
SWP 35030	1988 Dec 16.00	660.68	110
SWP 35096	1988 Dec 22.32	668.01	130
SWP 35126	1988 Dec 24.97	670.66	180
SWP 35243	1989 Jan 4.05	680.74	90
SWP 35308	1989 Jan 10.87	687.55	220
SWP 35379	1989 Jan 19.06	695.75	140
SWP 35401	1989 Jan 24.53	701.21	160
SWP 35505	1989 Feb 7.59	715.28	220
SWP 35686	1989 Mar 5.61	741.29	240
SWP 35822	1989 Mar 20.39	756.07	183
SWP 35940	1989 Apr 5.50	772.18	260
SWP 36035	1989 Apr 19.31	785.99	166
SWP 36171	1989 Apr 30.47	797.16	210
SWP 36258	1989 May 14.21	810.89	222
SWP 36279	1989 May 17.47	814.15	260
SWP 36539	1989 Jun 17.34	845.03	260
SWP 36578	1989 Jun 26.09	854.78	310
SWP 36670	1989 Jul 13.39	871.07	200
SWP 36676	1989 Jul 14.26	871.95	260
SWP 36801	1989 Aug 6.18	894.87	260
SWP 36968	1989 Sep 9.85	929.54	270
SWP 37062	1989 Sep 17.80	937.49	230
SWP 37088	1989 Sep 20.12	939.80	300
SWP 37236	1989 Oct 2.78	952.46	263
SWP 37424	1989 Oct 22.00	971.69	230
SWP 37574	1989 Nov 12.95	993.63	300
SWP 37798	1989 Dec 11.87	1022.55	300
SWP 37973	1990 Jan 8.77	1050.46	285
SWP 38055	1990 Jan 20.45	1062.13	280
SWP 38172	1990 Feb 9.62	1082.30	285
SWP 38307	1990 Mar 5.61	1106.29	285
SWP 38336	1990 Mar 12.35	1113.04	275
SWP 38536	1990 Apr 6.52	1138.20	285
SWP 38555	1990 Apr 9.27	1140.96	270
SWP 38866	1990 May 25.44	1187.13	285
SWP 39300	1990 Jul 25.29	1247.97	285
LWP camera (1975–3300 Å)			
LWP 10189[a]	1987 Feb 24.88	1.56	1.9s
LWP 10191	1987 Feb 24.97	1.66	1.1s
LWP 10193, 10195, 10198	1987 Feb 25.28	1.96	1.1s, 3.6s, 1.1s
LWP 10199	1987 Feb 25.83	2.51	1.1s
LWP 10202, 10203, 10205	1987 Feb 26.26	2.95	1.1s, 13s, 2.7s
LWP 10207	1987 Feb 26.50	3.18	2.3s
LWP 10210, 10211	1987 Feb 26.83	3.52	2.7s, 90s
LWP 10218	1987 Feb 27.50	4.18	5.6s
LWP 10220, 10221, 10222	1987 Feb 27.84	4.53	3m, 7.7s, 4m

TABLE 3—*Continued*

IUE Image	Date (UT)	Day	t_{exp}
LWP 10227, 10228	1987 Feb 28.96	5.65	28s, 12m
LWP 10230, 10231	1987 Mar 1.27	5.95	1m 16s, 4m
LWP 10233, 10234	1987 Mar 1.37	6.06	6m 30s, 1m 16s
LWP 10241, 10242, 10243, 10244	1987 Mar 2.24	6.92	2m 20s, 2m 30s, 2m 30s, 4m
LWP 10248, 10249	1987 Mar 2.84	7.53	2m 50s, 10m
LWP 10251, 10252, 10253, 10254, 10255	1987 Mar 3.25	7.93	1m 25s, 2m, 90m, 2m 10s, 2m 30s
LWP 10259, 10260	1987 Mar 4.01	8.69	40m, 5m
LWP 10270, 10271, 10272	1987 Mar 4.91	9.60	6m, 15m, 60m
LWP 10287, 10288, 10289	1987 Mar 6.72	11.41	4m 20s, 120m, 18m
LWP 10300, 10301	1987 Mar 8.74	13.43	6m, 50m
LWP 10302, 10303, 10304	1987 Mar 9.33	14.02	7m, 6m, 100m
LWP 10318, 10319	1987 Mar 13.53	18.21	7m, 24m
LWP 10322, 10323, 10324	1987 Mar 14.26	18.94	15m, 7m, 90m
LWP 10344, 10345, 10346	1987 Mar 16.58	21.26	7m, 24m, 110m
LWP 10349, 10350	1987 Mar 17.18	21.86	6m 45s, 50m
LWP 10351, 10352	1987 Mar 17.30	21.99	6m 55s, 90m
LWP 10371, 10372	1987 Mar 19.84	24.52	7m, 24m
LWP 10388, 10389, 10390	1987 Mar 22.59	27.27	7m, 24m, 90m
LWP 10401, 10402	1987 Mar 23.85	28.53	7m, 24m
LWP 10441, 10442	1987 Mar 28.33	33.02	230m, 6m
LWP 10445, 10446	1987 Mar 28.97	33.66	6m, 20m
LWP 10518, 10519, 10520	1987 Apr 8.54	44.22	5m 30s, 20m, 115m
LWP 10587, 10588	1987 Apr 16.66	52.35	5m 30s, 120m
LWP 10647, 10648	1987 Apr 26.66	62.33	4m, 55m
LWP 10664, 10665	1987 Apr 29.80	65.48	3m 35s, 55m
LWP 10669, 10670	1987 Apr 30.73	66.42	3m 35s, 25m
LWP 10683, 10684	1987 May 2.84	68.53	3m, 25m
LWP 10692, 10693	1987 May 4.61	70.30	2m 45s, 22m
LWP 10706, 10707	1987 May 7.71	73.39	2m 30s, 20m
LWP 10711, 10712	1987 May 8.03	73.71	3m 30s, 90m
LWP 10723, 10724	1987 May 9.67	75.35	2m 30s, 20m
LWP 10755, 10756	1987 May 13.63	79.32	2m 20s, 17m
LWP 10765, 10766	1987 May 14.86	80.55	2m 20s, 20m
LWP 10788, 10789	1987 May 19.52	85.20	2m 20s, 20m
LWP 10811, 10812	1987 May 22.68	88.36	2m 20s, 20m
LWP 10826, 10828	1987 May 25.13	90.81	2m 30s, 60m
LWP 10833, 10834	1987 May 25.82	91.51	2m 20s, 15m
LWP 10873, 10874, 10875	1987 May 30.39	96.08	6m 30s, 39m, 120m
LWP 10888, 10889	1987 Jun 1.73	98.41	2m 35s, 15m
LWP 10909, 10910	1987 Jun 4.74	101.42	2m 40s, 13m
LWP 10939, 10940	1987 Jun 7.60	104.29	2m 40s, 13m
LWP 10960, 10961	1987 Jun 9.10	105.79	2m 30s, 60m
LWP 10970, 10971	1987 Jun 10.94	107.63	2m 50s, 17m
LWP 11080, 11081	1987 Jun 25.05	121.73	4m 10s, 110m
LWP 11086, 11087	1987 Jun 25.78	122.46	4m 5s, 20m
LWP 11130, 11131	1987 Jul 1.34	128.03	4m 10s, 20m
LWP 11182, 11183	1987 Jul 10.94	137.62	4m 20s, 25m
LWP 11201, 11202	1987 Jul 12.74	139.42	4m 20s, 20m
LWP 11225, 11226	1987 Jul 17.01	143.70	20m, 4m
LWP 11254, 11255	1987 Jul 20.27	146.96	3m 50s, 16m
LWP 11281, 11282	1987 Jul 26.95	153.63	4m 30s, 35m
LWP 11311, 11312	1987 Aug 3.14	160.83	3m 40s, 15m
LWP 11369, 11370	1987 Aug 10.84	168.53	4m 20s, 40m
LWP 11436, 11437	1987 Aug 20.04	177.73	3m 30s, 13m
LWP 11500, 11501, 11502	1987 Aug 27.74	185.43	3m 40s, 20m, 90m
LWP 11503, 11504	1987 Aug 27.96	185.64	3m 10s, 12m
LWP 11534, 11535	1987 Sep 1.17	188.86	3m 10s, 12m
LWP 11588, 11589	1987 Sep 10.05	198.74	3m 10s, 12m
LWP 11672, 11673	1987 Sep 20.74	209.42	3m, 20m
LWP 11824, 11825, 11826	1987 Oct 9.06	227.75	3m, 12m, 35m
LWP 11953, 11954	1987 Oct 26.15	244.83	3m, 12m
LWP 11997, 11998	1987 Nov 2.89	252.58	3m, 12m
LWP 12083, 12084	1987 Nov 13.68	263.37	2m 45s, 20m
LWP 12167, 12168	1987 Nov 25.98	275.66	2m 50s, 10m
LWP 12235, 12236	1987 Dec 6.18	285.87	3m, 12m
LWP 12294, 12295	1987 Dec 16.49	296.18	2m 30s, 10m
LWP 12372, 12373	1987 Dec 25.86	305.54	3m, 12m
LWP 12410, 12411	1988 Jan 2.03	312.71	3m, 12m
LWP 12486, 12487	1988 Jan 13.54	324.22	3m 30s, 12m
LWP 12525, 12526	1988 Jan 19.13	329.82	12m, 3m

TABLE 3—*Continued*

IUE Image	Date (UT)	Day	t_{exp}
LWP 12558, 12559	1988 Jan 24.17	334.85	3m, 12m
LWP 12576, 12577	1988 Jan 27.79	338.47	3m, 60m
LWP 12623, 12624	1988 Feb 7.79	349.48	3m, 12m
LWP 12656, 12657	1988 Feb 13.23	354.92	3m, 25m
LWP 12677, 12678	1988 Feb 17.03	358.72	3m, 12m
LWP 12734, 12735	1988 Feb 25.73	367.41	12m, 3m
LWP 12789, 12790	1988 Mar 3.21	373.89	3m, 12m
LWP 12869, 12870	1988 Mar 17.22	387.90	3m, 30m
LWP 12942, 12943, 12944	1988 Mar 29.68	400.36	3m, 12m, 30m
LWP 12991, 12992	1988 Apr 5.96	407.65	3m 30s, 12m
LWP 13041, 13042	1988 Apr 14.19	415.87	3m 30s, 22m
LWP 13087, 13088	1988 Apr 21.57	423.26	3m 30s, 12m
LWP 13153, 13154	1988 May 1.92	433.61	4m, 12m
LWP 13193, 13194, 13195	1988 May 10.06	441.74	4m, 30m, 20m
LWP 13217, 13218	1988 May 13.42	445.11	4m, 12m
LWP 13236, 13237	1988 May 15.88	447.57	4m, 12m
LWP 13310, 13311	1988 May 26.58	458.27	12m, 4m
LWP 13387, 13388	1988 Jun 8.74	471.42	4m, 12m
LWP 13402, 13403, 13404	1988 Jun 11.10	473.79	4m, 60m, 20m
LWP 13489, 13490	1988 Jun 22.34	485.02	4m, 12m
LWP 13528, 13529	1988 Jun 29.62	492.31	60m, 4m
LWP 13573, 13574, 13575	1988 Jul 5.96	498.64	4m 30s, 60m, 23m
LWP 13624, 13625	1988 Jul 12.55	505.24	4m, 15m
LWP 13684, 13685	1988 Jul 18.25	510.94	4m 30s, 13m
LWP 13741, 13742	1988 Jul 25.88	518.56	4m 30s, 40m
LWP 13743, 13744	1988 Jul 26.52	519.20	4m 30s, 13m
LWP 13787, 13788	1988 Aug 4.66	528.34	5m, 15m
LWP 13813, 13814	1988 Aug 8.18	532.86	5m, 15m
LWP 13846, 13847, 13848	1988 Aug 14.75	538.43	4m 30s, 30m, 55m
LWP 13866, 13867	1988 Aug 17.34	541.03	6m, 18m
LWP 13896, 13897, 13898	1988 Aug 22.54	546.22	6m, 18m, 60m
LWP 14007, 14008, 14009	1988 Sep 7.35	562.04	6m 30s, 18m, 80m
LWP 14038, 14039, 14040	1988 Sep 12.79	567.47	4m 30s, 25m, 45m
LWP 14126, 14127	1988 Sep 26.14	580.82	6m 30s, 18m
LWP 14190, 14191	1988 Oct 8.71	593.39	8m, 25m
LWP 14229, 14230	1988 Oct 15.45	600.13	7m 30s, 25m
LWP 14348, 14349	1988 Oct 31.08	615.76	12m, 60m
LWP 14476, 14477	1988 Nov 17.04	632.72	9m, 25m
LWP 14692	1988 Dec 22.26	667.94	12m
LWP 14766	1989 Jan 4.06	680.74	14m
LWP 14799	1989 Jan 10.69	687.37	15m 30s
LWP 14865	1989 Jan 19.00	695.69	16m
LWP 14909, 14910	1989 Jan 24.53	701.22	13m, 45m
LWP 14981, 14982	1989 Feb 7.71	715.40	19m, 80m
LWP 15059, 15060	1989 Feb 19.01	726.70	21m, 53m
LWP 15133, 15134	1989 Mar 5.73	741.42	27m, 65m
LWP 15191, 15192	1989 Mar 13.88	749.56	31m, 90m
LWP 15216, 15217	1989 Mar 18.89	754.58	32m, 80m
LWP 15225, 15226	1989 Mar 20.25	755.93	60m, 15m
LWP 15307, 15308	1989 Apr 5.63	772.32	35m, 35m
LWP 15375	1989 Apr 19.23	785.92	40m
LWP 15391, 15392	1989 Apr 22.79	789.48	42m, 115m
LWP 15414, 15415	1989 Apr 30.60	797.28	40m, 90m
LWP 15512	1989 May 14.10	810.79	40m
LWP 15530, 15531	1989 May 17.48	814.16	45m, 78m
LWP 15641	1989 Jun 2.62	830.30	50m
LWP 15741	1989 Jun 17.46	845.14	55m
LWP 15771, 15772	1989 Jun 22.80	850.48	55m, 95m
LWP 15796	1989 Jun 26.96	854.64	60m
LWP 15855, 15856	1989 Jul 5.82	863.41	55m, 75m
LWP 15914, 15915	1989 Jul 14.41	872.09	55m, 46m
LWP 16076	1989 Aug 6.30	894.99	70m
LWP 16185	1989 Aug 21.38	910.06	150m
LWP 16235	1989 Aug 28.52	917.21	80m
LWP 16295, 16296	1989 Sep 7.55	927.23	80m, 80m
LWP 16313	1989 Sep 9.72	929.41	90m
LWP 16372	1989 Sep 17.69	937.37	70m
LWP 16380	1989 Sep 20.26	939.94	85m
LWP 16466	1989 Oct 2.65	952.33	90m
LWP 16527	1989 Oct 10.44	960.12	95m

TABLE 3—*Continued*

IUE Image	Date (UT)	Day	t_{exp}
LWP 16600	1989 Oct 22.12	971.80	80m
LWP 16751	1989 Nov 6.22	986.90	110m
LWP 16780	1989 Nov 13.09	993.77	95m
LWP 16841	1989 Nov 26.39	1007.07	100m
LWP 16855	1989 Nov 28.54	1009.22	100m
LWP 16911	1989 Dec 12.01	1022.69	90m
LWP 17113	1990 Jan 8.91	1050.60	110m
LWP 17189	1990 Jan 20.58	1062.27	94m
LWP 17329	1990 Feb 9.76	1082.44	105m
LWP 17413	1990 Feb 23.65	1096.33	120m
LWP 17475	1990 Mar 5.75	1106.43	105m
LWP 17519	1990 Mar 12.22	1112.91	90m
LWP 17543	1990 Mar 17.07	1117.75	150m
LWP 17702	1990 Apr 6.66	1138.35	112m
LWP 17714	1990 Apr 9.13	1140.82	120m
LWP 17783	1990 Apr 21.99	1153.67	140m
LWP 17987	1990 May 25.58	1187.27	100m
LWP 18440	1990 Jul 25.42	1248.11	85m

[a] Spectrum saturated for 2650–3000 Å.

be taken for line identification and spectral evolution studies (Benvenuti et al. 1982). During the first two weeks of *IUE* observations, the UV spectra from both these supernovae showed a strong UV continuum below 1500 Å with an excess over blackbody radiation extrapolated from the optical spectra. Furthermore, strong emission lines of highly ionized species such as N V 1240, Si IV 1400, and N III] 1750 were observed blueward of ~2000 Å. Fransson et al. (1984) showed that the UV excess may originate from inverse Compton scattering by energetic, thermal electrons ($T \sim 10^9$ K) produced just behind the outward moving shock front where the supernova ejecta interacts with the preexisting circumstellar envelope. The radiation from this shock wave dominates the continuum below 1500 Å, while the Comptonized flux which scatters back to the interior is the dominant source of energy for the UV emission lines. These high-energy photons cause the ionization and excitation of the species in the outer layers of the supernova envelope, where the density is lower and the ionizing radiation flux is higher than in the inner envelope, producing narrow emission lines through fluorescence.

The UV spectra from SN 1987A showed marked contrasts with these two "classical" SNe II. A large UV flux was seen in the first *IUE* spectra obtained (day 1.6) with a high photospheric temperature of about 14,000 K. The broad P Cygni features of Mg II at ~2800 Å indicated high expansion velocities in the debris extending up to 40,000 km s^{-1}. The extra UV continuum below 1500 Å and the highly ionized UV emission lines blueward of 2000 Å are missing in the spectra of SN 1987A, suggesting less interaction of the supernova ejecta with the intermediate circumstellar environment than SN 1979C and SN 1980K. In the next few days, a huge drop in flux is seen at all UV wavelengths. In less than 3 days (day 4.6), radiation blueward of 1600 Å decreased by a factor of 3000. At the same time, the spectral features changed dramatically: instead of a continuum, the spectrum consisted of broad absorption bands caused by iron peak elements. The spectral shape is very similar to that of Type Ia supernovae (SNe Ia), such as SN 1980N, and SN 1981B (Panagia & Gilmozzi 1991). Ultraviolet spectra were obtained for SN 1992A, another SN Ia, by both *IUE* (~2000–3300 Å) and the Faint Object Spectrograph (FOS) on *HST* (~1800–4800 Å) (Kirshner et al. 1993). The *HST* UV spectrum of SN 1992A taken 5 days past optical maximum is strikingly similar to that of SN 1987A observed at day 3.5 in the range 1800–3200 Å (Jeffery et al. 1994, Fig. 3), with both spectra showing broad absorptions at around 1930, 2180, 2380, 2600, and 3050 Å. In contrast, the UV spectrum for SN 1993J, a SN IIb, taken by FOS of *HST* about 18 days after the explosion does not show any obvious broad absorptions (Jeffery et al. 1994), and instead resembles SN 1979C and SN 1980K. Earlier UV spectra of SN 1993J taken with *IUE* also lack obvious broad absorptions and show only a strong UV continuum (Wamsteker et al. 1993; Sonneborn et al. 1993). These observations led Jeffery et al. (1994) to suggest that the interaction of the supernova ejecta with the circumstellar matter surrounding the progenitor is the source of differences in the UV behavior of supernovae. A smooth UV spectrum lacking in broadband absorptions caused by iron group elements is characteristic of supernovae which interacted with thick circumstellar envelopes. In the case of SN 1987A, the circumstellar material is present in the form of a ring, located 200 light-days from the supernova (Jakobsen et al. 1991; Plait et al. 1995), with little material in the immediate neighborhood. The ejecta of SN 1987A had relatively little interaction with the circumstellar matter compared to SN 1993J, SN 1980K, or SN 1979C. This may explain why the UV spectrum of SN 1987A resembles SNe Ia more than other SNe II.

The UV opacity is primarily that of line opacity. There are many strong and closely spaced resonance lines in the UV region, especially from the neutral or singly ionized iron group elements, such as Fe, Ni, and Ti. Assuming LTE, Branch (1987) computed the Sobolev line strengths of optical, infrared, and ultraviolet spectral lines at the photosphere of SN 1987A. Concerning the earliest phase of development, the only calculated the optical depths of lines for temperatures above 6000 K. He showed that the UV lines are stronger than the optical/IR lines, and the line strengths increase with decreasing temperature. Fransson (1994) obtained similar results and showed that even the low abundance elements in the envelope

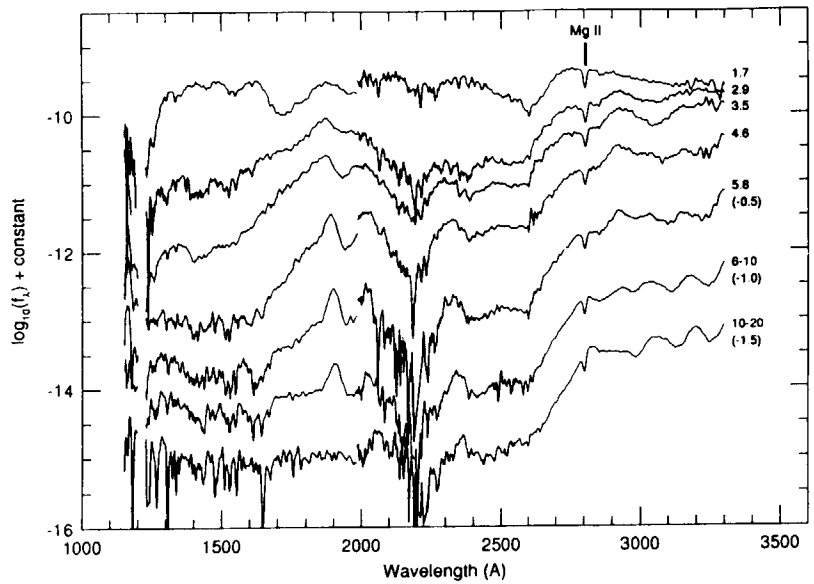

FIG. 2*a*

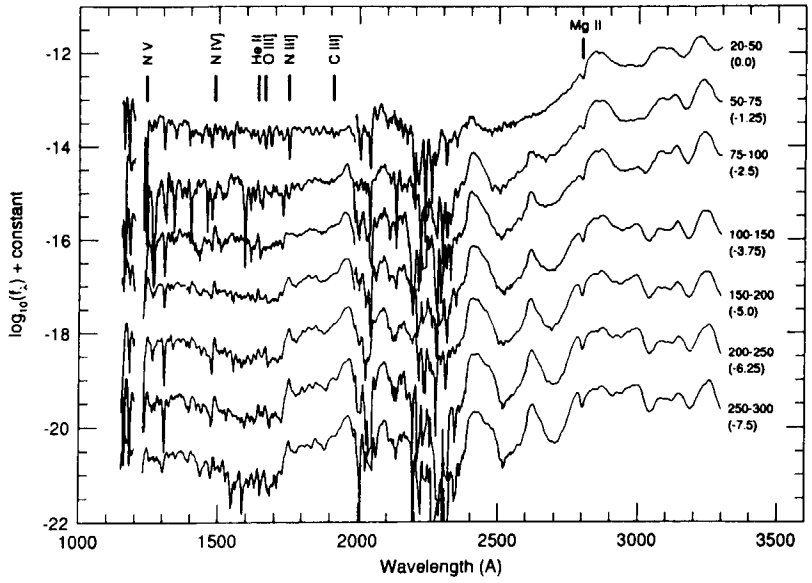

FIG. 2*b*

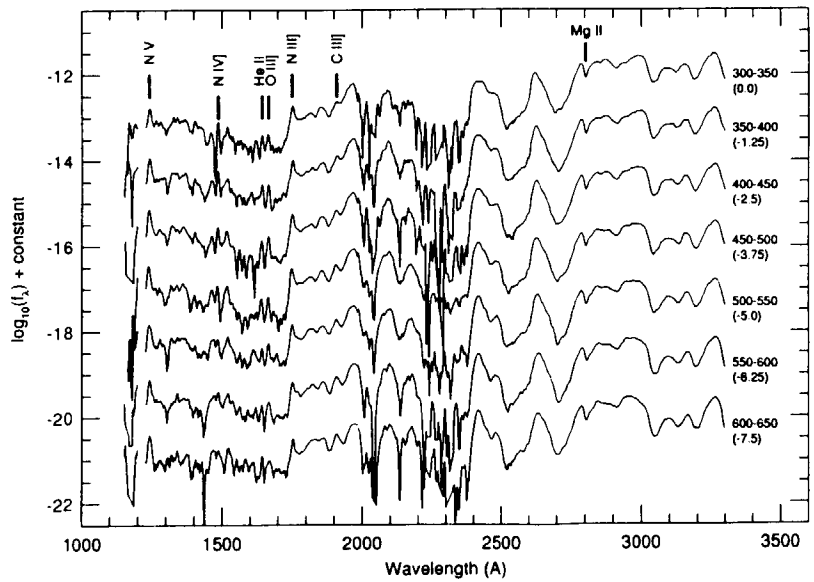

FIG. 2*c*

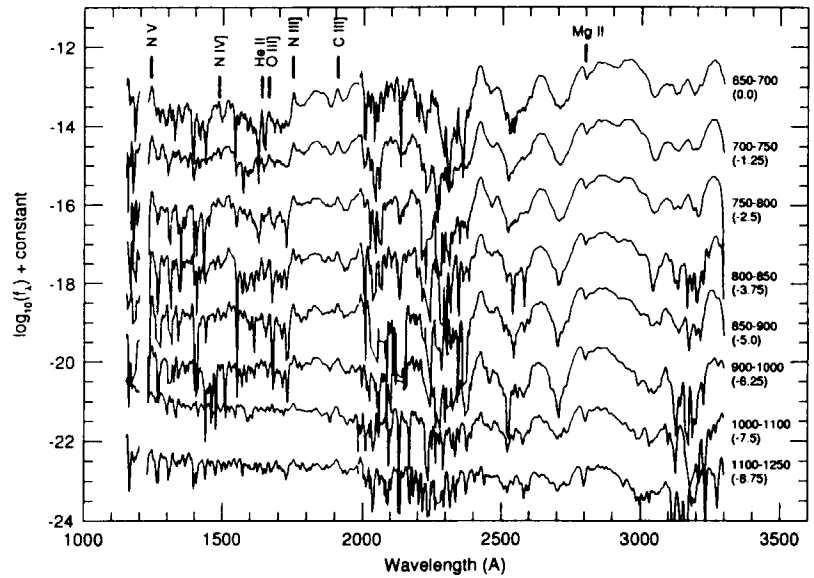

FIG. 2*d*

FIG. 2.—(*a*)-(*d*) Spectral evolution of SN 1987A in the wavelength range 1150–3300 Å. The spectra are corrected for interstellar reddening with $E(B-V)_{\text{galactic}} = 0.06$ and $E(B-V)_{\text{LMC}} = 0.09$. The number to the right of each spectrum represents the number of days after outburst and the displayed spectrum is the average over the indicated time period. Spectra shown are shifted vertically by the amount (in dex) as denoted in the bracket. However, the spectra taken in the first four days are not shifted because the huge flux decrease during that epoch provides sufficient spacing between successive spectra. The interstellar Mg II absorption line can be seen in all spectra. The emission lines N V 1240, N IV] 1486, He II 1640, O III] 1664, N III] 1750, and C III] 1909 are observed in the spectra taken after ~ day 90. These lines are in fact much narrower (FWHM $\lesssim 30$ km s^{-1}) than the widths in the low dispersion spectra.

and in the core have very large optical depths in the UV. In an atmosphere with a velocity range of 2000–20,000 km s^{-1}, typical of supernova expansion, each line occupies a wavelength band much greater than in a static atmosphere. The UV photons will be scattered from line to line by the gas in the core and envelope, while being redshifted each time. Some photons will stop resonance scattering and finally escape from the envelope by finding a wavelength "window" where the scattering lines are neither numerous nor thick enough to scatter the photons (Fransson 1994; Xu & McCray 1991), while some other photons may be destroyed by photoionization, the photoionization of the hydrogen atoms in the Balmer continuum (Xu & McCray 1991; Xu et al. 1992). The effective opacity of such an expanding atmosphere, the expansion opacity, has the net effect of line blanketing, that is, producing a quasi-continuum formed by many overlapping lines (Karp et al. 1977). In the UV region where there are a great number of densely spaced resonance lines, the line opacity is spread out in the observer frame frequency, thus enhancing the flux reduction. Wagoner, Perez, & Vasu (1991) studied the expansion opacity of a hydrogen-rich atmosphere similar to that of the outer layers of a SN II. Despite the fact that SN 1987A has a much smaller hydrogen envelope than other SNe II, we expect the model atmosphere calculations by Wagoner et al. (1991) will also be valid for the SN 1987A atmosphere because hydrogen is not the dominant source of opacity in the optical/UV region. They predict a substantial flux deficiency in the UV and that the UV flux deficiency increases with decreasing temperature. The expansion opacities in the wavelength region 1000–4000 Å increase by a factor of more than 100 as the temperature of the atmosphere drops from 12,000 to 5000 K, while the expansion opacities of the optical and IR region are not affected much by the drop in temperature. This suggests qualitatively why the UV spectrum remains opaque long after the optical spectrum has become optically thin. Thus at early times, if the temperature is high enough, we should observe no UV flux deficiency from line blanketing. For the late-time SN 1987A atmosphere, most of the lines depart significantly from LTE and the opacity calculations become very model-dependent.

The development of the UV spectra of SN 1987A in the earliest phases can be explained by the decrease in temperature of the ejecta and the increasing effects of line blanketing (Cassatella et al. 1987; Fransson et al. 1987; Kirshner et al. 1987b; Lucy 1987). At day 1.7 (Fig. 2), we were observing the cooling tail of a much hotter photosphere heated by the interaction of the explosion shockwave with the stellar surface. Hydrodynamical models of the shock breakout in SN 1987A by Ensman & Burrows (1992) showed that the UV burst occurred about 2 hr after the core collapse of the progenitor. In these models, the luminosity rises more than five orders of magnitude over an interval of a few hundred seconds and the effective temperature of the emitted radiation reaches about 5×10^4 K. And the observed UV spectrum showed a continuum with broad features. After the first *IUE* observation, the temperature of the supernova declined rapidly as the supernova atmosphere expanded and cooled. The net effect in the UV of the hundreds of blended iron group lines is that the UV continuum below 2600 Å disappeared below detection by about 3 days after outburst. Even the lines strong enough to give rise to P Cygni profiles were modulated by line blending due to the weak lines. The observed peaks in the spectra were the consequences of minima, or "windows," in selective opacity. The synthetic UV spectrum computed by Lucy (1987) confirmed that the trough observed in the *IUE* spectrum at day 3 in the region 2200–2600 Å is caused by the blending of more than 150 closely spaced lines of Fe II and Fe III. These lines would be individually strong enough to be observable if not blended together by differential expansion. This same process is responsible for the spectral and bolometric evolution of classical novae (Hauschildt et al. 1994).

After the dramatic changes in the early days in both the flux level and the spectral shape, the UV spectra showed only minor and slow variations at epochs after ~ day 150. We know that falling temperature in the early SN 1987A atmosphere due to expansion will lead to increased UV opacity. However, since the UV region is formed by lines with very large opacities, the spectral shape did not respond to the changes in opacity as quickly as it would if the opacity were lower (Jeffery & Branch 1990). This explains the slow evolution of the UV spectrum of SN 1987A after the initial phase. While the optical spectra obviously became nebular (optically thin) by ~ day 200, the UV spectra have remained photospheric (optically thick) due to the heavy line blanketing effects during the whole epoch of *IUE* observations.

McCray, Shull, & Sutherland (1987) predicted that after the initial drop in flux, there should be an "ultraviolet renaissance" in the UV region for SN 1987A. They suggested that as the supernova envelope expanded and became thin, the inner debris of the explosion would be revealed, releasing high-energy radiation originating from a hot photosphere caused by either the decay of radionucleides or a newly born pulsar. Fast electrons would be produced by Compton scattering of these high-energy photons, and the direct excitation of H, He, and heavy elements in the expanding debris by these electrons would produce radiation in UV and X-ray. The UV photons will be trapped by the substantial expansion opacity and come out as a quasi-continuum (Karp et al. 1977). They predicted a substantial UV continuum emerging from the supernova envelope about a few months after the explosion, and the UV spectrum to break up into an emission-line spectrum about one year later. This effect is similar to the one seen in classical novae where an increasing UV flux is observed as soon as the shell becomes transparent and the hot nova remnant ionizes the ejecta (Williams 1991; Saizar et al. 1992). However, this resurgence of UV radiation was not observed by either *IUE* or *HST*. One explanation is that the newly formed dust molecules in the supernova ejecta may have large ultraviolet opacity to absorb the UV radiation and re-radiate this luminosity in the IR continuum, as observed in some classical novae (Gehrz 1988). However, this is probably not applicable for SN 1987A. As we will see in § 5.2, instead we observe a *rise* in the UV flux relative to the bolometric luminosity, even after the epoch of dust formation. The failed prediction of a UV renaissance probably lies in the fact that the UV radiation originates from the Doppler blanketing of emission lines from mostly iron group elements and not from the scattering from high-energy photons.

3.2. *Time Evolution*

The three-dimensional plots shown in Figure 3 (SWP) and Figure 4 (LWP) illustrate vividly the time evolution of the SN

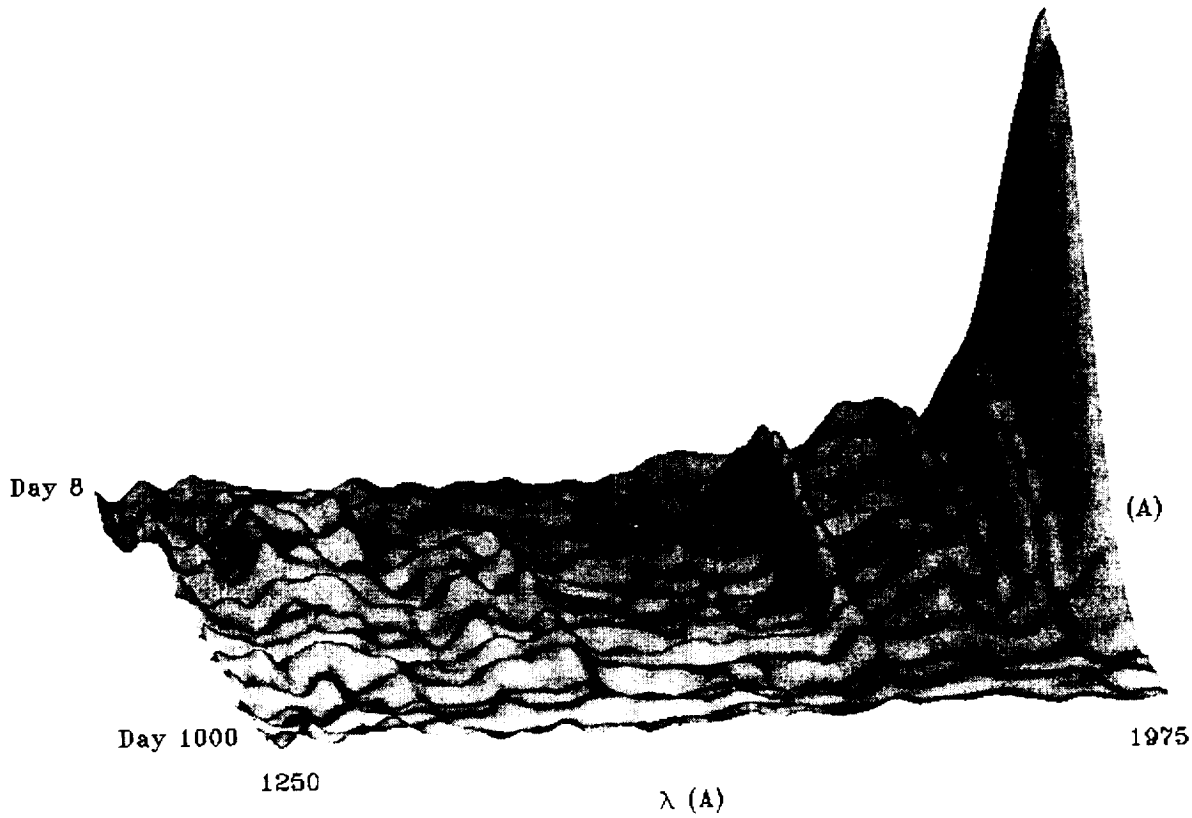

FIG. 3.—Three-dimensional plot of *IUE* SWP spectra (1250–1975 Å) of SN 1987A in time. The combined spectrum is binned at 4 Å in wavelength scale and 5 days in timescale. The plot is smoothed (boxcar = 5) in both the time and wavelength axes. The time evolution of broad band emission feature A (1980 Å) is shown.

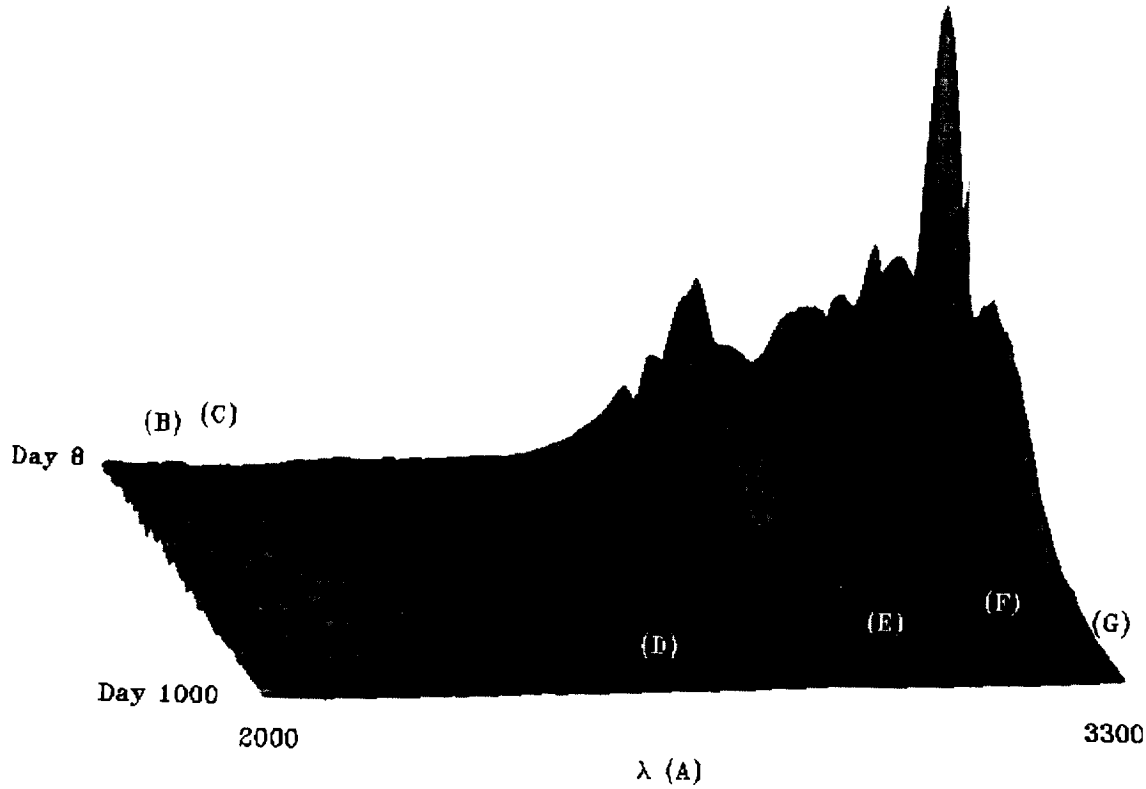

FIG. 4.—Three-dimensional plot of *IUE* LWP spectra (2000–3300 Å) of SN 1987A in time. The combined spectrum is binned at 6 Å in wavelength scale and 5 days in timescale. The plot is smoothed the same way as in Fig. 3. Notice that the flux scale is larger than that of Fig. 3 by a factor of 10. The time evolution of broad-band emission features B (2100 Å), C (2200 Å), D (2650 Å), E (3000 Å), F (3100 Å), and G (3247 Å) are shown.

1987A UV spectrum. In both figures, spectra taken before day 8 are excluded. The vertical scales of the two figures are different, with that of Figure 4 larger by a factor of 10. The change of the shape, magnitude, and strength of various spectral features can be studied despite the slow rate of evolution. Similar display of the time evolution of the SN 1987A spectrum is presented in Hanuschik & Thimm (1990) on the evolution of the fine spectroscopic structures of the spectral lines obtained at the Bochum telescope. Different time behaviors for different spectral features are demonstrated in Figure 5. The evolution of the SN 1987A spectrum in the range 2550–3300 Å, where most of the UV spectral features are located, is plotted. Evolution of the strength of individual features can be studied and compared. For example, the evolution of the strengths of the two emission features at 3000 Å (feature E in Figs. 4 and 5) and 3247 Å (feature G) are similar from around day 150 to day 800, but the maximum in flux for the 3247 Å feature at around day 85 is not observed in the 3000 Å feature. Thus it seems that the maximum observed at day 85 for the 3247 Å feature probably originates from a different ion, or from a different layer in the photosphere.

Since the UV spectrum consists of broad features formed by the blending of many weaker lines of similar wavelengths, it is a difficult task to identify the individual lines. Cassatella et al. (1987) identified the features between 2800 and 2950 Å during the first 30 days of observation as contributions from the Fe II multiplets. Also, the observed absorption blends near 3270, 3160, and 3015 Å are identified as the resonance lines of Ti II. Lyubimkov (1990) studied the spectra from the Soviet *ASTRON* satellite (to be discussed in § 4.1) and also concluded that these absorption blends result from strong Ti II multiplets such as λ3372 (No. 1 in the Martin, Fuhr, & Wiese 1988 list of Ti II multiplets), λ3331 (No. 7), λ3238 (No. 2), and λ3080 (No. 5). However, most other features seen in the UV spectrum of SN 1987A cannot be identified with a given line or multiplet of any particular species. Despite the lack of specific identification of many features in the spectra, two trends of their evolutions can be deduced: first, the absorption lines become narrower in time, the flux minima around 2500, 2700, and 3200 Å; and second, the emission maxima shift towards longer wavelengths, the flux maxima around 2650, 3000, 3100, and 3247 Å. Similar trends were also observed in the optical spectra (Catchpole et al. 1987; Phillips et al. 1988, 1990). There are many factors affecting the radiative transfer in the late-time supernova envelope—changes in temperature and non-LTE conditions, energy of gamma ray photons from radioactive nuclei, and dust formation, for example. However, the essential effect is probably the declining density as the inverse third power of time ($\rho \sim t^{-3}$) as the debris expands. Similar to other P Cygni absorptions, this expansion will cause the photosphere (above which the lines are formed) and the regions of large line opacity (the line-forming region) to recede to the inner, denser, more slowly expanding regions of the ejecta. The emission maxima will be shifted to longer wavelengths because their red sides are absorbed by strong lines which become narrower in time.

In order to study the redshift of the features with time, we have determined the peak wavelengths of six spectral features: 1980 (feature A in Fig. 3), 2100 (feature B in Figs. 4 and 5), 2200 (feature C), 2650 (feature D), 3100 (feature F), and 3247 Å (feature G). These features were chosen because their maxima are easily identifiable. A tenth-order polynomial was fitted to the part of the spectrum where the feature is located, and then we determined the wavelength maximum of the fitted

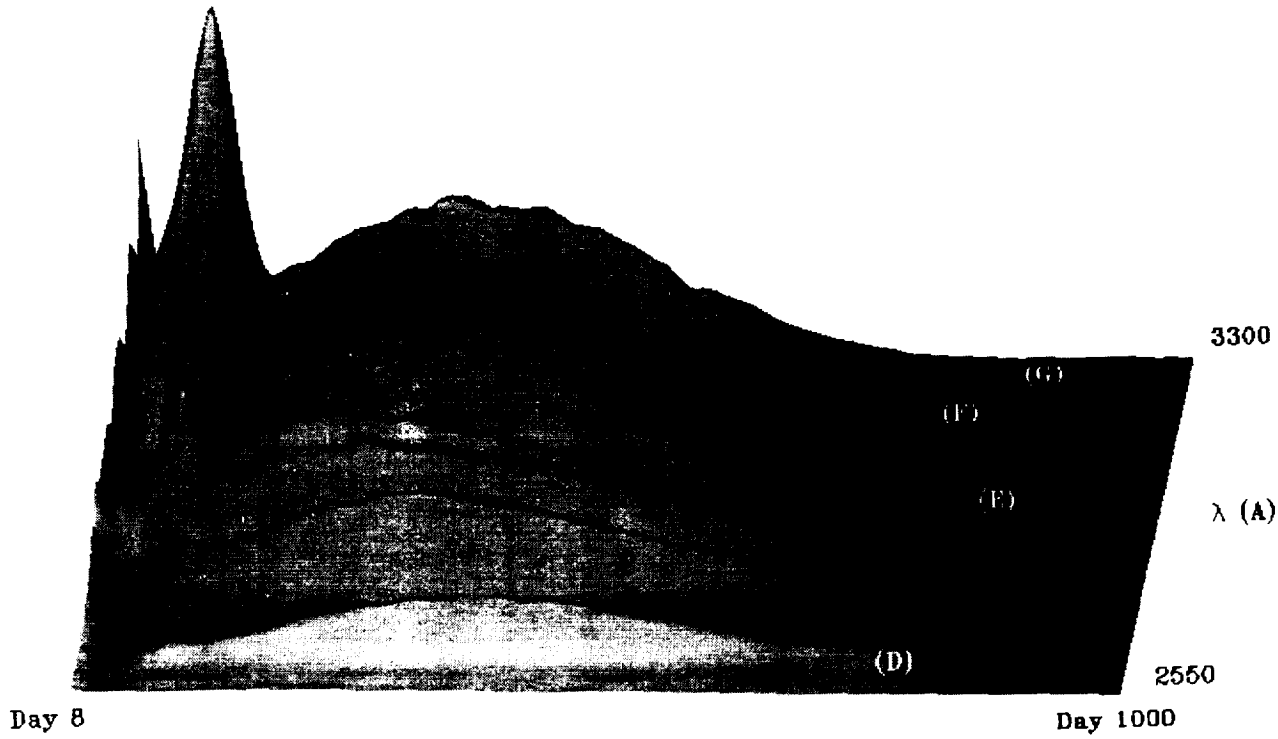

FIG. 5.—Same as Fig. 4 for the wavelength range 2550–3300 Å is shown for clearer display of the time evolution of the emission features D–G

polynomial. The evolutions of the peak wavelength for the six features are shown in Figure 6. There are fewer data points for the 2100 and 2200 Å features because we only included the spectra with good signal-to-noise in that wavelength region. The accuracy of the measurement is not significantly hampered by the resolution of the spectra because the supernova features remained quite broad. We found that except for the 3247 Å feature, the redshifting of the features from about day 120 to day 800 appears linear with time. Second, for the 3100 and 3247 Å features, additional phases of rapid redshifting are observed before day 120. At the same time, both these features showed a flux maximum around day 85, which were not seen for the 2100, 2200, and 2650 Å features (Fig. 4). We conclude that the UV radiation of these features from the two epochs (between day 10–120, and day 120–800) probably originated from species in different regions of the supernova atmosphere which have different velocities. The 1980 Å feature did not have maximum magnitude at day 85, yet there seems to be a rapid redshifting component from day 1 to day 10. However, we suspect that the two branches of the peak wavelength evolution are the results of two unrelated blends, instead of the same species, because the feature is not observed between day 10 and 55.

The precise radial velocities of these features cannot be determined without knowing the correct rest wavelengths. However, arbitrarily choosing an intermediate observed value as the rest wavelength introduces less than a 1% error in the rate of change of radial velocity. Velocity increases of 3.74, 4.09, 3.95, 3.85, and 4.38 km s^{-1} day^{-1} are determined from linear fits to the emission maxima of the 1980, 2100, 2200, 2650, and 3100 Å features respectively from day 120 to 800. The average rate of velocity increase is found to be 4.00 km s^{-1} day^{-1}. This result is surprisingly similar to the results obtained by fitting comparable data of the Hα P Cygni absorption minimum from day 120 to day 526. A straight line through the optical velocities of the Cerro Tololo Inter-American Observatory (CTIO) data shows that the rate of radial velocity change is 4.23 km s^{-1} day^{-1} (Phillips et al. 1988, 1990).

Further comparisons with optical results are provided by the development of the 3247 Å feature. Employing 3247 Å as the rest wavelength and assuming a radial velocity for the progenitor of +286 km s^{-1} (Wampler, Richichi, & Baade 1989), the variation of radial velocity with time can be determined. The radial velocity evolution of the 3247 Å feature is compared to that of the Fe II 5018 absorption, and the results are presented in Figure 7. The two sets of data agree extremely well starting from the first day of the detection of the 3247 Å feature at day 6.0. The agreement continued until day 45, after which they started to differ. The result suggests that the species contributing to the 3247 Å emission blend had the same velocity as Fe II from day 6 to day 45, implying that they originated from the same layer in the ejecta. There is also the possibility that the 3247 Å blend in fact has a Fe II origin from day 6 to day 45, while other components in the blend, possibly Ti II (Lyubimkov 1990), dominated afterward.

3.3. *Combined Optical-UV Spectra*

To better understand the evolution of SN 1987A, the ultraviolet *IUE* observations have been combined with the optical spectra taken at CTIO. From day 1 to day 130, the optical spectra covered the wavelength range 3700–7100 Å at a FWHM resolution of 5 Å (Phillips et al. 1988). From day 198 up to day 805, observations with wider wavelength coverage (3200–11,000 Å) but lower resolution (11–16 Å) were obtained (Phillips et al. 1990). An observation on day 1050 obtained at slightly higher resolution (10 Å FWHM) at the CTIO 4 m telescope is also included (Suntzeff et al. 1991). The optical spectra are combined with *IUE* data taken within 0.4 days before day 200, and within 2 days after day 200, when there are fewer optical and UV spectra available. The 32 UV + optical combined spectra are shown in Figure 8. Note that all the CTIO optical spectra taken prior to day 805 contained contamination from the field stars near SN 1987A, namely stars 2 and 3. As the supernova faded, the percentage of contamination from these field stars increased. The corrections for contamination are significant for spectra obtained after about day 600. For example, at day 600 about 35% of the flux at *U* and 17% at *I* comes from the field stars (Phillips et al. 1990). Spectrophotometry was obtained later for both star 2 and star 3 (Suntzeff et al. 1991; Walborn et al. 1993). However, in Figure 8, only the day 1050 spectrum has these two stars removed, where almost 70% of observed *U*-band flux is from stars 2 and 3. The optical spectra are corrected for interstellar extinction with the average extinction law of Cardelli, Clayton, & Mathis (1989). To be consistent with the correction of *IUE* data, we use $E(B-V)_{\rm total}$ of 0.15 and R_V of 3.1. Since the UV flux decreased at an enormous rate in the first few days of observation, a small time difference can lead to a big difference in observed flux. For example, in the earliest spectrum (day 1.7), the UV spectrum was collected 0.2 day earlier than the CTIO one. During the time the rate of change of UV flux in the near UV region of 3000–3300 Å is $\Delta F_\lambda/\Delta t \sim -0.1$ dex/day. Thus the UV flux level should be lowered by $\sim$0.02 dex for comparison with the optical data. However, this effect is only significant in the very early days of observations (before $\sim$ day 6) when the UV flux was plummeting, with $\Delta F_\lambda/\Delta t$ as large as ~ -0.6 dex/day in the overlap region (as discussed further in § 5).

In Figure 9, λf_λ is plotted with λ (1150–11,000 Å) for the combined UV + optical spectra taken at selected dates to illustrate the energy budget in the UV and optical regions for SN 1987A. On the first day of observation at day 1.7, the energy output of the supernova is more or less evenly distributed from about 1300 Å to the red end of the optical spectrum. (The steep drop blueward of 1300 Å is not an instrumental artifact.) The radiation energy in the UV range 1250–3300 Å, $E_{\rm UV}$, is 38% of that in the optical + UV range 1250–7150 Å, $E_{\rm UV+optical}$. This is compared to the value of 35% if the energy were evenly distributed in all wavelengths. Within the next few days, the distribution of the radiation energy changed swiftly. By day 4.6, most of the energy radiated from the supernova is from the optical regime and the value of $E_{\rm UV}/E_{\rm UV+optical}$ dropped to 2.4%. The UV flux level continued to decrease while the optical flux was increasing, releasing the hydrogen recombination energy. At day 44, the energy level coming out from the optical region is about 10^4 times of that in the UV and the ratio $E_{\rm UV}/E_{\rm UV+optical}$ dropped to 0.05%. After reaching the maximum at day 85, the optical flux started to decay linearly, while the UV remained steady (§ 5.2, Fig. 16). At day 198, the optical flux

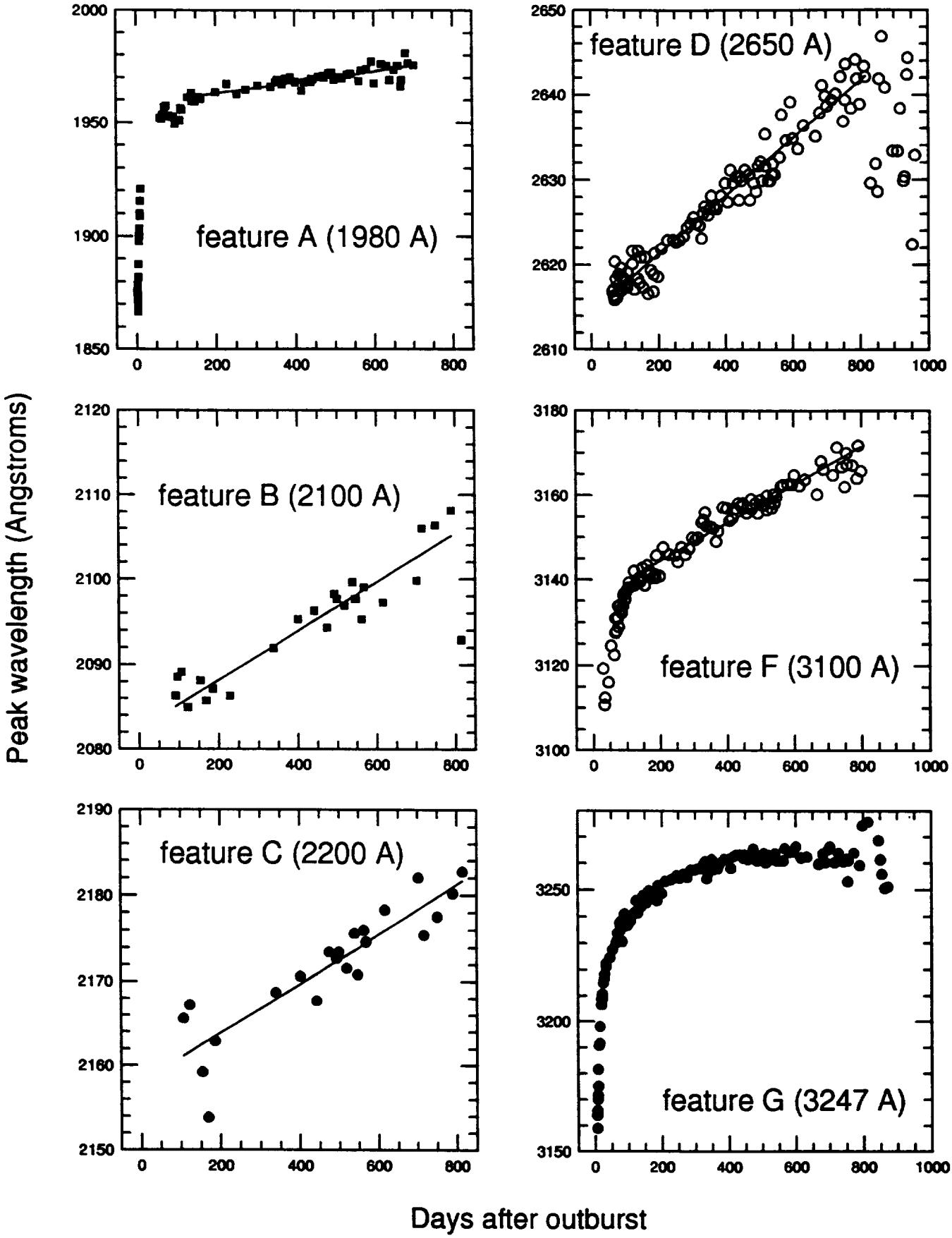

FIG. 6.—Time evolution of the measured peak wavelength for the broad band emission features A, B, C, D, F, and G. The linear fits to the features (except G) from day 120 to 800 also shown.

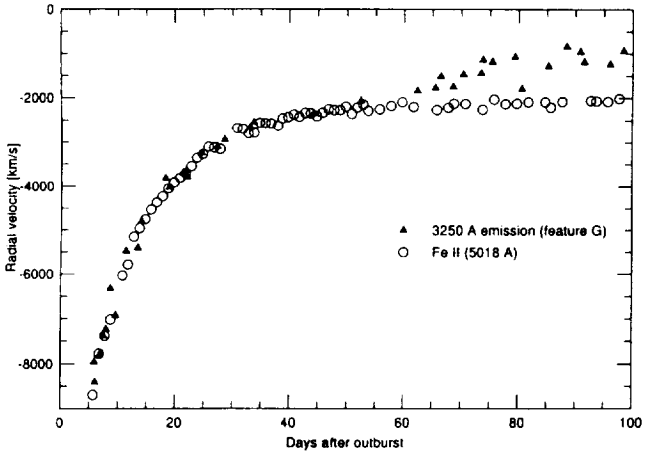

FIG. 7.—Comparison of the measured radial velocity of feature G (3247 Å) with that of the Fe II 5018 absorption line measured at CTIO (Phillips et al. 1988). The radial velocity of the progenitor is assumed to be +286 km s^{-1}.

was lower that seen on day 44. But at the same time, the UV flux was *higher* than that of the level at day 44. Therefore, while the energy emitted at optical and UV wavelengths differed by about one order of magnitude at day 423 ($E_{UV}/E_{UV+optical} \simeq 2\%$), they are nearly at the same level at day 715 ($E_{UV}/E_{UV+optical} \simeq 14\%$). As the supernova aged, relatively more energy of SN 1987A comes from the ultraviolet region compared to the optical.

4. COMPARISONS TO OTHER ULTRAVIOLET OBSERVATIONS

4.1. *ASTRON Satellite*

The UV spectra from *IUE* are compared with the results from the Soviet *ASTRON* satellite. The "Astrophysical Station *ASTRON*" was launched on 1983 March 23, and it continued to function until mid-1988. The detailed characteristics of the satellite were described by Boyarchuk et al. (1986). It consisted of two instruments, one of which is a f/10 Ritchey-Chretien ultraviolet telescope. The detector consists of a three-channel photoelectric scanning spectrometer covering the spectral regions 1050–3500 Å.

Fifteen ultraviolet spectra were taken with *ASTRON* on SN 1987A covering the spectral range 2600–3500 Å from day 9 to day 394 (Boyarchuk et al. 1987; Lyubimkov 1990). With the supernova observed through an entry aperture 1′ in diameter at a resolution of 28 Å, the *ASTRON* spectra should contain flux from star 2 and star 3 in the field of SN 1987A. However, in the spectral region where *IUE* and *ASTRON* overlap (2800–3300 Å, low signal-to-noise for the 2600–2800 Å data), the flux level of the background stars, 4.4×10^{-14} ergs cm^{-2} s^{-1} $Å^{-1}$, is less than 4% of the flux of the supernova during the *ASTRON* observation epochs. Thus the background stars did not have significant flux contribution to the *ASTRON* spectra. These spectra and the corresponding *IUE* data as observed (before reddening corrections) at similar epochs are presented in Figure 10. Each successive *ASTRON* spectrum has been shifted down 0.2 dex relative to the preceding one to avoid overlaps. All *IUE* spectra displayed in Figure 10 are smoothed to the resolution of the *ASTRON* observations. Each successive *IUE* spectrum is also shifted down by 0.2 dex, except for day 120.5, which is downshifted 0.4 dex relative to the preceeding spectrum. The two sets of observations generally agree well on the spectral shapes and the relative strengths of the spectral features in the overlapping region. However, the absolute flux measured for these features were systematically different, with the *IUE* results higher by ~0.02–0.1 dex. The difference probably results from the different UV calibration techniques for the two satellites.

4.2. *VBLUW Photometry*

The *IUE* results can also be compared with the ground-based *VBLUW* Walraven photometry. Walraven photometry for SN 1987A was measured at the 91 cm Dutch Telescope of the European Southern Observatory (ESO) at La Silla, Chile. The *W*-band of the system, with effective wavelength of 3236 Å and FWHM bandwidth of 157 Å, provides a useful comparison to the near-ultraviolet results of *IUE*. Photometry results from day 1 to day 393 (1988 March 22) were obtained, and some of the early results have been discussed by Cristiani et al. (1987) and Pel et al. (1987). The *IUE* spectra, not corrected for reddening, are convolved with the transmission function of the *W*-band as provided by J. W. Pel. The *W*-band photometry can thus be directly compared with the mean flux density $F_\lambda(P)$, which is given by the expression

$$F_\lambda(P) = \frac{\int_0^\infty P(\lambda) f_\lambda(\lambda) \lambda d\lambda}{\int_0^\infty P(\lambda) \lambda d\lambda}, \qquad (1)$$

where $P(\lambda)$ is the filter passband and $f_\lambda(\lambda)$ is the spectroscopic flux (Horne 1988). Equal weight is given to equal photon number rather than equal photon energy in equation (1). In Figure 11, both the *IUE* synthesized mean flux results and the *W*-band photometry data are presented. This provides a convenient link between ground-based photometry and the *IUE* data. The accuracy of the *W*-band photometric data on SN 1987A is about 0.005 dex (Pel et al. 1987). The two sets of data agree extremely well—the rms difference between the two data sets is 0.02 dex. We conclude that the absolute calibration of the LWP spectra at ~3200 Å is correct within an error of ≲5% and the calibration procedures used by the *ASTRON* generate results in which the mean flux appears lower by ~15%.

5. THE UV LIGHT CURVE OF SN 1987A

5.1. *UV Photometry*

The *IUE* spectra have been integrated over a limited number of broad-wavelength intervals so that time variations of the observed flux can be studied. The detection range of the LWP is divided into three wide bands: short, S: 1975–2500 Å; middle, M: 2500–3000 Å; long, L: 3000–3300 Å (not to be confused with the infrared *M* and *L* bands). The flux collected from the SWP camera (1150–1975 Å) is also integrated. We did not correct the SWP photometry for the circumstellar lines because of their small contribution to the total flux (<2%). The wave-

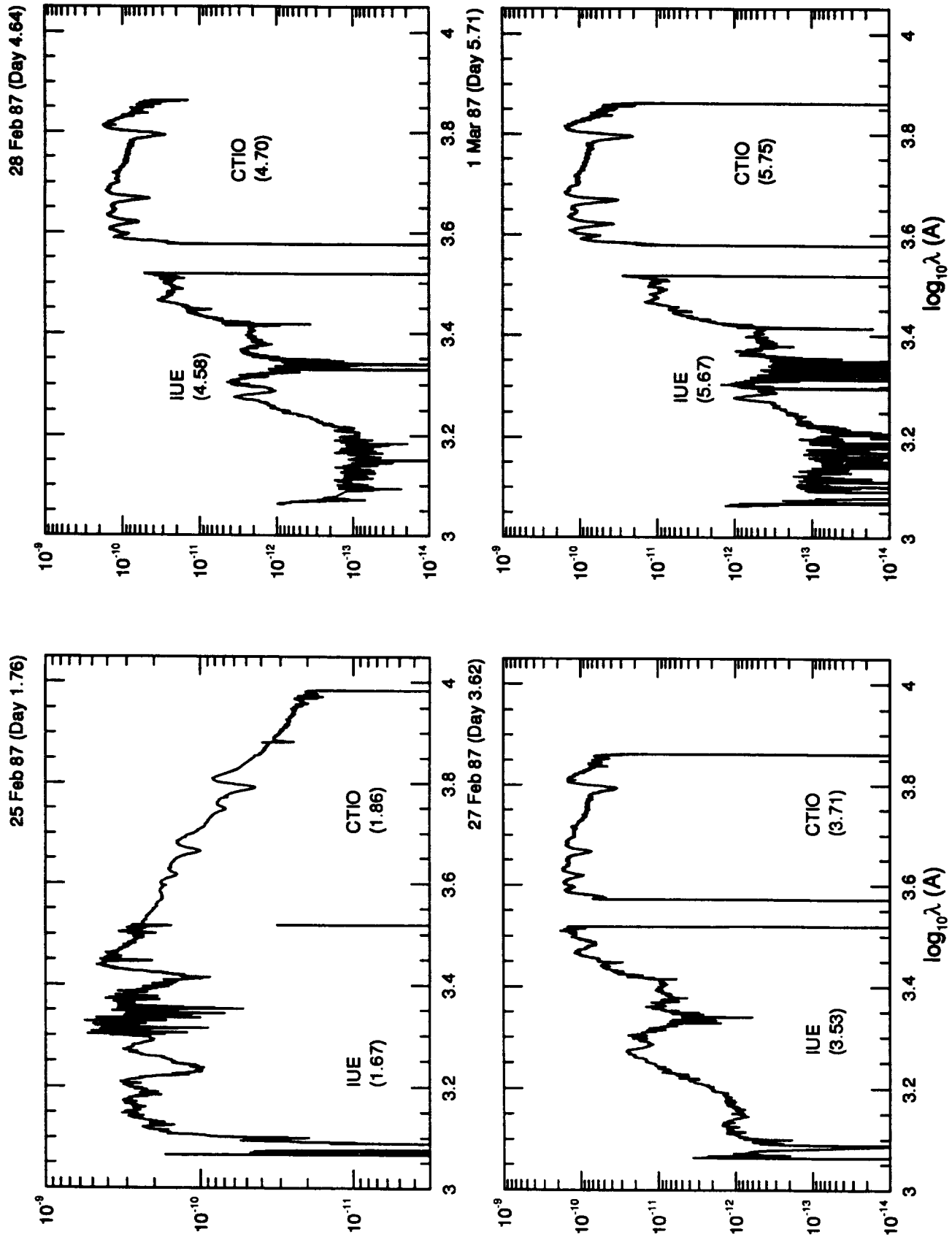

FIG. 8*a*

FIG. 8.—(*a*)–(*h*) The combined UV and optical spectra of SN 1987A. Notice that both the horizontal axis (wavelength) and the vertical axis (flux) are logarithmic. The optical spectra are obtained from CTIO (Phillips et al. 1988, 1990; Suntzeff et al. 1991). The optical spectra are corrected for interstellar extinction with the Cardelli et al. (1989) law with $E(B-V)_{host} = 0.15$ and $R_V = 3.1$.

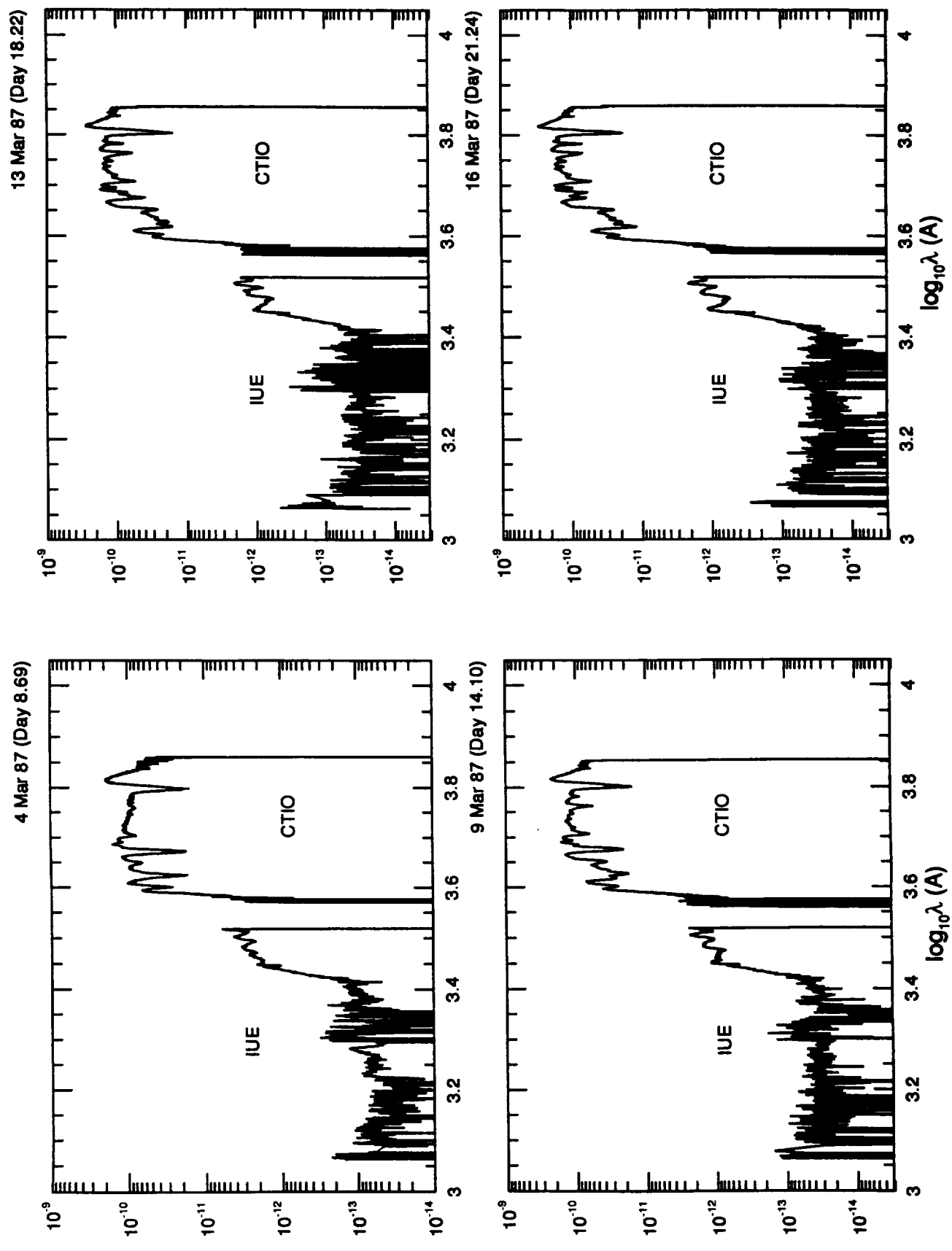
4 Mar 87 (Day 8.69)
9 Mar 87 (Day 14.10)
13 Mar 87 (Day 18.22)
16 Mar 87 (Day 21.24)
IUE
CTIO
f_λ (erg cm^{-2} s^{-1} A^{-1})
$\log_{10}\lambda$ (A)

FIG. 8*b*

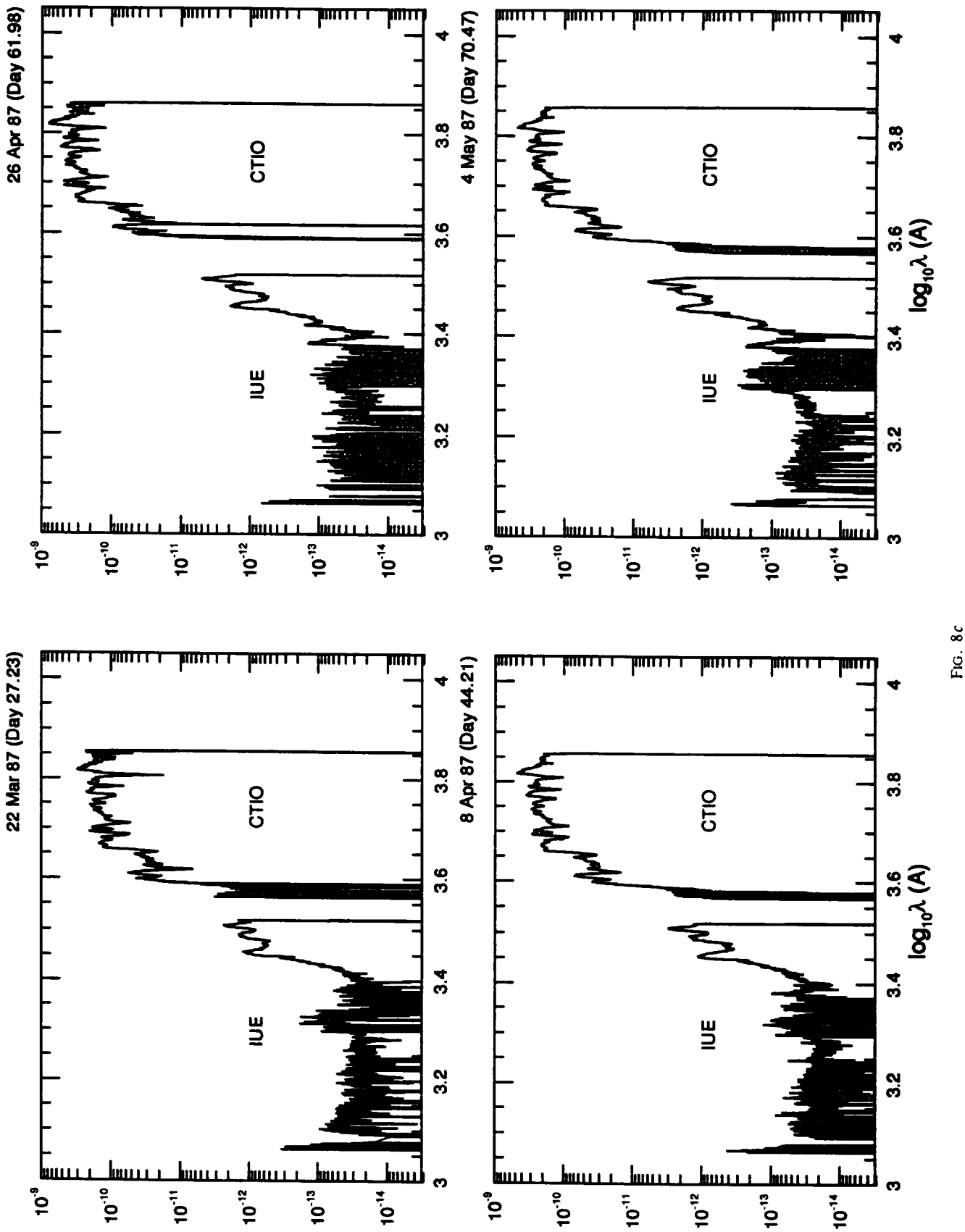
22 Mar 87 (Day 27.23)
8 Apr 87 (Day 44.21)
26 Apr 87 (Day 61.98)
4 May 87 (Day 70.47)
IUE
CTIO
f_λ (erg cm^{-2} s^{-1} A^{-1})
$\log_{10}\lambda$ (A)

FIG. 8c

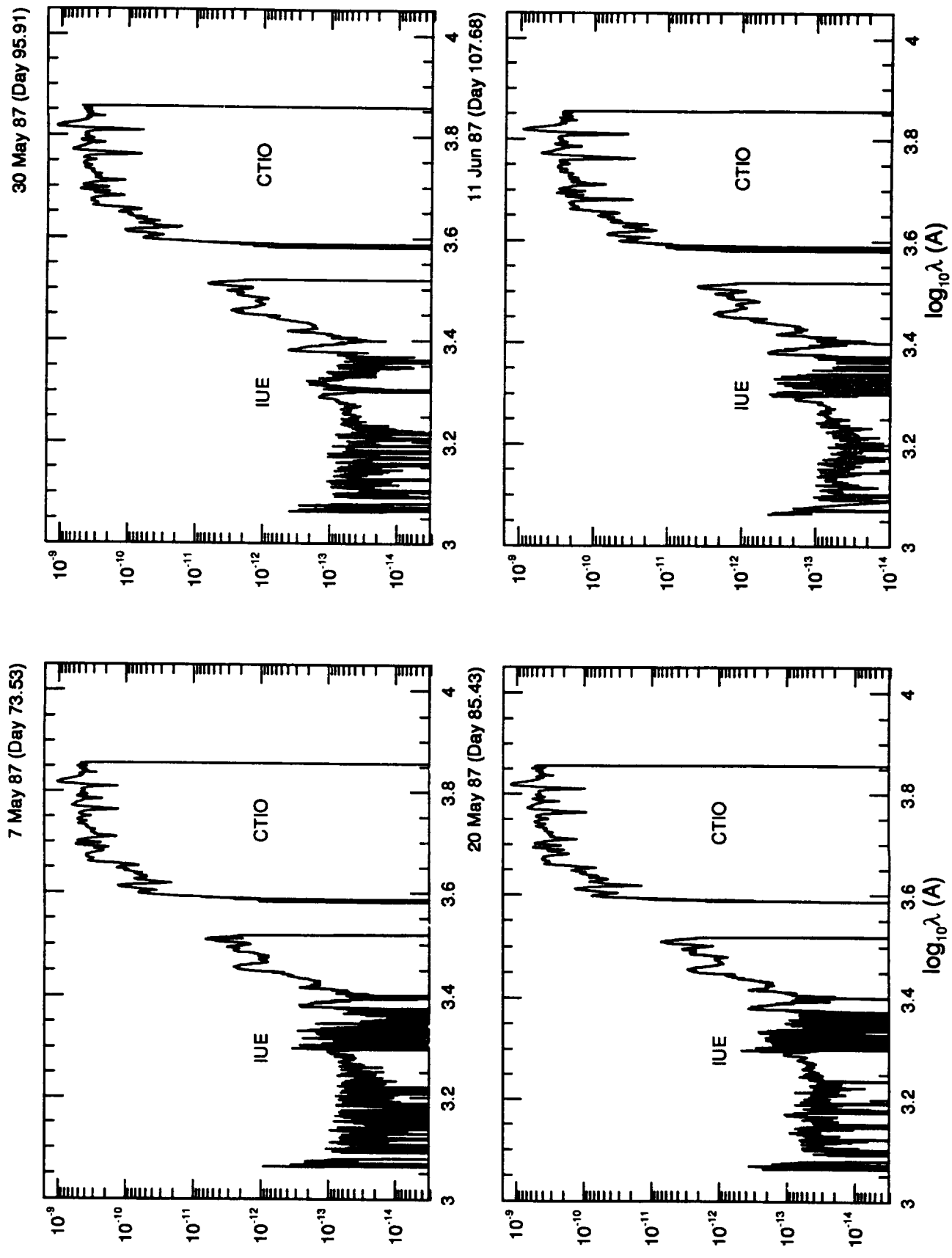
7 May 87 (Day 73.53)
20 May 87 (Day 85.43)
30 May 87 (Day 95.91)
11 Jun 87 (Day 107.68)
IUE
CTIO
f_λ (erg cm^{-2} s^{-1} A^{-1})
$\log_{10}\lambda$ (A)

FIG. 8*d*

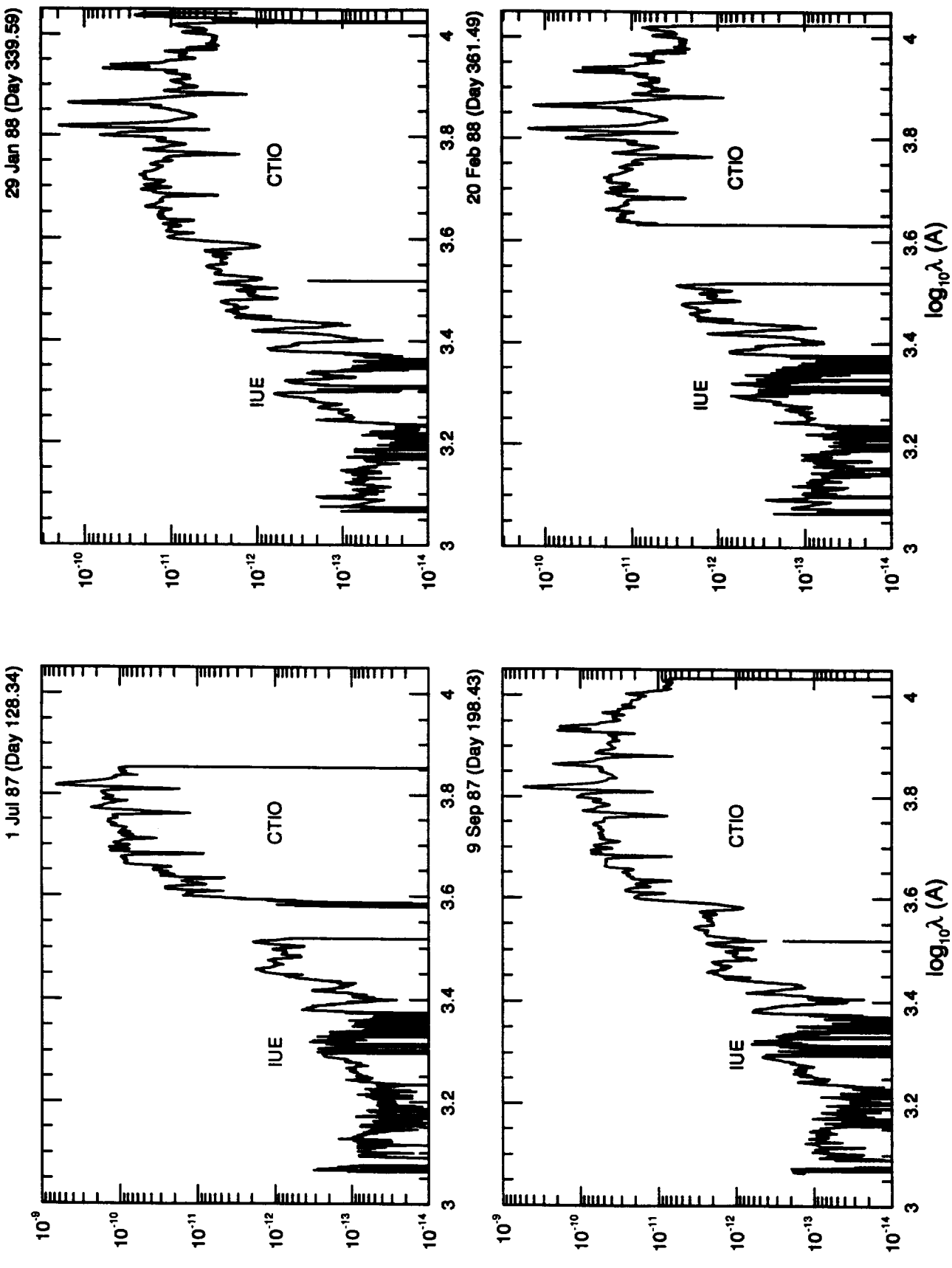
1 Jul 87 (Day 128.34)
9 Sep 87 (Day 198.43)
29 Jan 88 (Day 339.59)
20 Feb 88 (Day 361.49)
IUE
CTIO
f_λ (erg cm^{-2} s^{-1} A^{-1})
$\log_{10}\lambda$ (A)

FIG. 8e

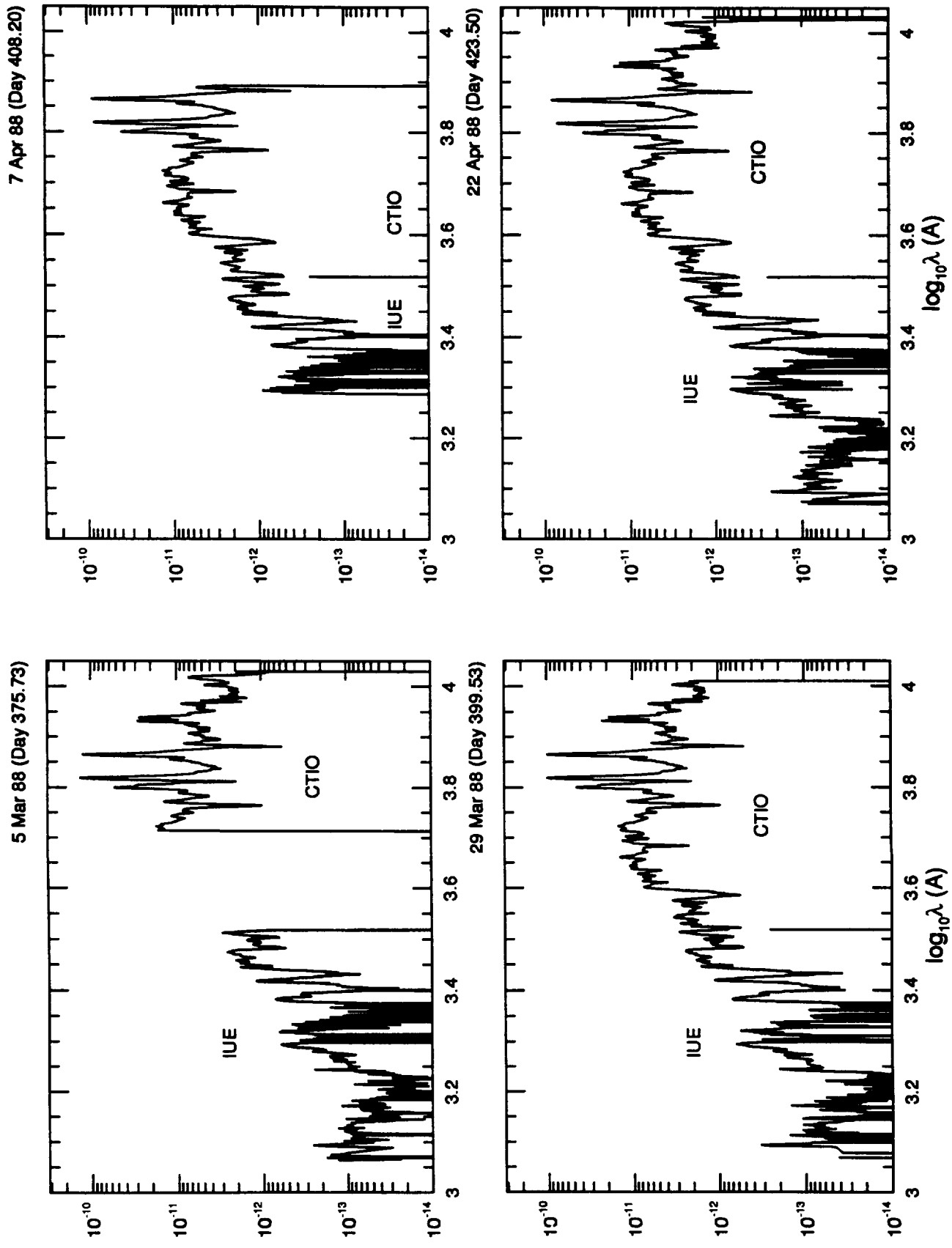
5 Mar 88 (Day 375.73)
29 Mar 88 (Day 399.53)
7 Apr 88 (Day 408.20)
22 Apr 88 (Day 423.50)
IUE
CTIO
f_λ (erg cm^{-2} s^{-1} A^{-1})
$\log_{10}\lambda$ (A)

FIG. 8*f*

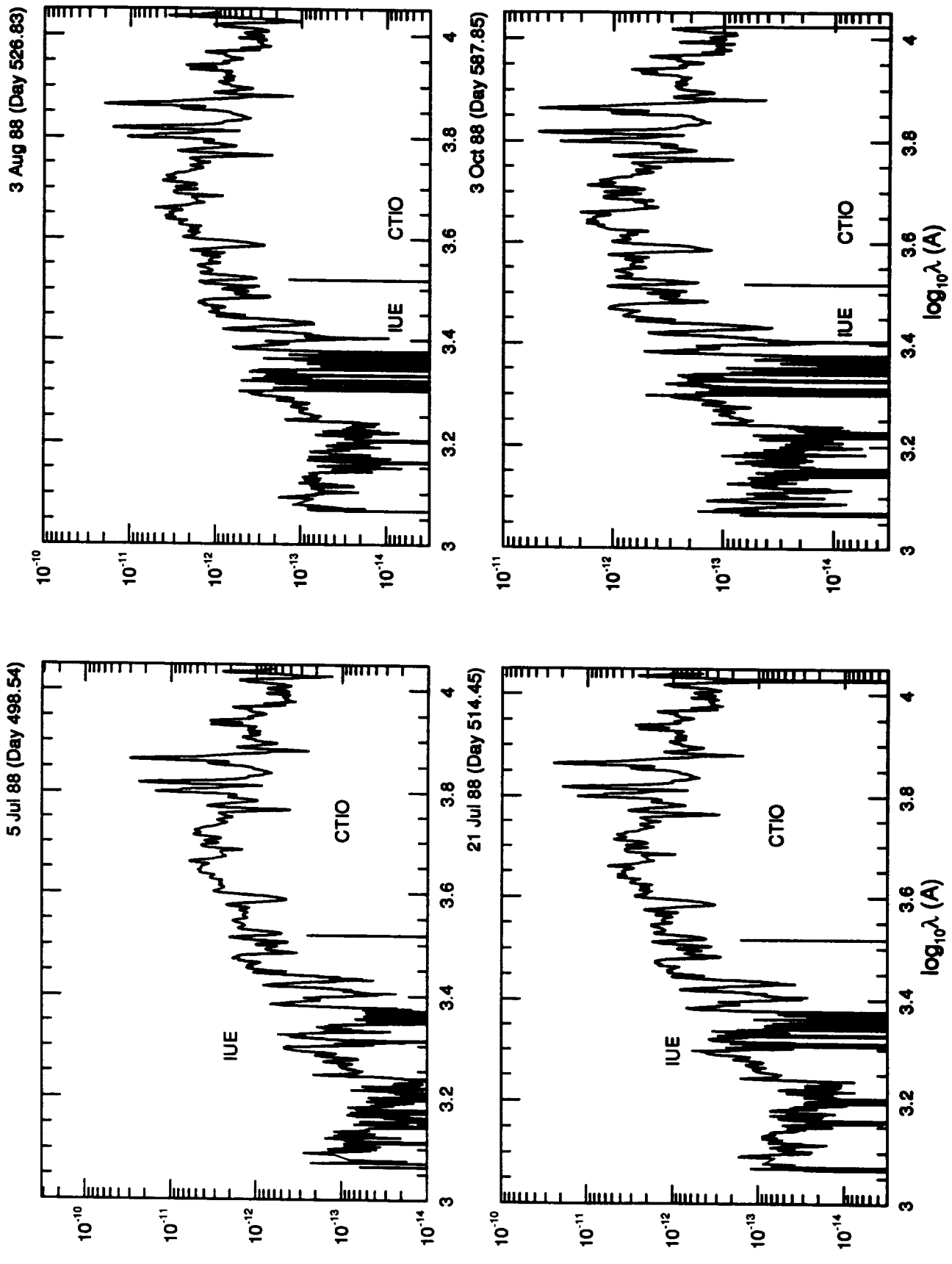
3 Aug 88 (Day 526.83)
3 Oct 88 (Day 587.85)
5 Jul 88 (Day 498.54)
21 Jul 88 (Day 514.45)
IUE
CTIO
f_λ (erg cm^{-2} s^{-1} A^{-1})
$\log_{10}\lambda$ (A)

FIG. 8g

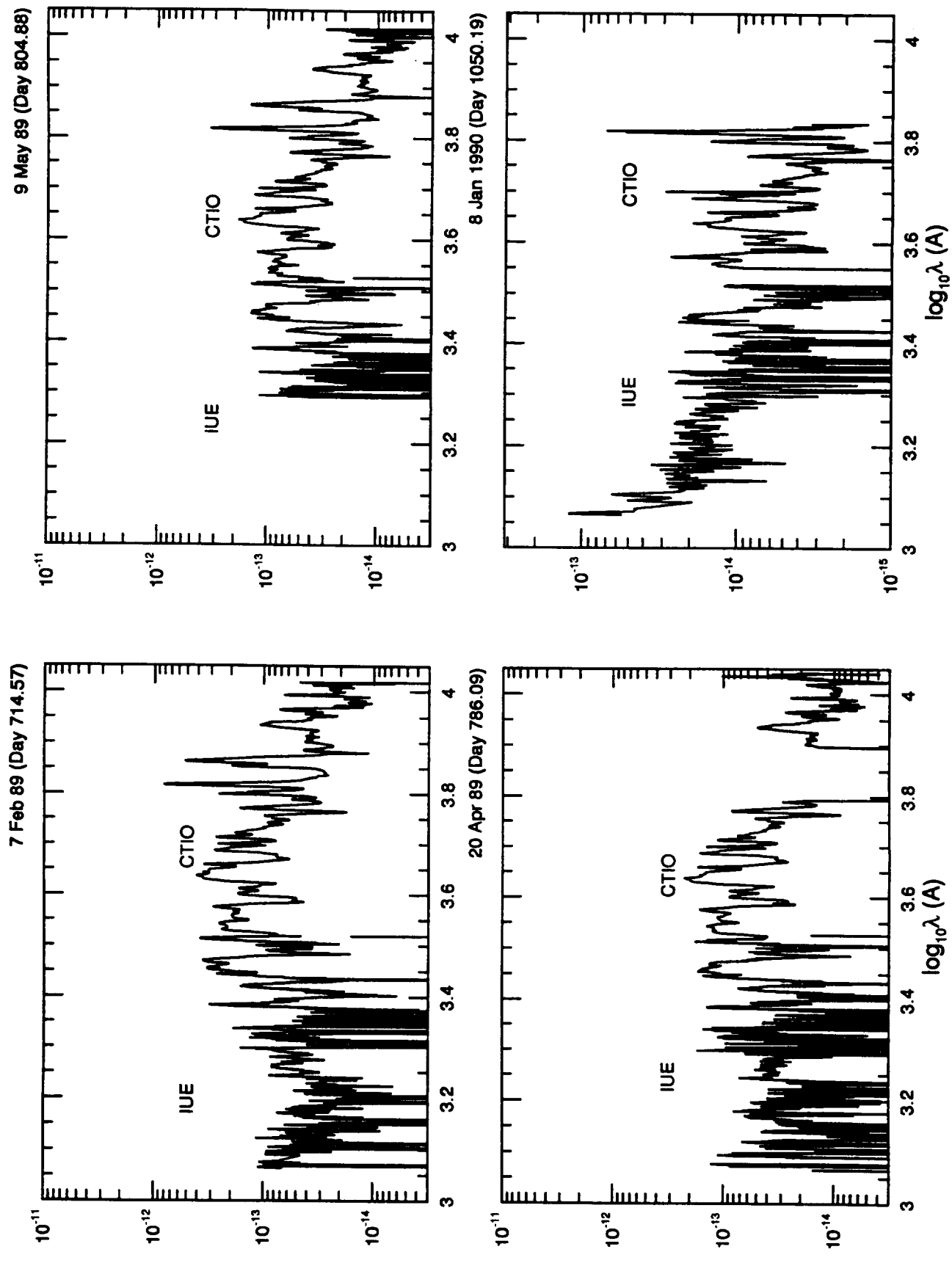
9 May 89 (Day 804.88)
8 Jan 1990 (Day 1050.19)
7 Feb 89 (Day 714.57)
20 Apr 89 (Day 786.09)
IUE
CTIO
f_λ (erg cm^{-2} s^{-1} A^{-1})
$\log_{10}\lambda$ (A)

FIG. 8*h*

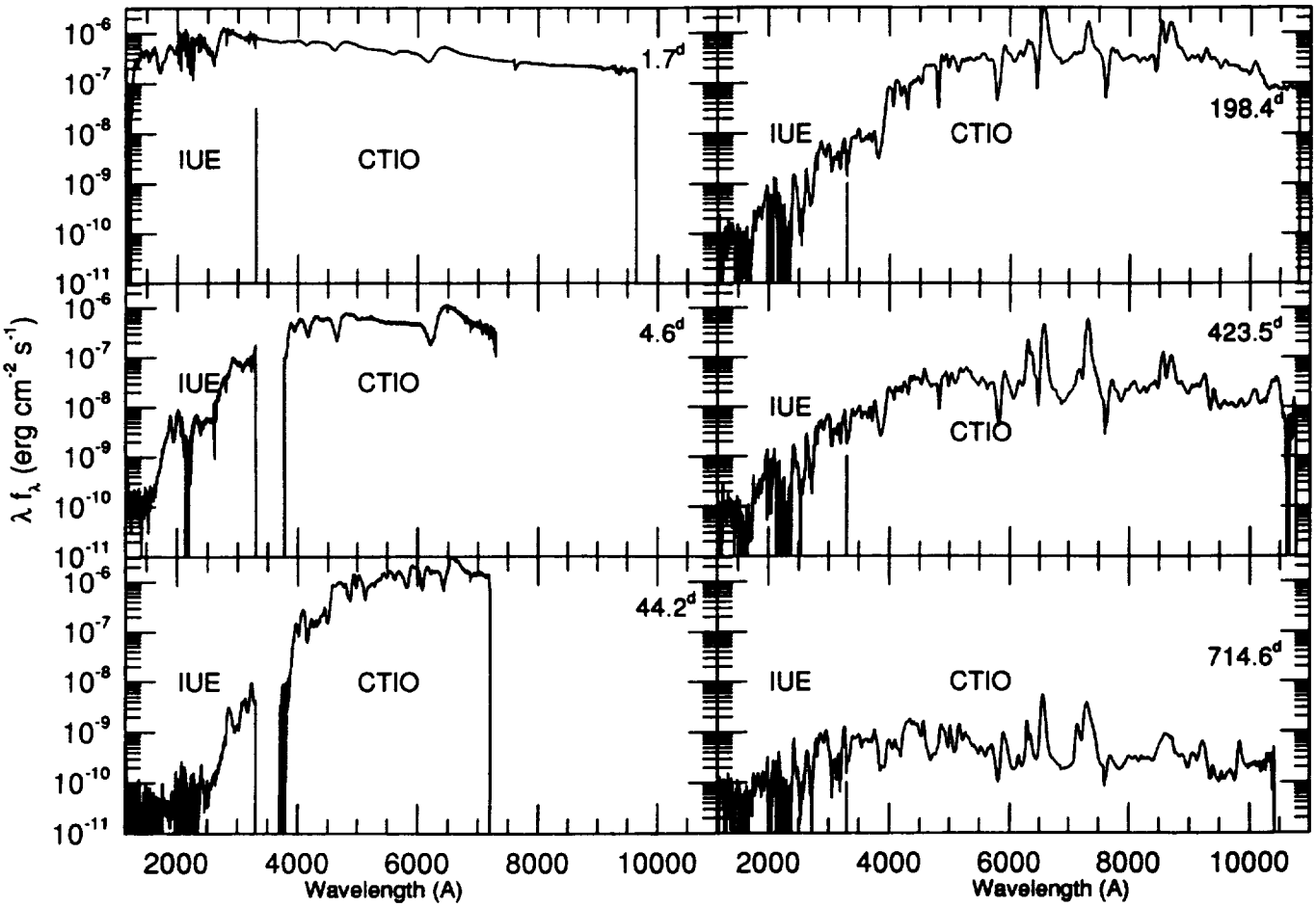

FIG. 9.—Plots of λf_λ vs. λ (1150–11,000 Å) at selected dates to show the energy distribution in the spectra of SN 1987A

length band from 1199 to 1227 Å is excluded from the SWP integration because of strong geocoronal Lyα emission. The UV light curves from these wavelength bands for the first 15 days after the explosion are presented in Figure 12. The integrated mean flux density of the waveband from λ_i to λ_f is determined by the formula

$$F_\lambda = \frac{\int_{\lambda_i}^{\lambda_f} w_\lambda f_\lambda(\lambda)\lambda d\lambda}{\int_{\lambda_i}^{\lambda_f} w_\lambda \lambda d\lambda}, \qquad (2)$$

where w_λ is the Lyα notch filter such that $w_\lambda = 0$ from 1199 to 1227 Å and $w_\lambda = 1$ elsewhere. The flux from SN 1987A plummeted over the first few days of observations for all the UV wavelength bands. The decrease continued throughout the 15 day period, though it was much slower after day 8. The time development of the integrated flux from the SWP band is very similar to that of the S band, while the M and L bands showed different temporal developments. During the initial drop, the short-wavelength bands declined much more rapidly than the long-wavelength bands. During the first 5 days of *IUE* observations, the integrated flux of the wavelength bands shortward of 2500 Å decreased by a factor of 2000, while the flux from the wavelength bands longward of 2500 Å decreased by a factor of 100. This steep drop in UV flux is accompanied by a large variation of the UV spectral characteristics as discussed in § 3.

The dramatic initial drop in UV flux can be explained by the rapid temperature decrease in the photosphere of the supernova, and also the corresponding increase in expansion opacity with the falling temperature (§ 3.1). We are probably seeing the cooling tail of a much hotter photosphere which was present on the day of outburst when the shock emerged from the stellar interior of Sk −69 202. The effects of the falling photospheric temperature are illustrated in Figure 13 where the combined optical + UV spectra of the SN 1987A for day 1.7 and day 4.6 are fitted by blackbody spectra of temperatures 11,700 and 7500 K, respectively. The measured temperatures are determined by fitting the *IUE* and optical/IR colors (Hamuy et al. 1988). The scale of the blackbody spectrum was determined by demanding the integrated fluxes of the observed and blackbody spectra to be equal for the range 5000–6200 Å (approximately the *V* band). For the day 1.7 spectrum, all the flux points from UV to the *M* band are used for the fit. After that, the UV and *U*-band fluxes are systematically lower than a blackbody and thus only the *B* to *L* magnitudes are used for the fit to the day 4.6 spectrum. The initial temperature drop

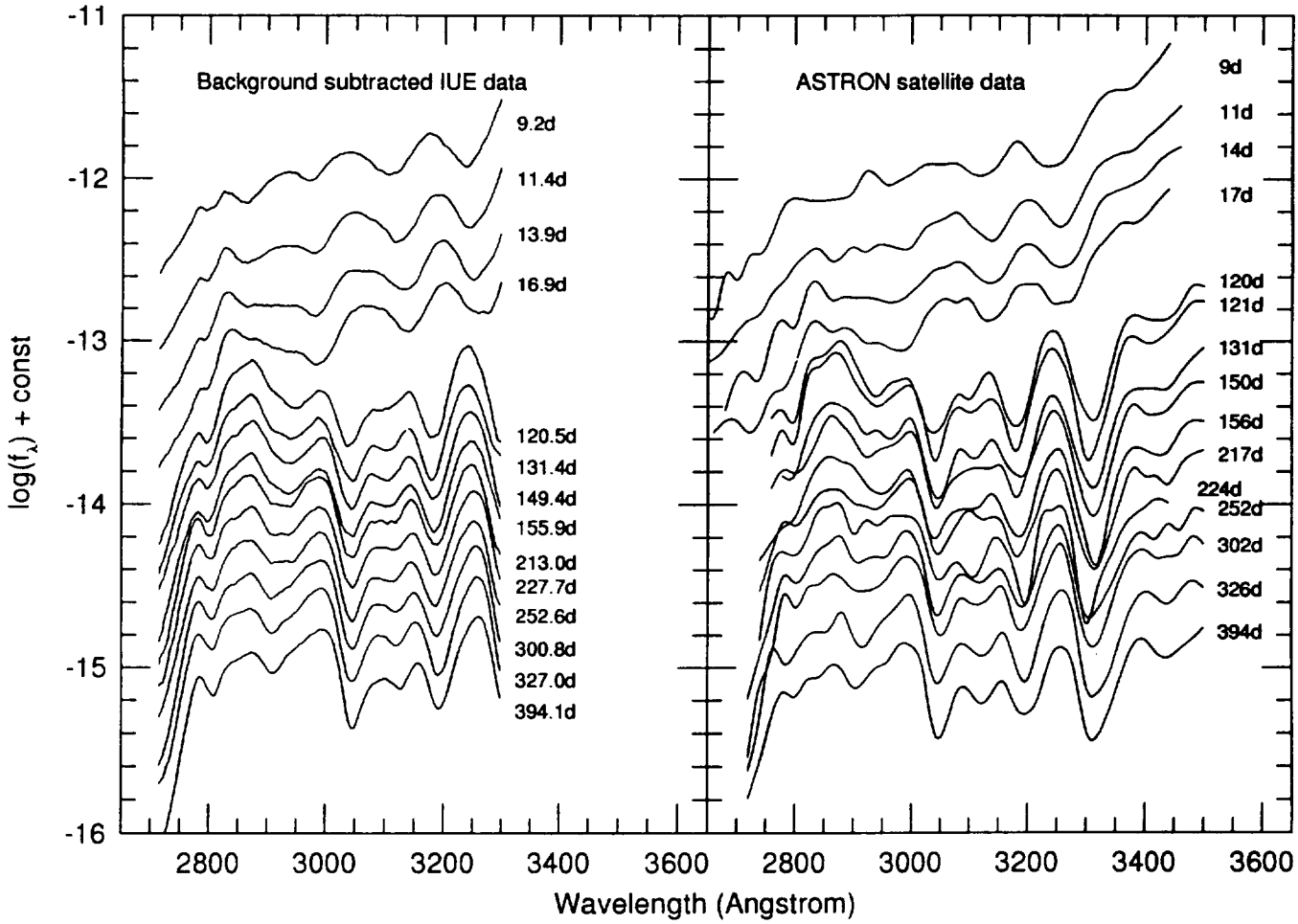

FIG. 10.—The UV spectra taken by the *ASTRON* satellite compared with the *IUE* data at similar dates. The *IUE* data is smoothed to the resolution of the *ASTRON* data (28 Å). Each successive spectrum is shifted downwards by 0.2 dex for clarity of display. The only exception is the *IUE* spectrum taken at day 120.5, which is shifted down by 0.4 dex. Neither set of data is corrected for interstellar extinction.

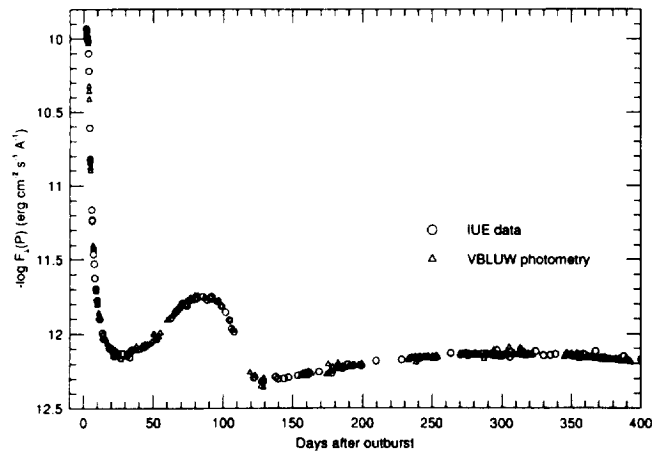

FIG. 11.—Comparison of the Walraven *W*-band photometry (λ_{eff} = 3236 Å; FWHM = 157 Å) with the convolved *W*-band *IUE* spectrophotometry results.

has two effects on the evolution of the UV flux. First, decreasing temperature causes the blackbody emission maximum to shift from the UV regime (~2500 Å) to the blue optical region (~3900 Å). Second, the falling temperature vastly increases the expansion opacity of the supernova atmosphere (Wagoner et al. 1991). They showed that at 5000 K, the UV expansion opacity is about 10^4 times that of the optical/IR. At day 1.7, the UV flux level slightly exceeded that of the blackbody fit. However, in two days, the situation quickly reversed and SN 1987A showed definite UV flux deficiency relative to blackbody fits to the optical.

We tried to estimate the effects of increased opacity in UV during the earliest stage of the supernova. The ratio between the integrated UV flux of the observed *IUE* spectrum and the fitted blackbody spectrum is computed for the first 15 days of observations. The temperature fits from Hamuy et al. (1988) are used to construct the blackbody spectra. Because of the similar time development of the S and SWP band flux in the early phase (Fig. 12), they are combined for the calculation (the SWP+S band). The results for the integrated flux ratio of the SWP+S, M, and L bands, along with the full *IUE* band,

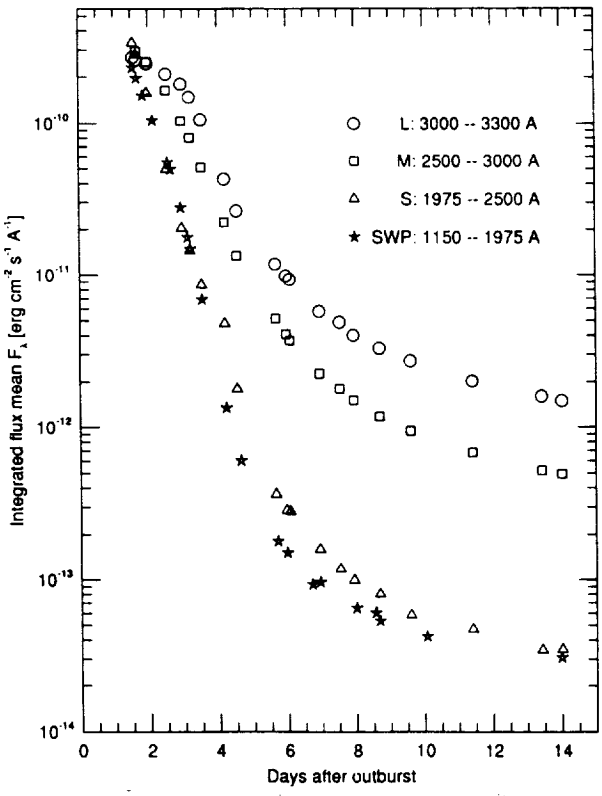

FIG. 12.—UV light curves of SN 1987A of various wavelength bands for the first 15 days after outburst.

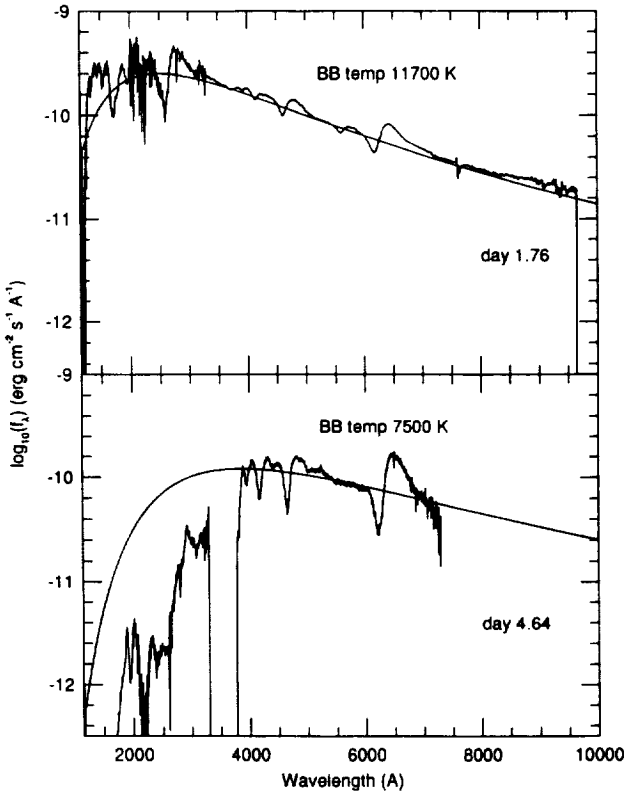

FIG. 13.—Comparing the earliest UV + optical spectrum of SN 1987A at day 1.7 (extinction corrected) with the blackbody spectrum of temperature 11700 K. The BB temperature is obtained by fitting the optical and IR colors (Hamuy et al. 1988). The spectrum at day 4.6 and the blackbody spectrum of 7500 K is also presented.

are presented in Figure 14. We notice that the UV deficiencies increased with time for all the wavebands. While the UV flux level is about 40% *above* the blackbody radiation at day 1.7, it dropped to be only 10% of the blackbody flux around day 5, and 1% around day 14. Second, the UV deficiency is more significant in the shorter wavelength band. The SWP+S band is more underluminous to a blackbody than the L band by about one order of magnitude between day 4 and 14. This is probably caused by the enormous line-blanketing effects in the wavelength region below 2600 Å with the presence of many strong Fe II lines.

Figure 12 shows that the UV flux decreases more rapidly at shorter wavelength during the early days of observations. This can also be seen in Figure 15, where the rates of decrease of the *IUE* flux, $-\Delta F_\lambda/\Delta t$ (expressed in unit of magnitude day^{-1}), in various wavebands are plotted against time. The earliest UV flux decay rates measured at day 2 are 1.93, 0.56, and 0.20 mag day^{-1}, for the SWP+S, M, and L wavebands, respectively. The rates of change of the optical U, B, and V bands photometry are also included in the figure. No interstellar extinction correction has been applied to the *IUE* data so that direct comparison between the rates of flux change in the optical and in the UV is possible. From day 3.8 through day 813, the $UBV(RI)_{KC}$ photoelectric observations taken at CTIO (Hamuy & Suntzeff 1990) are used, while prior to day 3.8, the *UBVRI* photoelectric observations by Shelton (1993) are used to compute the rate of change of flux in U, B, and V. Discrepancies exist between the two data sets, mostly because of the

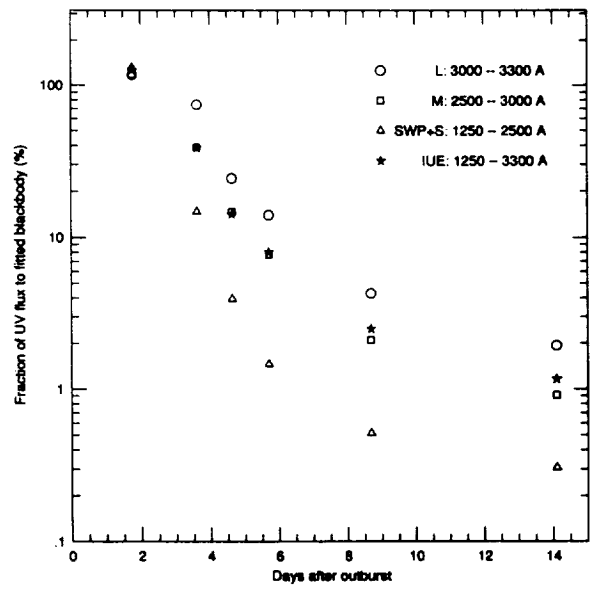

FIG. 14.—Ratios between observed flux and the fitted blackbody spectrum in various UV wavelength bands.

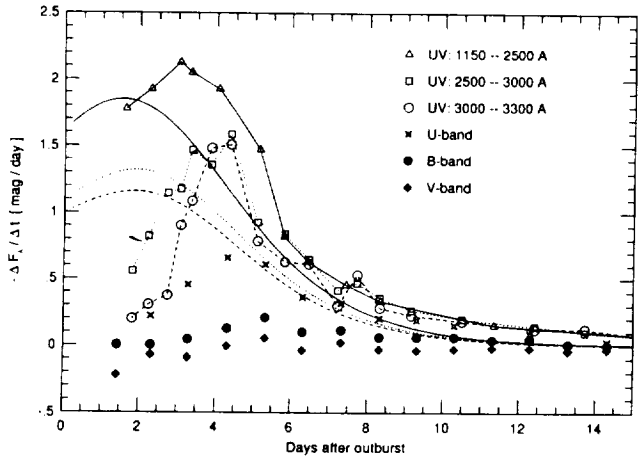

FIG. 15.—Rate of change of flux in time for various UV wavelength bands and optical photometry. The optical photometry data are from Shelton (1993) and the CTIO observatory (Hamuy & Suntzeff 1990). The smooth lines show the rates of change of UV flux for the fitted blackbody spectrum with temperature $T(t) = T_0[1 + k \exp(-\alpha t)]$, where $T_0 = 5900$ K, $k = 3.0$ and $\alpha = 0.54$. The SWP+S (*solid line*), M (*dotted line*), L (*broken line*) results are shown.

different filter passbands used. However, for the first few days after outburst, we estimate that the error involved should be less than ~0.03 mag. The trend of slower decay rates with longer wavelength extends to the *U* and *B* bands in the optical regime. In fact, the *V* band flux, along with *R* and *I* band fluxes (not plotted here), *increases* during the early days of observation. The decay rate for the SWP+S band reached a maximum of 2.13 mag/day at day 3.1, while the decay rates for both the M and L bands reached maxima 1.3 days later at day 4.4, with the value of 1.59, and 1.51 mag/day, respectively. After that, the decline in UV flux became slower with time in all wavebands. Despite the big differences in the initial decay rates observed in the various wavelength bands, all the UV bands decay at similar rates starting from around day 6.5, reaching a value of ~0.15 mag/day at day 14. The slow down of flux decay in all UV bands may probably be explained by the diffusion of energy which was deposited by the passage of the initial shock. However, the exact understanding of the phenomenon requires detailed modeling of the UV radiation from the atmosphere at the early stages.

The evolution of $-\Delta F_\lambda/\Delta t$, for a fitted blackbody is also presented in Figure 15. We estimate $\Delta F_\lambda/\Delta t$ by $\partial F_\lambda/\partial t = (\partial F_\lambda/\partial T)(\partial T/\partial t)$. $\partial F_\lambda/\partial T$ is determined by differentiating the Planck's function, while $\partial T/\partial t$ is calculated by fitting the early temperature data from CTIO (Hamuy et al. 1988) to a simple analytic expression $T(t) = T_0[1 + k \exp(-\alpha t)]$. The values $T_0 = 5900$ K, $k = 3.0$ and $\alpha = 0.54$ are used for the fit. This model is able to reproduce the general temporal behaviors of $-\Delta F_\lambda/\Delta t$ observed in all UV wavebands. The peaks of flux change rate occur earlier for the shorter wavelength bands (day 1.4 for SWP+S band) than the long-wavelength ones (day 1.8 for M and L bands). However, the peaks generated by the model occurred about 2 days earlier than the observed values and the model peaks for the M and L bands are too broad compared to the data. This calculation reaffirms the notion that the initial drop in temperature alone is not sufficient to completely explain the early behavior of the UV flux.

The light curves from day 1 to day 1248 for all the UV wavelength bands are illustrated in Figure 16. The integrated *IUE* mean flux densities from equation (2), without reddening corrections, are transformed to magnitude with the formula

$$\text{magnitude} = -2.5 \log_{10}(\text{integrated flux}) + \text{constant}, \quad (3)$$

where the value of *constant* is chosen for clarity of display. Following the fast decay of UV flux in the early days of observation, each of the UV light curves ceased to decrease when a minimum at day 30 was reached. For the two UV wavelength bands longward of 2500 Å (M and L), observed flux reached a maximum at ~day 85 before reaching minimum again at ~day 125. The UV flux from SN 1987A then increased slowly to another maximum at ~day 350 before its ultimate decline. The rate of decay increased from ~day 350 to ~day 650, and remained constant until ~day 900. During this constant decay epoch, the flux decline is faster for longer wavelengths (0.0109 and 0.0129 mag/day for M and L band respectively). It is difficult to determine the rate of decay of the light curves after day 900 as the supernova became dimmer. But the M-band light curve, which has the highest signal to noise at late times, suggests that the UV light curves decline at a slower rate from

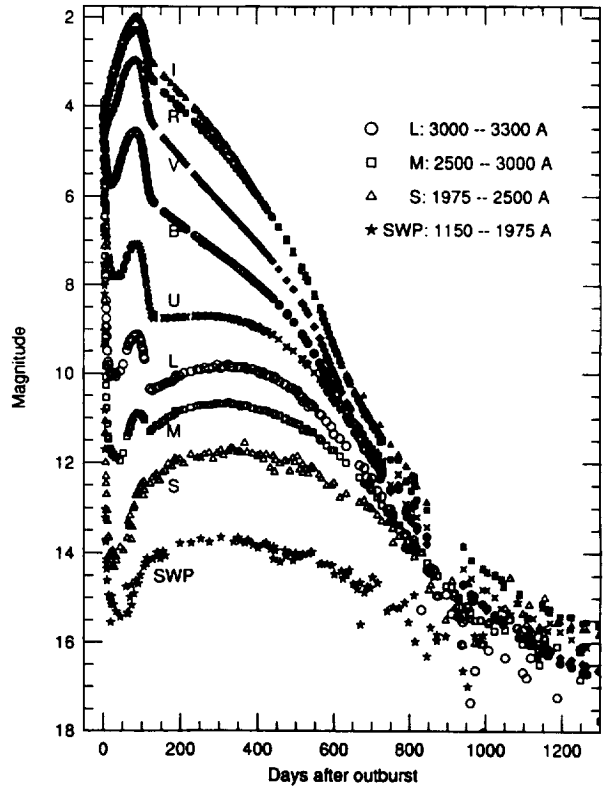

FIG. 16.—Light curves of SN 1987A for both the UV and optical wavelength bands from day 1 to day 1300. The optical photometry data are from Shelton (1993), Hamuy & Suntzeff (1990), and Walker & Suntzeff (1991). The UV broad-band spectrophotometry results are shifted vertically for clarity of display.

~day 950 until the final data point at day 1248. For the two wavelength bands shortward of 2500 Å (SWP and S), the temporal development of the light curve is similar, except that the second maximum near day 85 is not observed. The rate of decay for the constant decay epoch from day 650 to day 800 is 0.0092 mag/day for both wavebands. Moreover, the similarity between the SWP and S band flux evolution as noticed in the early days of observation continued in the late epoch. The two light curves did not start to differ in shape until ~day 900, when additional radiation from the variable star 3 might be present in the SWP spectra (to be discussed later).

In Figure 16, the UV spectrophotometry results are compared with the optical light curves from the CTIO data, which include the photoelectric photometry results from day 3.8 to 813 (Hamuy & Suntzeff 1990), and the CCD *UBVRI* photometry measurements from day 680 to 1469 (Walker & Suntzeff 1991). Early photometric results by Shelton (1993) from day 1.0 to 3.7 are also included despite the slight difference between the filters used. We can see that with decreasing wavelength from *I* band to far-UV, the magnitude of the light curve's second maximum around day 85 gradually diminishes. This maximum in fact disappeared for wavelength bands below 2500 Å. On the other hand, after day 125, the decline of *V*, *R*, and *I* light curves are within 15% of the *e*-folding time of the radioactive decay of ^{56}Co (111.3 d), and the *B* band had a less rapid decline of ~160 days (Suntzeff et al. 1988). However, this decline is not observed in the *U* band and UV photometric measurements. Instead, the development of a third maximum around day 350 can be seen with decreasing wavelength. Both the disappearance of the second maximum of the UV light curves around day 85 and the appearance of the third maximum maximum around day 350 with decreasing wavelengths are probably related to the changes of the ionization and excitation stages of the iron group elements. However, a plausible interpretation of the UV light curves is not possible without correct modeling of the opacities with the changing temperature, density, and composition of the photosphere.

5.2. *UVOIR Total Bolometric Luminosity*

The total integrated UV light curve (1150–3300 Å) of SN 1987A is shown in Figure 17. The same reddening correction as described in § 2.3 is applied to the data, i.e., $E(B-V)_{\rm total} = 0.15$. Only epochs with both SWP and LWP spectra taken within 5 hr are investigated. The spectra are combined for calculations and a total of 96 measurements are obtained. Also shown in Figure 17 is the total ultraviolet-optical-infrared (UVOIR) bolometric light curve of SN 1987A. The CTIO and ESO groups have previously computed the UVOIR bolometric light curve based on broadband *U* to *M* photometry for the early days of observations (Suntzeff & Bouchet 1990), and *U* to Q_0 photometry for the late-time observations (Suntzeff et al. 1991; Bouchet et al. 1991). The ESO and CTIO results differ from each other after day 616 because of the differences in the IR flux measurements. In these compilations, the UV flux was included in the total bolometric flux calculations for only the first 14 days. After day 14, the UV contribution was assumed to be negligible, and thus only the optical/IR luminosities, $L_{\rm OIR}$, are presented. While this omission was justified before ~day 200, the UV flux contributes an increasing fraction of

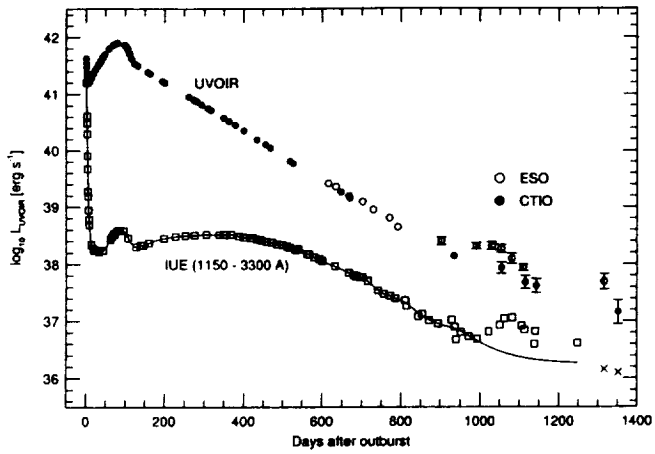

FIG. 17.—Revised UVOIR bolometric light curve of SN 1987A with UV data included from day 1 to 1352. Results from both CTIO (*filled circles*) and ESO (*open circles*) are shown. Errors are less than the symbol size if not shown. The total UV light curve measured from *IUE* data (*squares*) and the spline fit to the UV light curve used for calculations of the bolometric luminosity are plotted. Extrapolations of the spline fit beyond the final UV flux points are also shown (*crosses*).

the total bolometric luminosity as time progresses. Therefore, we tried to add the UV flux contributions after day 14 to the bolometric data after day 14 from both the CTIO and ESO groups. Moreover, the *IUE* data that had been included for bolometric calculations before day 14 were not processed for the corrections described in § 2 such as appropriate combination, background subtraction, camera degradation, and so on. Therefore, the early bolometric fluxes before day 14 are recalculated with our new processed set of *IUE* data. The revised bolometric luminosity data, including the contributions of UV at all epochs, for SN 1987A are given in Table 4A and 4B, for the results from the CTIO and ESO groups, respectively. A distance modulus to the LMC of 18.5 is assumed.

Before day 14, we started with the UV to *M*-band bolometric luminosity data as described in Suntzeff & Bouchet (1990). The separate UV and optical/IR components of the bolometric flux used in the calculation are obtained (N. Suntzeff, private communications). We fit a spline to our new UV light curve to estimate the UV fluxes on days with OIR measurements. The interpolated UV flux is added to the measured OIR flux to obtain the UVOIR bolometric luminosity. The adjustment is ~0.06 dex for the first day of observation (day 1.14), and it decreases with time. By day 10, the adjustment to the bolometric luminosity became <0.001 dex. Notice that the first two OIR measurements (day 1.14 and 1.51) were made before the earliest *IUE* observation (day 1.66). Thus extrapolation of UV data is required for the bolometric flux calculations for the two dates day 1.14 and 1.51. We estimated that the extrapolation will not induce large enough error to change the error quoted for the bolometric luminosity (0.02 dex).

After day 14, we started with the *U* to Q_0 bolometric luminosity data of the CTIO (Suntzeff et al. 1991) and ESO (Bouchet et al. 1991) groups. Again, we interpolate the UV light curve with a spline to estimate the UV fluxes on days with optical/IR measurements. This method works fine for epochs before ~day 900. However, after day 900, as the supernova

TABLE 4

A. BOLOMETRIC LUMINOSITY OF SN 1987A FROM CTIO (SUNTZEFF & BOUCHET 1990; SUNTZEFF ET AL. 1991) AND THE NEW UVOIR BOLOMETRIC LUMINOSITY WITH *IUE* RESULTS INCLUDED

Day	CTIO $\log(L_{UVOIR})$[a] (ergs s^{-1})	$\log(L_{UV})$ (ergs s^{-1})	New $\log(L_{UVOIR})$ (ergs s^{-1})	$\sigma \log(L_{bol})$	Day	CTIO $\log(L_{UVOIR})$[a] (ergs s^{-1})	$\log(L_{UV})$ (ergs s^{-1})	New $\log(L_{UVOIR})$ (ergs s^{-1})	$\sigma \log(L_{bol})$
1.14	41.687	41.446	41.628	<0.02	103.70	41.829	38.514	41.829	<0.02
1.51	41.582	41.275	41.546	<0.02	104.70	41.812	38.500	41.812	<0.02
1.85	41.493	41.118	41.476	<0.02	106.70	41.787	38.473	41.787	<0.02
2.70	41.373	40.722	41.372	<0.02	108.70	41.755	38.446	41.755	<0.02
3.65	41.294	40.226	41.288	<0.02	110.70	41.722	38.421	41.722	<0.02
4.70	41.245	39.613	41.237	<0.02	111.70	41.706	38.409	41.706	<0.02
5.64	41.219	39.288	41.215	<0.02	115.70	41.630	38.367	41.630	<0.02
6.82	41.211	38.972	41.207	<0.02	122.70	41.544	38.316	41.544	<0.02
7.81	41.206	38.806	41.203	<0.02	132.10	41.501	38.311	41.501	<0.02
8.79	41.215	38.679	41.213	<0.02	157.10	41.390	38.358	41.390	<0.02
9.80	41.225	38.573	41.225	<0.02	158.10	41.389	38.362	41.389	<0.02
10.79	41.237	38.491	41.237	<0.02	159.10	41.381	38.366	41.381	<0.02
13.80	41.293	38.348	41.293	<0.02	164.10	41.361	38.383	41.361	<0.02
14.80	41.309	38.326	41.309	<0.02	195.00	41.230	38.448	41.231	<0.02
19.70	41.371	38.261	41.371	<0.02	198.00	41.214	38.452	41.215	<0.02
24.80	41.438	38.220	41.438	<0.02	201.00	41.202	38.456	41.203	<0.02
25.80	41.449	38.229	41.449	<0.02	260.80	40.950	38.504	40.952	<0.02
30.80	41.504	38.234	41.504	<0.02	273.90	40.894	38.508	40.896	<0.02
32.80	41.525	38.219	41.525	<0.02	280.90	40.869	38.511	40.871	<0.02
33.80	41.536	38.214	41.536	<0.02	293.00	40.812	38.517	40.814	<0.02
34.80	41.544	38.210	41.544	<0.02	308.80	40.744	38.521	40.747	<0.02
35.80	41.556	38.208	41.556	<0.02	316.80	40.712	38.519	40.715	<0.02
36.80	41.569	38.208	41.569	<0.02	348.80	40.576	38.517	40.580	<0.02
37.80	41.584	38.209	41.584	<0.02	361.80	40.518	38.517	40.522	<0.02
39.70	41.607	38.215	41.607	<0.02	377.80	40.450	38.510	40.455	<0.02
42.70	41.640	38.231	41.640	<0.02	399.70	40.351	38.473	40.357	<0.02
43.70	41.653	38.238	41.653	<0.02	433.00	40.186	38.434	40.194	0.02
44.70	41.668	38.245	41.668	<0.02	455.70	40.100	38.396	40.109	0.02
46.70	41.688	38.260	41.688	<0.02	468.00	40.040	38.385	40.050	0.02
47.70	41.699	38.268	41.699	<0.02	518.10	39.803	38.295	39.816	0.02
58.70	41.796	38.382	41.796	<0.02	526.10	39.761	38.264	39.775	0.02
59.70	41.805	38.395	41.805	<0.02	648.00	39.25	37.92	39.27	0.04
68.70	41.861	38.494	41.861	<0.02	670.00	39.14	37.84	39.16	0.04
73.70	41.880	38.516	41.880	<0.02	935.00	38.12	36.86	38.14	0.07
74.70	41.885	38.458	41.885	<0.02	1055.00	37.91	36.60	37.93	0.10
79.70	41.899	38.553	41.899	<0.02	1115.00	37.65	36.50	37.68	0.11
80.70	41.901	38.584	41.901	<0.02	1143.00	37.59	36.46	37.62	0.12
98.70	41.867	38.569	41.867	<0.02	1352.00	37.12	36.10	37.16	0.21
101.60	41.844	38.540	41.844	<0.02					

B. LATE-TIME BOLOMETRIC LUMINOSITY OF SN 1987A FROM ESO (BOUCHET ET AL. 1991) AND THE NEW UVOIR BOLOMETRIC LUMINOSITY WITH *IUE* RESULTS INCLUDED

Day	ESO $\log(L_{OIR})$ (ergs s^{-1})	$\log(L_{UV})$ (ergs s^{-1})	New $\log(L_{UVOIR})$ (ergs s^{-1})	$\sigma \log(L_{bol})$	Day	ESO $\log(L_{OIR})$ (ergs s^{-1})	$\log(L_{UV})$ (ergs s^{-1})	New $\log(L_{UVOIR})$ (ergs s^{-1})	$\sigma \log(L_{bol})$
615.91	39.408	38.013	39.425	0.007	903.10	38.383	36.934	38.398	0.066
634.80	39.352	37.964	39.369	0.005	991.56	38.300	36.689	38.311	0.055
667.85	39.177	37.850	39.197	0.016	1030.50	38.303	36.633	38.312	0.068
701.85	39.075	37.771	39.096	0.018	1054.30	38.258	36.598	38.267	0.070
728.75	38.932	37.617	38.953	0.033	1081.13	38.080	36.556	38.093	0.090
770.71	38.786	37.451	38.806	0.049	1110.08	37.920	36.510	37.937	0.056
791.67	38.622	37.386	38.646	0.042	1316.00	37.680	36.158	37.693	0.133

[a] For time before day 14, the UVOIR bolometric luminosity L_{UVOIR} data is tabulated. After day 14, the OIR luminosity L_{OIR} is tabulated.

dimmed, an increasing fraction of the observed UV flux is from the background stars, and it becomes hard to correctly determine the UV contribution to the UVOIR bolometric luminosity at the very late epochs ($\gtrsim$ day 900).

In Figure 17, we observed a bump in the UV light curve between about day 1000 to 1150. The bump remains even after careful removal of star 4 as described in § 2.2. Most of the UV flux we measured at late times comes from star 2 and star 3. Since star 3 is a Be star, it is possible that the additional flux is from star 3, which is known to be a variable. With the back-

ground flux determined by averaging spectra over the epoch from day 1301 to day 1567 (§ 2.2), our net UV flux measurement is vulnerable to variations in the background stars on shorter time scales. This idea is strengthened after studying the $UBV(RI)_{KC}$ photometry of star 3 taken by Walborn et al. (1993) which is reproduced in Figure 18. Magnitudes in all optical bands change with time and variations of the order of ~0.3 mag are observed. During the period day 1080–1220, star 3 was exceptionally bright across all wavelength bands. The coincidence in time of maximum optical emission from star 3 with the epoch of extra UV flux provides evidence that this extra flux is mostly from star 3. We estimate that a variation of 15% in the UV flux from star 3 would be sufficient to explain the detected increase. Be stars are known to be variables in both UV and optical regions. A 50% decrease in UV flux has been detected in a Be star (Barylak & Doazan 1986), thus a 15% variation over 1 year seems plausible.

The other potential explanation for the bump in the UV light curve is that the extra flux comes from the supernova itself. A possible evidence is that the increase of the UV flux around day 1070 is at about the same time as the increase in ESO bolometric luminosity observed around day 1035. At this very late time, the UVOIR bolometric luminosity was dominated (~80%) by infrared radiation longward of 10 μm. In fact, the ESO 10 μm and 20 μm broadband photometric light curves display bumps of ~0.8 mag near day 1030 (Bouchet et al. 1991). However, the optical light curves of the CTIO data, for which the supernova was resolved from its neighboring stars, did not show bumps at a similar epoch (Walker & Suntzeff 1991). We cannot think of any physical process originated from the supernova which can explain the increase of flux in far-IR and UV at the same time without increasing the optical output. Thus it seems unlikely the extra flux observed is intrinsic from the supernova.

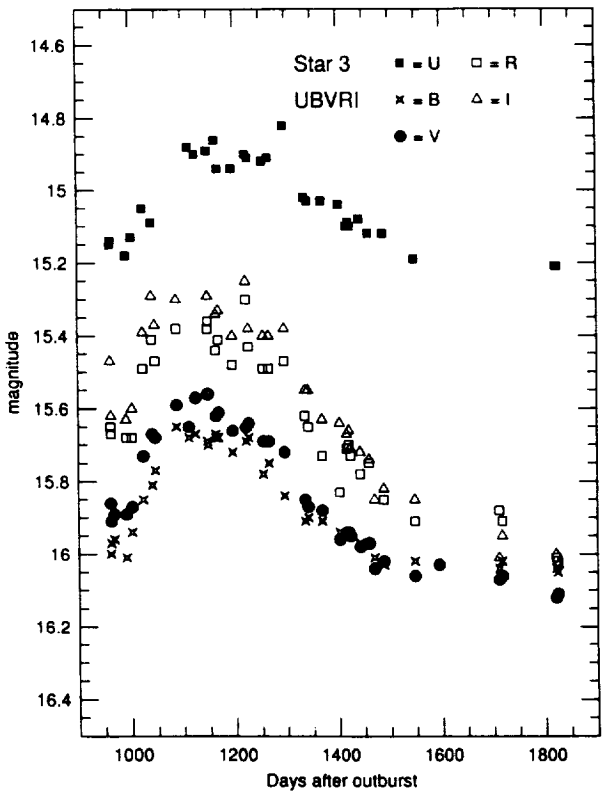

FIG. 18.—The *UBVRI* photometry of Star 3 taken by Walborn et al. (1993).

With the ESO 10 and 20 μm broadband photometric results taken with a 5″ aperture, we suggest that the observed increase of flux near day 1030 may be explained by the variable IR behavior of the Be stars. While studies of the far-IR variability of Be stars are not available, studies of the near-IR variability of Be stars show that the fraction of Be stars that are variables increases with wavelength and the amplitude of variations increases with wavelength (Dougherty & Taylor 1994). Walborn et al. (1993) observed variations in the near-IR photometry of star 3 of ~1 mag between day 1150 and day 1870. Thus we suggest it is possible that star 3 also vary in magnitude of ~1 mag in the far-IR bands to explain the bumps observed in the light curves near day 1030.

Assuming that the extra flux in the bump of the UV light curve seen between day 1000–1150 is from the variable star 3, we tried to estimate the fraction of the observed UV flux that was originated from the supernova in the last spectrum of the data set (day 1248). By comparing the *IUE* data from day 1 to 800 with the *HST* data (§ 7) from day 1278 to 2431, we estimated that at day 1248, only about 40% of our "background" subtracted SWP flux and about 57% of the LWP flux are indeed from the supernova. Thus we estimated that 46% of the total "background"-subtracted *IUE* flux at day 1248 is from the supernova itself by adding the SWP and LWP flux components. Using this estimate and the observed total *IUE* measurements from day 1 to day 1000 (excluding the noisy data points around day 940), we can fit a spline and estimate the UV contributions to the total UVOIR bolometric luminosity at epochs with OIR measurements. Notice that extrapolation of UV light curve beyond the last day of observation is required for the last CTIO and ESO data points (day 1352 and 1316, respectively). However, since the UV contribution to the total bolometric flux is less than 10% at late times, we estimate that the errors quoted in the Suntzeff et al. (1991) and Bouchet et al. (1991) papers will not be altered by the inclusion of the extrapolated UV fluxes. The extrapolated UV flux values for day 1316 and 1352 are marked by crosses in Figure 17. The fitted spline to the UV light curve with the adjusted day 1248 flux is shown in Figure 17 and the interpolated UV fluxes at dates with OIR measurements are presented in the second column of Table 4. The adjusted UVOIR bolometric luminosity data are presented in the third column of Table 4A and 4B, respectively, for CTIO and ESO measurements. The inclusion of UV flux added less than 0.001 dex to the total bolometric luminosity by day 164. However, the contribution of UV increases with time—by day 468, inclusion of UV flux added 0.01 dex to the total bolometric flux. At the final date of calculation, day 1352, the UV flux added 0.04 dex to the previous bolometric luminosity calculations.

As seen in Figure 17, both the bolometric luminosity and the UV flux from SN 1987A show an early decrease in magnitude. While the bolometric light curve reached a brief minimum at ~day 8, the UV light curve did not reach its minimum until ~day 18 and it remained at the minimum for another month

before it started to increase. Despite differences in their prior developments, both light curves reached maxima at ~day 90 before they decreased again. By ~day 120, the rate of decrease for UVOIR flux changed to the one suggested by the radioactive decay of ^{56}Co. The UV flux instead increased slowly to a maximum at ~day 350 before it started to drop exponentially around day 600. Beyond ~day 900, both curves seemed to have s slowed their rate of decrease. From Figure 17, it is obvious that the UV fraction of the total UVOIR luminosity increases with time. The time development of this fraction is presented in Figure 19. At the first day of *IUE* observation (day 1.66), emission in UV represents 46% of the radiation from SN 1987A. This fraction decreased steeply in the next few days. By day 18, less than 0.1% of the bolometric radiation was from the *IUE* bands. The F_{UV}/F_{UVOIR} ratio reached a minimal value of 0.004% at ~day 45. After that date, the contribution of UV flux started and continued to increase afterward. By day 800, UV accounted for ~7% of the total UVOIR bolometric luminosity of SN 1987A, and the compilation here is the only source where it has been included. The correct determination of the late-time bolometric flux from the supernova is especially important to the identification its energy source. Fransson & Kozma (1993) suggest that after ~day 800, time-dependent effects due to long recombination and cooling times would lead the supernova ejecta to a "frozen" state, causing the emitted flux to be larger than the instantaneous radioactive energy deposition. Thus the observed supernova luminosity will be higher than that of the instantaneous energy input. Quantitative tests of this theory demand a set of correctly determined bolometric luminosity data, as given in Table 4.

6. CONNECTION WITH DUST CONDENSATION

6.1. *Dust Condensation in SN 1987A Ejecta*

By comparing the atmospheric conditions in SN 1987A with classical novae, Gehrz & Ney (1987) suggested that dust grains would condense in the expanding ejecta when the temperature cools down to 1000 K. They predicted that the dust condensation would occur by late 1987 or early 1988 (~day 300). A similar study by Dwek (1988) made the same prediction and suggested that dust would form in the ejecta by $t \approx 400$ days. Hints of dust condensation came from the optical/IR photometric and spectroscopic observations of the supernova. In Roche et al. (1989), they reported that the mid-IR continuum emission (8–13 μm), which had been fading steadily since ~day 120, began to increase on day 465 and continued to do so up to day 578. However, the authors suggested that this emission originated from an IR echo. With subsequent observations Roche, Aitken, & Smith (1993) concluded that the bulk of the mid-IR continuum flux originated instead from the newly formed dust in the ejecta which absorbed the optical photons and reradiated that energy in the IR region. Meikle et al. (1993) studied the 4 μm flux continuum and also suggested that dust condensation occurred as early as ~day 350. At about the same time, the optical photometry data were fading at a rate faster (see Fig. 16) than the previous epoch. The increase in IR luminosity compensated for the optical deficit so that the overall bolometric light curve continued to follow the decay of ^{56}Co (Whitelock et al. 1989; Suntzeff & Bouchet 1990).

However, it was the spectroscopic evidence that was decisive in confirming the presence of condensed dust in the SN 1987A ejecta. Around day 530, the line profiles of optical emission lines, such as Mg I] 4571, [O I] 6300, 6363, Hα, and [C I] 9823, 9849, became asymmetrical and blueshifted by 500–700 km s^{-1} (Danziger et al. 1989). Lucy et al. (1989) explained this shift as the consequence of obstruction of the far side of the supernova ejecta by dust formed in the inner core of the supernova atmosphere, within the line-forming region. Moreover, the bluer lines showed larger blueshifts, suggesting that some dust is optically thin. However, the condensation efficiency would be very small ($\lesssim 10^{-3}$) if the only dust formed were small-sized grains (~0.01 μm) uniformly distributed in the ejecta. Lucy et al. (1991) resolved the problem by constructing a model with dust grains concentrated in optically thick clumps with filling factor $\lesssim 1$, while a diffuse distribution of small dust grains exists between these opaque clouds. They are able to obtain a better fit to the IR spectrum than their previous model (Lucy et al. 1989) in which only uniformly distributed dust grains are condensed. This clumping of the condensed dust is probably the reason the predicted optical-UV photometric "blackout" in Gehrz & Ney (1987) and Dwek (1988) did not occur. This picture is consistent with the model constructed by Wooden et al. (1993) to match the IR observations from the Kuiper Airborne Observatory (KAO) from day 60 to day 775. In their model, the dust grains are clumped and these dust clumps emit a single-temperature gray-body spectrum in the infrared continuum of SN 1987A so that most of the energy emitted redward of 6 μm comes from the dust. The dust temperature dropped from $T_g \approx 400$ K at day 615 to $T_g \approx 265$ K at day 775. Bouchet et al. (1991) also fit a blackbody to the infrared photometric data for day 1316 and obtained $T_g \approx 140$ K.

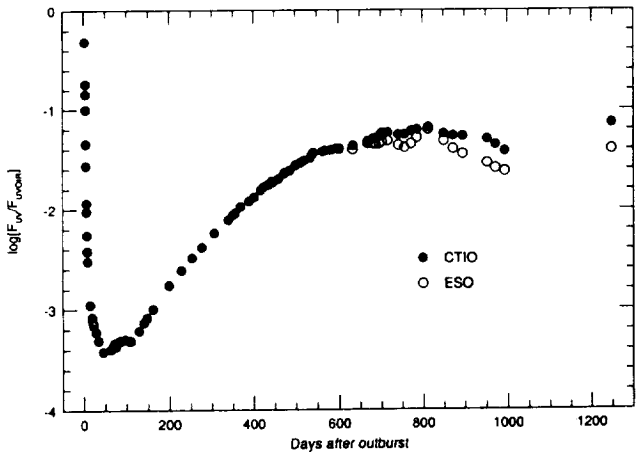

FIG. 19.—Fraction of UV emission to the total emission for SN 1987A. The integrated UV flux is compared with the adjusted UVOIR bolometric luminosity (Table 4) measured by CTIO (*filled circles*) and ESO (*open circles*).

6.2. *UV Color Evolution*

As seen in the optical + UV spectra in Figure 8, and the ratio of UV contribution to total bolometric luminosity in Figure 19, SN 1987A is getting bluer in time. To investigate this

change quantitatively and to evaluate the effect of the forming dust on the UV emission, we define an ultraviolet "color" by subtracting the logarithm of integrated flux in the wavelength band 1600–2500 Å from the logarithm of integrated flux in the band 2500–3300 Å. The spectra in the range 1150–1600 Å are not included in the study because of their low signal to noise and the contamination by background stars. The time evolution of this UV color is shown in Figure 20. After climbing to a early maximum at day 6 and stayed there until day 75, the UV color dropped, approximately in linear fashion, to a value of ~0.8 by day 125. Then the color remained at about the same level for about a year (day 125–460) before it took a sudden turn toward the blue and started to decrease, more or less linearly, until the end of our observing period. To examine the origin of the latter dip in color, the spectra just before and after day 460 are compared. The average spectrum for the period day 500–550 is divided by the average spectrum of day 350–400 and the result is presented in Figure 21. The fluctuation of the ratio seen in the wavelength range 2200–2390 Å is caused by the very low signal observed. Unfortunately, this is where part of the 2175 Å "bump" of interstellar extinction is located. This bump, though not as prominent in the LMC as in the Galaxy (Fitzpatrick 1985), is the most prominent feature of the interstellar reddening function in the UV. However, by noticing the relative flux change in the 2040–2200 Å range where stronger signals from the supernova are detected, we conclude that the 2175 Å bump is not the dominant factor in the variation of the UV color. In fact, the change of color is not caused by the change of flux of any particular feature. Instead, it is caused by an overall change that seems to increase the flux toward shorter wavelength, resulting in a general "bluing" of the spectrum as time goes by.

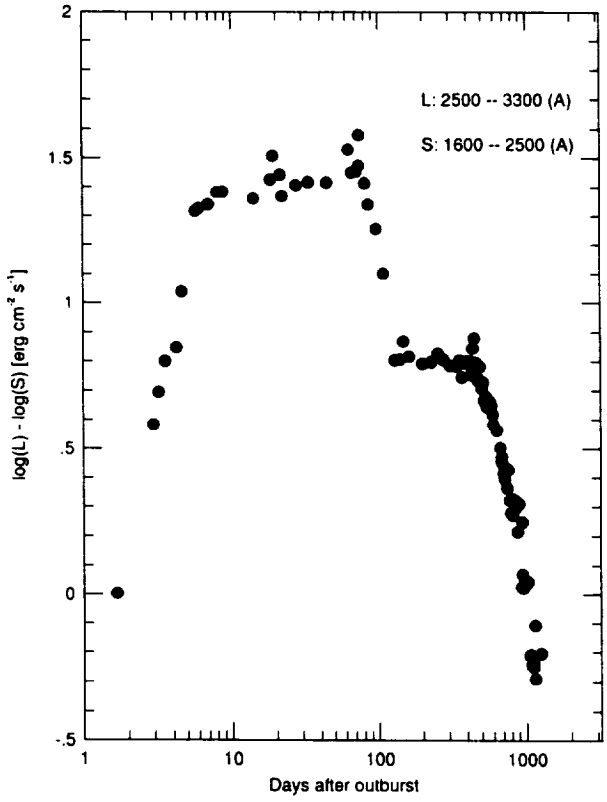

FIG. 20.—The evolution of the UV color with $\log_{10}$(time) (see text for definition of the UV color). Note that when the supernova gets redder in UV, it will have a higher value of UV color.

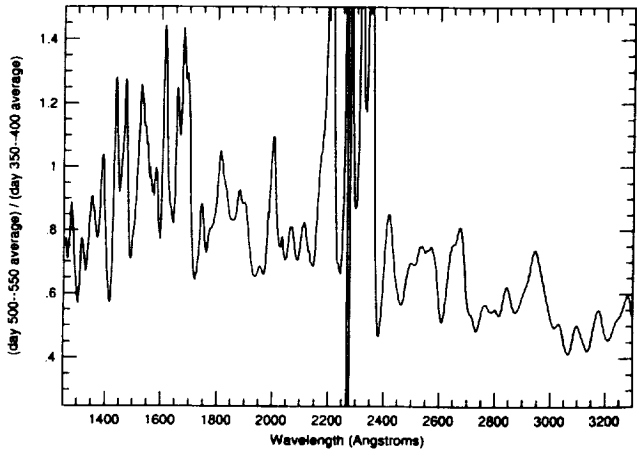

FIG. 21.—Ratio of the average UV spectrum taken just before dust formation (day 350–400) over the average UV spectrum taken just after dust formation (day 500–550). (We assume that dust formation took place around day 460.) The fluctuations in the range 2200–2390 Å are caused by the very low signal from the supernova in these two epochs.

The time at which the UV color took a sharp turn to the blue is also the time when dust formation is believed to occur in the ejecta (day 450). Ordinary interstellar dust causes flux extinction that increases with decreasing wavelength in the ultraviolet range, except for the distinct 2175 Å bump. The fact that the supernova was getting bluer despite the dust formation suggests that the short-wavelength ultraviolet radiation did not suffer any extra extinction by the newly formed dust. In any case, the dust does not resemble interstellar dust in its extinction properties in the UV. This is similar to what was seen in Nova Cassiopeiae 1993 in the UV where the formation of "gray" dust was observed (Shore et al. 1994). The solution of this problem lies in the composition, size, and distribution of the condensed dust.

6.3. *On the Reddening Properties of Dust in SN 1987A*

The supernova ejecta consist of regions of different elemental compositions and physical properties, which might lead to the condensation of different types of grains. Lucy et al. (1991) suggested that the condensation of "astronomical silicate" (Draine & Lee 1984) of radius 100 Å, mostly in clumps, could explain both the steepening in the rate of decline of the [Si I] 1.65 μm line flux and provide a better fit to the 10–20 μm continuum. However, the [Si I] 1.65 μm line is very sensitive to changes in temperature (Fransson & Chevalier 1987), and thus its rapid decline may not be totally attributed to the condensation to silicates. Using the theory of homogeneous nucleation and grain growth, Kozasa, Hasegawa, & Nomoto (1989, 1991) modeled the condensation of clumped silicate and oxide grains (radius ~ 10–100 Å), such as $MgSiO_3$, Al_2O_3, and Fe_3O_4, to obtain fits to the observed 10 μm IR light curve. In the model by Wooden et al. (1993), the graybody radiation of the supernova in the mid- and far-infrared after ~day 400 is

explained by the presence of some heavily clumped dust clouds which are optically thick, with a total surface area filling factor of ~0.5. Spyromilio & Graham (1992) suggested that the falling of the gaseous Fe II near-IR emission could be explained by the combined effects of the rapid drop of temperature (below 500 K), and that a fraction of Fe^+ got tied up in optically thick clumps of dust to escape the rapid cooling. In their efforts to model the light curves of neutral and singly ionized Fe, Ni, and Co infrared emission lines, Li, McCray, & Sunyaev (1993) also constructed a model of the supernova atmosphere with some iron-rich clumps with a total filling factor of ~0.5. This suggests that the newly formed dust may be rich in iron-group elements. This conclusion is supported by the study of Wickramasinghe & Wickramasinghe (1993). They argued that in the heavily non-LTE conditions of the supernova atmosphere, the condensation of metallic iron might precede the formation of iron oxide, thus leading to the production of "iron whiskers." These metallic iron needles of radius 100 Å and length 1 mm are shown to have the necessary mass absorption coefficients to explain the lack of observed flux in the far-infrared to microwave range (3 μm to 30 cm) in the day 1300 spectrum of SN 1987A. As described in § 3, the UV spectrum of SN 1987A is dominated by the heavily blanketed lines of iron group elements, especially Fe II. The combined effects of decreased opacities of iron lines with the formation of iron rich dust, and increased absorption by the condensed dust, may explain the evolution of the UV color near the epoch of dust formation.

As described in § 3, the UV radiation from the supernova went through a series of resonance scatterings before escaping from the envelope. Fransson (1994) pointed out that since the effects of dust absorption are prominent for optical lines, we should see a larger fraction of the UV radiation, with a much larger path length due to resonance scattering, to be absorbed, thermalized, and emerge in the infrared after dust condensation. However, such a large drop in flux in UV is not observed (see Fig. 16). In fact, the supernova continued to grow bluer in the UV even as dust condensation proceeded. This effect might be caused by dust grains with *decreasing* absorption coefficients with decreasing wavelength in the UV. For small grains (radius $\lesssim \lambda/10$), Rayleigh scattering is the dominant scattering process and its effect goes with the inverse fourth power of the wavelength. We found that neither the "astronomical silicate" (radius ~ 100 Å) proposed by Lucy et al. (1991), nor the oxides and silicates grains (radius ~ 10–100 Å) proposed by Kozasa et al. (1991), nor the iron whiskers (radius 100 Å; length 1 mm) proposed by Wickramasinghe & Wickramasinghe (1993), has the correct absorption cross section dependence with wavelength to explain the bluing effects in the UV. Thus we would need different components in the dust other than the these small sized grains. With larger sized grains, Mie scattering will be increasingly more important. If the dust is in front of the UV source, the effect of forward scattering could work to make the spectrum bluer. Lucy et al. (1989) derived a constraint on the size of the dust grains ("astronomical silicate" radius $\lesssim$ 500 Å) to explain the bluing of the optical emission lines. We hope a constraint on the grain size can be determined with the UV color information.

One alternate explanation for the bluing of the spectra in UV following dust formation is as follows: dust condensation started in the cooler part of the ejecta. If some of the dust clumps formed are totally black, the newly condensed dust will effectively block out the lowest temperature material in the supernova envelope. Therefore, even though the flux from the supernova was declining, the temperature of the UV radiation could go up. And as a consequence, the UV color would get bluer in time. A detailed inhomogeneous model of the supernova debris is needed to see whether this effect can account for the observations.

7. COMPARISON WITH *HST* RESULTS

The *IUE* data form an essential record that will prove useful for interpreting future observations of SN 1987A with the *Hubble Space Telescope* (*HST*). Observation of SN 1987A was part of the science assessment program to test the performance of the telescope. Continuing observations of the supernova were carried out by the Supernova INtensive Study (SINS) GO program. The Faint Object Camera (FOC) aboard the *HST* has the resolution capability (0".022) to resolve the supernova from its neighboring stars. It also has the sensitivity to detect the fading supernova after it has become too faint for *IUE* measurements. The first *HST* UV observations of SN 1987A were taken on 1990 August 24 (day 1277.8) with the FOC f/96 through the F175W and F275W filters (Jakobsen et al. 1991). Further results on the expansion of the supernova debris and photometry were also published (Jakobsen, Macchetto, & Panagia 1993) based on a second set of observations made at 1991 December 13 (day 1754.3), and also in Jakobsen et al. (1994) based on the first set of post-COSTAR observations. Complete photometric results from the SINS SN 1987A observations will be presented in Kirshner et al. (1995).

The UV photometry in the *HST* bands for epochs before *HST* deployment can be obtained by convolving the *IUE* spectra with the FOC filter passbands. We convolved the *IUE* spectra with the FOC f/96 F175W filter function (peak wavelength 1730 Å, FWHM 714 Å) and F275W filter function (peak wavelength 2740 Å, FWHM 594 Å) using the CALCPHOT task in the SYNPHOT program of the Space Telescope Science Data Analysis System (STSDAS) (Bazell 1990). The CALCPHOT task is capable of synthesizing FOC photometry corresponding to the selected *HST* filter bands with the input spectrum using equation (1). The input UV spectra are corrected for neither the parent galaxy redshift nor interstellar extinction so that the derived spectrophotometric data can be compared directly to the photometric measurements. The synthesized FOC photometry results for the filters F175W and F275W are shown in Figures 22*a* and 22*b*, respectively.

The synthesized photometry results from *IUE* spectra can be compared with the photometry directly measured from the *HST* FOC images obtained under the SINS program. It is fortunate that the first UV observation of SN 1987A by *HST* was made not long after the signal from the supernova in UV was too weak for detection by *IUE*. Six sets of observations have been made at day 1278, 1754, 1876, 2031, 2260, and 2431 with images from both the F175W and F275W filters (except at day 1754, when only the F275W image is taken). The complete log of the FOC UV data set is given in Table 5. In all the FOC images, the SN 1987A is superimposed on the outer part of the point spread function (psf) of star 2 and star 3, which are both well saturated in the center in all the frames. The flux from the

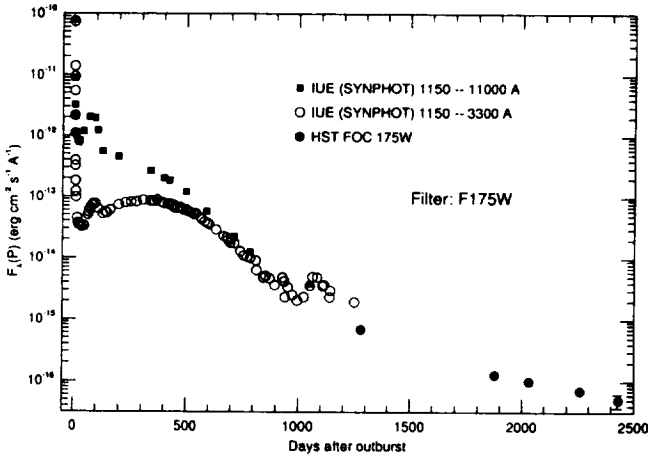

FIG. 22a

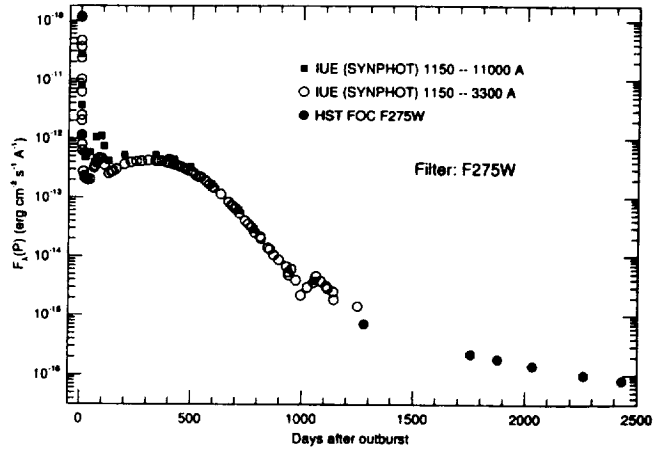

FIG. 22b

FIG. 22.—(*a*)–(*b*) The F175W and F275W light curves of SN 1987A from the *IUE* and *HST* observations. The filled squares are the results from the SYNPHOT program by convolving the *IUE* data with the *HST* observing passbands. The open circles are the SYNPHOT results of convolving the combined UV + optical data with the *HST* passbands. The filled circles represent the measured photometry from *HST* images.

two asymmetric halos represents the major source of contamination to the correct photometric measurement for the supernova. The DAOPHOT II program was used to create a model of the entire 3″ psf of star 2 (Stetson 1991). This model was subtracted from the *HST* image. The same model was scaled to the flux magnitude of star 3 and subtracted from the image. This procedure is valid despite the fact that both star 2 and star 3 are saturated at the center of the FOC images for both passbands because we are only interested in determining the flux from the supernova, which is located at the periphery of the psf of the two stars. The flux from the supernova is measured by integrating over a small circle (5 pixels, 0″.11). The result is multiplied by the fraction of encircled energy (22%) in the psf at the radius of 0″.11. This fraction is determined from the high signal to noise images of SN 1992A (Kirshner et al. 1993) obtained with the FOC f/96 F175W and F275W filters. These images provided good measurements of the encircled energy as a function of psf radius. The absolute UV photometry measurements by FOC is correct to ~10%–15% (P. Hodge, private communications) with the major uncertainty coming from the determination of the standard star flux. The photometry measurements in this present work are ~15%–40% lower than the previously published results from the day 1278 and day 1754 data (Jakobsen et al. 1991, 1993). The discrepancy is probably caused by the different methods employed in removing the fluxes from star 2 and star 3 in the images.

TABLE 5

HST UV OBSERVATIONS OF SN 1987A WITH FAINT OBJECT CAMERA (FOC)

Date (UT)	Day	Filter	t_{exp} (s)
1990 Aug 24.0	1277.7	F175W	838 + 838
1990 Aug 24.1	1277.8	F275W	838
1991 Dec 13.6	1754.3	F275W	1200 + 838
1992 Apr 13.7	1876.4	F175W	2000
1992 Apr 13.7	1876.4	F275W	2000
1992 Sep 15.7	2031.4	F175W	2000
1992 Sep 15.7	2031.4	F275W	2000
1993 May 1.9	2259.6	F175W	2500
1993 May 1.8	2259.5	F275W	2500
1993 Oct 20.3	2431.0	F175W	1500 + 1700
1993 Oct 20.3	2431.0	F275W	1450 + 1550

There is one detail not to be overlooked while comparing the *IUE* and *HST* results—both the F175W and F275W filters have extensive red leaks that include optical light beyond the observed limit of the *IUE* cameras at 3300 Å (Nota, Jedrzejewski, & Hack 1993). In Figure 22, the open circles represent the synthesized FOC photometry results obtained with the SYNPHOT program with *IUE* data (1150–3300 Å) as the input. To study the effects of the red leaks, the results from the SYNPHOT program with the combined UV + optical data (1150–11000 Å) as the input spectra are also plotted (*filled squares*). We can see that neglecting the supernova flux longward of 3300 Å can cause a significant underestimate of the UV photometry. At day 44, excluding flux above 3300 Å will result in FOC-band UV photometry 35 and 3 times lower than the full photometry for F175W and F275W filters, respectively. For the F175W filter, even though the transmittance beyond 4000 Å is less than 0.3% of that at the transmission maximum at 1730 Å, on day 44 the flux in the optical regime is $\sim 10^4$ times larger than that at 1730 Å. The overall effect is that the UV photometry measurement with the F175W filter at day 44 would have about 97% of the flux originated redward of 3300 Å. Similarly, for the F275W filter, while the transmittance beyond 4000 Å is less than 0.75% of that at 2740 Å, the flux in the optical regime is about 500 times larger than that around 2740 Å at day 44. Thus only about one-third of the collected light through the F275W filter would have come from the UV. As mentioned in § 5.2, as the supernova ages, relatively more flux of SN 1987A comes from the ultraviolet region as compared to optical. Therefore, the difference between the SYNPHOT results using UV + optical input and UV only in-

put diminishes with time. For observations after ~day 700 for F175W and after ~day 400 for F275W, the underestimate of synthesized photometry caused by the cutoff at 3300 Å becomes negligible.

The *IUE* and *HST* results agree well for measurements made with the F275W filter around day 1250, the time at which the *IUE* satellite was not sensitive enough for further detection of the dimming SN 1987A, and when we started our program with *HST* on SN 1987A. This confirms that our method of background stellar subtraction for *IUE* is accurate, as compared to the one employed by SFdC93, which erroneously generated a late-time flux ~ 10–15 times higher than our study. Our *IUE* and *HST* F175W results agree only moderately well around day 1250, with the *IUE* measurement about 0.5 dex higher than the *HST* results. This is probably caused by the additional flux detected from the variable star 3 as described in § 5.2.

8. CONCLUSION

We have described the details to create a complete set of ultraviolet spectra taken by the *IUE* satellite on SN 1987A. We hope that this data set will contribute toward understanding the late stage of stellar evolution, the supernova explosion mechanism, and evolution of the explosion debris. The major problem we faced in the data reduction process has been the removal of the flux contributions from nearby field stars. No previous analysis has had background measurements of sufficient accuracy. Our *IUE* results are consistent with other UV observations such as Walraven *VBLUW* photometry and *HST* images.

The complexity of the line blending in the UV region implies that detailed analysis is needed to obtain abundances and even line identification in the supernova atmosphere. Early *IUE* and optical spectra had been used for modeling the SN 1987A atmosphere (Harkness & Wheeler 1988; Eastman & Kirshner 1989; Schmutz et al. 1990; Hauschildt & Ensman 1994) to understand the effects of scattering and geometry of the expanding envelope. LTE synthetic spectral analysis for the optical and UV spectral data taken by *HST* had been done on SN 1992A, a SN Ia (Kirshner et al. 1993), and SN 1993J, a SN II (Jeffery et al. 1994). The UV behavior of supernovae is closely related to the degree of interaction of the supernova ejecta with the circumstellar materials. For supernovae with thick circumstellar envelopes, such as SN 1979C, SN 1980K, and SN 1993J, relatively smooth UV spectra are observed, whereas for SNe Ia and SN 1987A, which had a weaker radio display and hence a more dilute circumstellar medium, showed UV-deficient spectra with broad band absorption caused mostly by singly ionized iron group elements. The UV deficit is caused by expanding atmospheres with moderately steep density profiles, together with a huge number of resonance lines of the iron group elements providing the UV opacity. These closely separated lines blended under the expansion and caused the line-blanketing effect, and the broad features observed will naturally emerge from the blending of the strongest absorption lines.

With the *IUE* data now swamped by star 2 and 3 (both B stars), future long-term monitoring of SN 1987A in UV depends on observing programs with the *HST*. The *HST* corrective optics will provide significant improvements in photometry by confining the flux from star 2 and star 3 to a small region far from SN 1987A. While post-COSTAR FOC or WFPC2 images can provide continuous UV light curve coverage (Jakobsen et al. 1994), the FOS should provide spectroscopic data on both the expanding debris and the circumstellar ring (Wang et al. 1994). Even though the supernova is fading in UV at present, it can become bright again in the future. The opaque UV atmosphere may turn transparent and reveal the stellar interior composition of the progenitor, Sk −69°202, right before the explosion. The UV spectrum then becomes a emission-line spectrum, and it should prove to be helpful in determining the masses of newly produced elements such as C, Mg, and Si, which all have strong lines in the UV region.

The circumstellar ring can also become a bright source of UV radiation when it is hit by the envelope of SN 1987A. Luo, McCray, & Slavin (1994) predicted that this will occur in 12 ± 3 years after explosion (AD 1999 ± 3). The shocked ring will become a bright source of optical, UV, and X-ray emission (Luo & McCray 1991; Luo et al. 1994; Suzuki, Shigeyama, & Nomoto 1993; Masai & Nomoto 1994). Ultraviolet emission lines of He, C, N, and O will all be rising in brightness (up to $\sim 10^{-12}$ ergs cm^{-2} s^{-1}) when the shock occurs and will stay bright a few year after the shock (Luo et al. 1994). The time evolution of these emission lines can be studied in detail with future *HST* observations.

We are extremely grateful to the staff at both the GSFC and VILSPA *IUE*. Observatories for supporting the continuous observing program of SN 1987A by the *IUE* satellite, especially Yoji Kondo for his energetic advocacy of this work. We would also like to acknowledge the following people for sharing the data with us: M. Phillips, N. Suntzeff for the ground-based CTIO spectroscopy, photometry of SN 1987A, stars 2 and star 3; J. W. Pel for the *VBLUW* photometry; L. S. Lyubimkov for the ASTRON spectra. C. S. J. Pun would also like to thank D. Jeffery, B. Schmidt, and P. Höflich for many insightful discussions on SN 1987A; T. Kozasa, and N. C. Wickramasinghe for their comments on dust condensation; S. M. Dougherty for the discussions on Be stars. This work was supported in part by NASA grant NAG 5-841.

APPENDIX

We have included the full set of processed *IUE* spectra on SN 1987A (both LWP and SWP) listed in Tables 2 and 3 in the AAS CD-ROM Series, Volume 5. The combined optical + UV spectra presented in Figure 8 are also included. Please consult the documentation included in the data file for further information.

REFERENCES

Arnett, W. D., Bahcall, J. N., Kirshner, R. P., & Woosley, S. 1989, ARA&A, 27, 629

Barylak, M., & Doazan, V. 1986, A&A, 159, 65

Bazell, D. 1990, Space Telescope Science Institute Newsletters, 7(3)

Benvenuti, P., Sanz Fernández de Córdoba, L., Wamsteker, W., Macchetto, F., Palumbo, G. C., & Panagia, N. 1982, ESA SP-1046
Bionta, R. M., et al. 1987, Phys. Rev. Lett., 58, 1494
Blades, J. C., Wheatley, J. M., Panagia, N., Grewing, M., Pettini, M., & Wamsteker, W. 1988a, ApJ, 332, L75
———. 1988b, ApJ, 334, 308
Boggess, A., et al. 1978, Nature, 275, 2
Bouchet, P., Danziger, I. J., & Lucy, L. B. 1991, AJ, 102, 1135
Boyarchuk, A. A. 1984, Soviet Sci. Rev. E: Astrophys. Space Phys., 5, 225
Boyarchuk, A. A., Gershberg, R. E., Zvereva, A. M., Petrov, P. P., Severnyi, A. B., Terebizh, A. V., Khua, Ch. T., & Sheikhet, A. I. 1987, Soviet Astron. Lett., 13, 311
Branch, D. 1987, ApJ, 320, L177
Cardelli, J. A., Clayton, G. C., & Mathis, J. S. 1989, ApJ, 345, 245
Cassatella, A., Fransson, C., van Santvoort, J., Gry, C., Talavera, A., Wamsteker, W., & Panagia, N. 1987, A&A, 177, L29
Catchpole, R. M., et al. 1987, MNRAS, 229, 15P
Chevalier, R. A. 1992, Nature, 355, 691
Christiani, S., et al. 1987, A&A, 177, L5
Crenshaw, D. M. 1988, *IUE* NASA Newsletter, 35, 51
Danziger, I. J., Gouiffes, C., Bouchet, P., & Lucy, L. B. 1989, IAU Circ., No. 4746
de Boer, K., Grewing, M., Richtler, T., Wamsteker, W., Gry, C., & Panagia, N. 1987, A&A, 177, L37
Dougherty, S. M., & Taylor, A. R. 1994, MNRAS, 269, 1123
Draine, B. T., & Lee, H. K. 1984, ApJ, 285, 89
Dupree, A. K., Kirshner, R. P., Nassiopoulos, G. E., & Raymond, J. C. 1987, ApJ, 320, 597
Dwek, E. 1988, ApJ, 329, 814
Dwek, E., & Felten, J. E. 1992, ApJ, 387, 551
Eastman, R. G., & Kirshner, R. P. 1989, ApJ, 347, 771
Ensman, L., & Burrows, A. 1992, ApJ, 393, 742
Fitzpatrick, E. L. 1985, ApJ, 299, 219
———. 1986, AJ, 92, 1068
Fitzpatrick, E. L., & Walborn, N. R. 1990, AJ, 99, 1483
Fransson, C. 1994, in Supernovae, Les Houches Summer School Course 10, Session 54, 1990, ed. S. Bludman, R. Mochkovitch, & J. Zinn-Justin (Amsterdam: Elsevier), 677
Fransson, C., Benvenuti, P., Gordon, C., Hempe, K., Palumbo, G. G. C., Panagia, N., Reimers, D., & Wamsteker, W. 1984, A&A, 132, 1
Fransson, C., Cassatella, A., Gilmozzi, R., Kirshner, R. P., Panagia, N., Sonneborn, G., & Wamsteker, W. 1989, ApJ, 336, 429
Fransson, C., & Chevalier, R. A. 1987, ApJ, 322, L15
Fransson, C., Grewing, M., Cassatella, A., Panagia, N., & Panagia, N. 1987, A&A, 177, L33
Fransson, C., & Kozma, C. 1993, ApJ, 408, L25
Garhart, M. P. 1992a, *IUE* NASA Newsletter, 48, 98
———. 1992b, *IUE* NASA Newsletter, 48, 80
Gehrz, R. D. 1988, ARA&A, 26, 377
Gehrz, R. D., & Ney, E. P. 1987, Proc. Natl. Acad. Sci., 84, 6961
Gilmozzi, R. 1988, Proc. Astron. Soc. Australia, 7, 397
———. 1990, in Evolution in Astrophysics: IUE in the Era of New Space Mission, ed. E. Rolfe, ESA SP-310, 125
Gilmozzi, R., et al. 1987, Nature, 328, 318
Gochermann, J., Goudfrooij, P., & Schmidt-Kaler, Th. 1989, A&A, 213, 333
Gould, A. 1994a, ApJ, 425, 51
———. 1994b, ApJ, submitted
Hamuy, M., & Suntzeff, N. B. 1990, AJ, 99, 1146
Hamuy, M., Suntzeff, N. B., González, R., & Martin, G. 1988, AJ, 95, 63
Hanuschik, R. W., & Thimm, G. J. 1990, A&A, 231, 77
Harkness, R. P., & Wheeler, J. C. 1988, Proc. Astron. Soc. Australia, 7, 431
Harris, A. W., & Sonneborn, G. 1987, in Exploring the Universe with the IUE Satellite, ed. Y. Kondo (Dordrecht: Reidel), 729
Hauschildt, P. H., & Ensman, L. M. 1994, ApJ, 424, 905
Hauschildt, P. H., Starrfield, S., Austin, S., Wagner, R. M., Shore, S. N., & Sonneborn, G. 1994, ApJ, 422, 831
Hillebrandt, W., & Höflich, P. 1989, Rep. Prog. Phys., 52, 1421
Hirata, R., et al. 1987, Phys. Rev. Lett., 58, 1490
Horne, K. 1988, in New Directions in Spectrophotometry, ed. A. G. Davis Philip, D. S. Hayes, & S. J. Adelman (Schenectady, New York: L. Davis), 145
Imshennik, V. S., & Nadëzhin, D. K. 1989, Soviet Astrophys. & Space Phys. Rev., vol. 8, ed. R. A. Syunyaev (London: Harwood), 1
Jakobsen, P., Jedrzejewski, R., Macchetto, F., & Panagia, N. 1994, ApJ, 435, L47
Jakobsen, P., Macchetto, F., & Panagia, N. 1993, ApJ, 403, 736
Jakobsen, P., et al. 1991, ApJ, 369, L63
Jeffery, D. J., & Branch, D. 1990, in Jerusalem Winter School for Theoretical Physics, vol. 6, Supernovae, ed. J. C. Wheeler, T. Piran, & S. Weinberg (Singapore: World Scientific), 149
Jeffery, D. J., et al. 1994, ApJ, 421, L27
Karp, A. H., Lasher, G., Chan, K. L., & Salpeter, E. E. 1977, ApJ, 214, 161
Kirshner, R. P., & Gilmozzi, R. 1989, in Exploring the Universe with the IUE Satellite, ed. Y. Kondo (2d ed.; Dordrecht: Reidel), 771
Kirshner, R., Sonneborn, G., Cassatella, A., Gilmozzi, R., Wamsteker, W., & Panagia, N. 1987a, IAU Circ., No. 4435
Kirshner, R. P., Sonneborn, G., Crenshaw, D. M., & Nassiopoulos, G. E. 1987b, ApJ, 320, 602
Kirshner, R. P., et al. 1993, ApJ, 415, 589
———. 1995, in preparation
Kozasa, T., Hasegawa, H., & Nomoto, K. 1989, ApJ, 344, 325
———. 1991, A&A, 249, 474
Li, H., McCray, R., & Sunyaev, R. A. 1993, ApJ, 419, 824
Lucy, L. B. 1987, A&A, 182, L31
Lucy, L. B., Danziger, I. J., Gouiffes, C., & Bouchet, P. 1989, in IAU Colloq. 120, Structure and Dynamics of the Interstellar Medium, ed. G. Tenorio-Tagle, M. Moles, & J. Melnick (New York: Springer), 164
———. 1991, in Supernovae, ed. S. E. Woosley (New York: Springer), 82
Lundqvist, P. 1991, in ESO/EIPC Workshop: SN 1987A and Other Supernovae, ed. I. J. Danziger & K. Kjär (Garching: ESO), 607
Luo, D., & McCray, R. 1991, ApJ, 379, 659
Luo, D., McCray, R., & Slavin, J. 1994, ApJ, 430, 264
Lyubimkov, L. S. 1990, Soviet Astron., 34, 239
Martin, G. A., Fuhr, J. R., & Wiese, W. L. 1988, J. Phys. Chem. Ref. Data Supp., 17(3), 1
Masai, K., & Nomoto, K. 1994, ApJ, 424, 924
McCray, R. 1991, in Supernovae and Stellar Evolution, ed. A. Ray & T. Velusamy (Singapore: World Scientific), 1
———. 1993, ARA&A, 31, 175
McCray, R., Shull, J. M., & Sutherland, P. 1987, ApJ, 317, L73
Meikle, W. P. S., Spyromilio, J., Allen, D. A., Varani, G.-F., & Cumming, R. J. 1993, MNRAS, 261, 535
Mũnoz Peiro, J. R. 1985, *IUE* NASA Newsletter, 27, 27
Nomoto, K., Shigeyama, T., Kumagai, S., Yamaoka, H., & Suzuki, T. 1994, in Supernovae, Les Houches Summer School Session 54, 1990, ed. S. Bludman, R. Mochkovitch, & J. Zinn-Justin (Amsterdam: Elsevier), 489
Nota, A., Jedrzejewski, R., & Hack, W. 1993, Hubble Space Telescope Faint Object Camera Instrument Handbook, version 4.0 (Baltimore: STScI)
Panagia, N. 1984, in Supernovae as Distance Indicator, ed. N. Bartel (Berlin: Springer), 14
Panagia, N., & Gilmozzi, R. 1991, in ESO/EIPC Workshop: SN 1987A and Other Supernovae, ed. I. J. Danziger & K. Kjär (Garching: ESO), 575
Panagia, N., Gilmozzi, R., Cassatella, A., Wamsteker, W., Kirshner, R. P., & Sonneborn, G. 1987a, IAU Circ., No. 4514
Panagia, N., Gilmozzi, R., Macchetto, F., Adorf, H.-M., & Kirshner, R. P. 1991, ApJ, 380, L23
Panagia, N., et al. 1980, MNRAS, 192, 861
———. 1987b, A&A, 177, L25
Pel, J. W., et al. 1987, in Proc. ESO Workshop on SN 1987A, ed. I. J. Danziger (ESO: Garching-bei-München), 97
Phillips, M. M., Hamuy, M., Heathcote, S. R., Suntzeff, N. B., & Kirhakos, S. 1990, AJ, 99, 1133
Phillips, M. M., Heathcote, S. R., Hamuy, M., & Navarrete, M. 1988, AJ, 95, 1087
Plait, P., Chevalier, R., & Kirshner, R. 1992, IAU Circ., No. 5592
Plait, P. C., Lundqvist, P., Chevalier, R. A., & Kirshner, R. P. 1995, ApJ, 439, 730
Podsiadlowski, P. 1992, PASP, 104, 717
Roche, P. F., Aitken, D. K., & Smith, C. H. 1993, MNRAS, 261, 522
Roche, P. F., Aitken, D. K., Smith, C. H., & Jones, S. D. 1989, Nature, 337, 533

Saizar, P., et al. 1992, ApJ, 398, 651
Sanz Fernández de Córdoba, L. 1993, A&A, 276, 103 (SFdC93)
Savage, B., Jenkins, E., Joseph, C., & de Boer, K. 1989, ApJ, 345, 393
Schmutz, W., Abbott, D. C., Russell, R. S., Hamann, W.-R., & Wessolowski, U. 1990, ApJ, 355, 255
Scuderi, S., Panagia, N., Gilmozzi, R., Kirshner, R. P., & Challis, P. M. 1995, ApJ, submitted
Seaton, M. J. 1979, MNRAS, 187, 73P
Shelton, I. K. 1993, AJ, 105, 1895
Shore, S. N., Starrfield, S., Gonzalez-Riestra, R., Hauschildt, P. H., & Sonneborn, G. 1994, Nature, 369, 539
Sonneborn, G. 1991, in Supernovae, ed. S. E. Woosley (New York: Springer), 125
Sonneborn, G., Altner, B., & Kirshner, R. P. 1987, ApJ, 323, L35
Sonneborn, G., Fransson, C., Cassatella, A., Gilmozzi, R., Kirshner, R. P., Lundqvist, P., Panagia, N., & Wamsteker, W. 1994, ApJ, submitted
Sonneborn, G., Rodriguez, P. M., Wamsteker, W., Fransson, C., & Kirshner, R. 1993, IAU Circ., No. 5754
Spyromilio, J., & Graham, J. R. 1992, MNRAS, 255, 671
Stetson, P. B. 1991, in 3rd ESO/ST-ECF Data Analysis Workshop, ed. P. J. Grosbøl & R. H. Warmels, ESO Conf. and Workshop Proc. 38 (ESO: Garching-bei-München), 187
Suntzeff, N. B., & Bouchet, P. 1990, AJ, 99, 650
Suntzeff, N. B., Hamuy, M., Martin, G., Goméz, A., & González, R. 1988, AJ, 96, 1864
Suntzeff, N. B., Phillips, M. M., Depoy, D. L., Elias, J. H., & Walker, A. R. 1991, AJ, 102, 1118
Suzuki, T., Shigeyama, T., & Nomoto, K. 1993, A&A, 274, 883
Teays, T. J., & Garhart, M. P. 1990, IUE NASA Newsletter, 41, 94
Turnrose, B. E., & Thompson, R. W. 1984, *IUE* Image Processing Information Manual, Version 2.0
Wagoner, R. V., Perez, C. A., & Vasu, M. 1991, ApJ, 377, 639
Walborn, N. B., Phillips, M. M., Walker, A. R., & Elias, J. H. 1993, PASP, 105, 1240
Walborn, N. B., Prévot, M. L., Prévot, L., Wamsteker, W., González, R., Gilmozzi, R., & Fitzpatrick, E. L. 1989, A&A, 219, 229
Walker, A. R., & Suntzeff, N. B. 1990, PASP, 102, 131
———. 1991, PASP, 103, 958
Wampler, E. J., Richichi, A., & Baade, D. 1989, in IAU Colloq. 120, Structure and Dynamics of the Interstellar Medium, ed. G. Tenorio-Tagle, M. Modes, & J. Melnick (Berlin: Springer), 190
Wamsteker, W., Gilmozzi, R., Cassatella, A., & Panagia, N. 1987a, IAU Circ., No. 4410
Wamsteker, W., Rodriguez, P. M., Gonzalez, R., Sonneborn, G., & Kirshner, R. 1993, IAU Circ., No. 5738
Wamsteker, W., et al. 1987b, A&A, 177, 21
Wang, L., D'Odorico, S., Gouiffes, C., & Wampler, J. 1992, IAU Circ., No. 5449
Wang, L., et al. 1994, in preparation
Whitelock, P. A., et al. 1989, MNRAS, 240, 7P
Wickramasinghe, N. C., & Wickramasinghe, A. N. 1993, Ap&SS, 200, 145
Williams, R. E. 1991, in IAU Colloq. 122, Physics of Classical Novae, ed. A. Cassatella & R. Viotti (Berlin: Springer), 215
Wooden, D. H., Rank, D. M., Bregman, J. D., Witteborn, F. C., Tielens, A. G. G. M., Cohen, M., Pinto, P. A., & Axelrod, T. S. 1993, ApJS, 88, 477
Xu, Y., & McCray, R. 1991, in Supernovae, ed. S. E. Woosley (New York: Springer), 444
Xu, Y., McCray, R., Oliva, E., & Randich, S. 1992, ApJ, 386, 181